Major Project -II
SOME EXPERIMENTAL AND COMPUTATIONAL STUDIES ON A SINGLE CYLINDER DIESEL ENGINE ON BLENDS OF CALOPHYLLUM METHYL ESTER AND DIESEL

Submitted to **Delhi Technological University** in partial fulfilment of the requirement for the award of the Degree of

Master of Technology

In

Thermal Engineering

By

CHINMAYA MISHRA (2K11/THE/06)

UNDER THE SUPERVISION OF

Dr. Naveen Kumar

Professor & Head

Mechanical Engineering Department

Delhi Technological University, Shahabad Daulatpur

Bawana Road, Delhi-110042, INDIA

July-2013

This piece of academic research is humbly dedicated

to my parents

Smt. Sadhana Mishra

and

Sri. Pravat Kumar Mishra

DECLARATION

I, hereby declare that the work embodied in the dissertation entitled **"SOME EXPERIMENTAL AND COMPUTATIONAL STUDIES ON A SINGLE CYLINDER DIESEL ENGINE ON BLENDS OF CALOPHYLLUM METHYL ESTER AND DIESEL"** in partial fulfilment for the award of degree of MASTER of TECHNOLOGY in "THERMAL ENGINEERING", is an original piece of work carried out by me under the supervision of Prof. Naveen Kumar, Mechanical Engineering Department, Delhi Technological University. The matter of this work either full or in part have not been submitted to any other institution or University for the award of any other Diploma or Degree or any other purpose what so ever.

(CHINMAYA MISHRA)

M.Tech (Thermal Engineering)

Roll No.: 2K11/THE/06

CERTIFICATE

This is to certify that the work embodied in the dissertation entitled **"SOME EXPERIMENTAL AND COMPUTATIONAL STUDIES ON A SINGLE CYLINDER DIESEL ENGINE ON BLENDS OF CALOPHYLLUM METHYL ESTER AND DIESEL"** by **CHINMAYA MISHRA, (**Roll No.-**2K11/THE/06)** in partial fulfilment of requirements for the award of **Degree of Master of Technology in Thermal Engineering**, is an authentic record of student's own work carried by him under my supervision.

This is also certified that this work has not been submitted to any other Institute or University for the award of any other diploma or degree.

(Dr. Naveen Kumar)

Professor & Head

Mechanical Engineering Department

Delhi Technological University

Delhi- 110042.

ACKNOWLEDGEMENT

Apart from personal efforts, the success of any project depends largely on the encouragement and guidance of many others. I take this opportunity to express my gratitude to the people; their guidance, support, encouragement and all the above blessing that have been instrumental to achieve this endeavour.

First and foremost, I would like to thank the almighty and my parents for creating, nurturing and enabling me up to this level of intellectual, spiritual and academic maturity. I would like to show my greatest appreciation, heartfelt sense of gratitude and indebtedness to Prof. Naveen Kumar. I can't say that the word "thank you" is enough for his tremendous support and help. I feel motivated and encouraged every time I attend his company. Without his encouragement and guidance this project would not have been materialized.

I would very much like to extend my sincere thanks to CASRAE lab attendants Mr. Manoj Kadiyan and Mr. Kamal Nain for their friendly help always. I further extend my gratitude to my friends Ashish Kumar Singh, Alhassan Yahya and Usharani Rath my juniors Anuj Pal, Manas Chitrans, Jayati Takkar and Vishvendra Singh Tomar for their dedicated moral, technical and physical support all the time just as a constant companion for the successful completion of this project.

.

CHINMAYA MISHRA

M.TECH (Thermal Engineering)

Roll No.-2K11/THE/06

ABSTRACT

Bio-origin liquid fuels like vegetable oil and animal fat are seriously considered as promising alternative fuels to crude oil derivatives worldwide. In this context, Government of India approved the National Policy on Biofuels in December 2009 to substitute 20% of net mineral diesel consumption by biodiesel. However, the ambitious plan of producing sufficient biodiesel to meet the mandate of 20 percent diesel substitution by the year 2012 was not realized. Excessive reliance on Jatropha curcas as the lonely oilseed and the inability to produce sufficient feedstocks was one of the major reasons cited in this context. In the light of the above fact, the present research deals with the comprehensive study of another potential alternative oilseed "Calophyllum Inophyllum" for biodiesel production which can support Government of India's biofuel policy and may significantly increase the feedstock availability. The research work was divided into four major domains. The two stage process, comprising of acid catalysed esterification followed by base catalysed transesterification to produce biodiesel from the high free fatty acid (FFA) Calophyllum vegetable oil was optimized using response surface methodology. A three level-five factors central composite rotatable design was set up. The process parameters like catalyst concentration, reaction time and temperature were taken as factors in the experimental design. For the acid catalysed stage, %FFA and for the base catalysed stage, %yield of biodiesel were considered as the response. Based on the designed test matrix the experiments were carried out and the results were analysed in design of experiment software 8.0.7.1. The optimum conditions for the acid catalysed stage was predicted as 1.5% catalyst concentration, 60 minutes reaction time and 65°C reaction temperature leading to 4.74% FFA from the initial value of 23.52%. For the alkaline stage, 0.88% catalyst, 62.75°C temperature, 90 minutes reaction time resulted in an optimal yield of 96.48% biodiesel. Based on the optimum condition bulk quantity of Calophyllum methyl ester was (CME) was produced. In the second stage of the project, fatty

acid profile and various physico-chemical as well as fuel properties of CME were experimentally investigated. The results of the gas chromatography study of CME indicated that the fuel is rich in oleic and linoleic acid. Properties like viscosity, density, calorific value, oxidation stability etc. were measured and found satisfactorily within the limits of ASTM and other standards. The third stage of the research comprised of fuel blend development, diesel engine test rig development and a set of exhaustive engine trial for performance, emission and combustion studies. Various test fuel for the engine trial were CME10, CME20, CME30, CME40 and CME100 with 10%,20%, 30%, 40%and 100% volume wise substitution of mineral diesel by CME. The results indicated higher engine performance for CME10 and CME20 as compared to mineral diesel. Other higher blends showed marginal reduction in engine performance. CME and its blends exhibited lower emissions of carbon monoxide, total hydrocarbon and smoke. However, emissions of oxides of nitrogen were increased with increase in CME volume fraction in the test fuel. The total combustion duration (TCD) of CME10 and CME20 were less than the baseline data and other higher blends. With increase in volume fraction of CME in the blend ignition delay was reduced from 11°CA for neat diesel to 7°CA for neat CME. Another notable observation in combustion study was the trend of increased % heat release in the diffusion phase with increase in CME volume fraction that leads to smoother engine operation. In the fourth stage of the study, a three dimensional Computational Fluid Dynamics (CFD) simulations involving in-cylinder air flow and biodiesel combustion was carried out using ANSYS14 IC Engine modeller. Experimental and CFD results showed good correlations with quantitative error of 0.58 % obtained for peak in-cylinder pressure.

Keywords –Alternative fuel, biodiesel, central composite rotatable design, combustion, computational fluid dynamics, diesel engine, emission, performance, response surface methodology, etc.

CONTENTS

LIST OF FIGURES

LIST OF PLATES

NOMENCLATURE

Symbols/Abbreviations

CME100	Calophyllum Methyl Ester (100% by vol)
CME10	Blend of 10% CME and 90% diesel.
CME20	Blend of 20% CME and 80% diesel
CME30	Blend of 30% CME and 70% diesel
CME40	Blend of 40% CME and 60% diesel
Baseline	Neat diesel
^0CA	Degrees of crank angle rotations.
BMEP	Brake mean effective pressure
CO	Carbon monoxide
CO_2	Carbon dioxide
THC	Total unburnt hydrocarbons,
NO_x	Oxides of nitrogen.
BTE	Brake thermal efficiency.
BSEC	Brake specific energy consumption.
ppm	Parts per million
H_2	Hydrogen gas.
^0C	Degree Celsius
^0K	Degree Kelvin
cSt	Centi-Stoke
DI	Direct injection
MJ/Kg	Mega joules per kilogram
kWh	Kilo-watt-hour

RPM	Rotations per minute
BTDC	Before top dead center
MFB	Mass fraction burnt
TCD	Total combustion duration
CHR	Cumulative heat release
ATDC	After top dead center
cc	Centimeter cube
wt. %	Percentage by weight
HRR	Heat release rate
$\frac{dQc}{d\theta}$	Net HRR per ^{0}CA
$\frac{dQc}{d\theta}$	Wall heat loss rate per ^{0}CA
P	In-cylinder Pressure
V	Volume
m	Mass
R	Universal gas constant
T	Temperature
Cp	Specific heat at constant pressure
Cv	Specific heat at constant volume
h	Convective heat transfer co-efficient
A	Piston wall area
γ	Specific heat ratio
Tw	Cylinder wall temperature
Tj	Ambient temperature
v/v	Volume wise substitution

INTRODUCTION

1.1 ENERGY SCENARIO: INDIAN PERSPECTIVE

The word energy is derived from the Greek word *"energeia"*, which means the work capacity. It possibly appeared for the first time in the work of Aristotle in 4th century BCE [1]. Two billiard balls colliding, for example, may come to rest, with the resulting energy becoming sound and perhaps a bit of heat at the point of collision [2]. The modernization of human civilizations from rural societies to affluent urban ones was made possible through the employment of modern technology based on multitude of scientific advances all of which is driven by energy [3].

Globalization and rapid economic growth has resulted in exhaustive use of energy resources worldwide. In this race, resurging India with rapid economic growth and large human population is putting huge pressure on global energy supply and environmental sustainability. This can be explained by certain trends exhibited by post reformed India and its energy intensive economy.
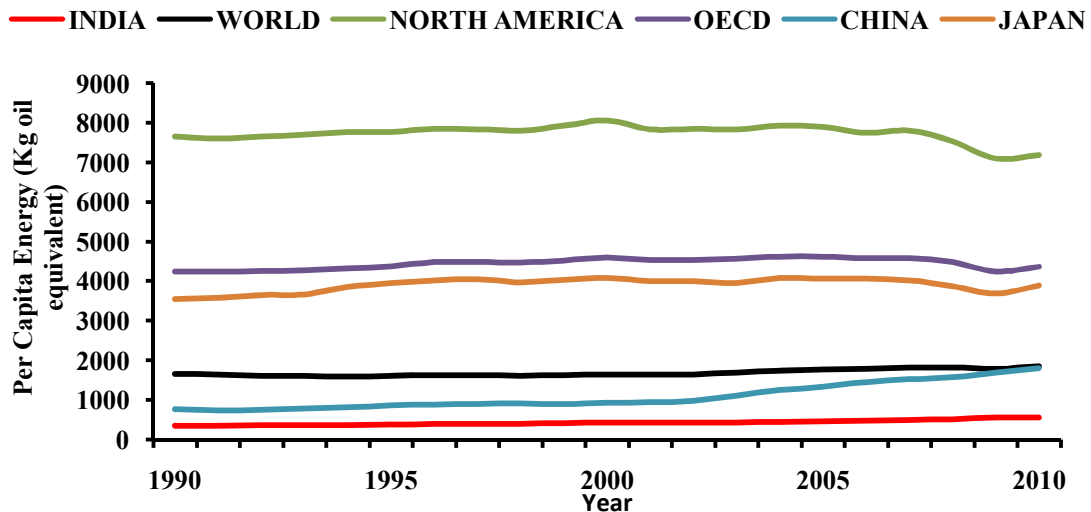
Fig.1.1: Per capita energy consumption in India, world and developed countries1990-2010[4].

Fig.1.1 describes the growth pattern in per capita energy consumption between the period 1990-2010of India, world and some developed countries. As per the above data, per

capita energy consumption in India was 565.63 kgoe in 2010 which has increased significantly from 362.49 kgoe in 1990 with an average annual growth rate of 2.8%. During the same period global average per capita energy consumption was found to increase from 1662.65kgoe in year 1990 to 1851.005kgoe in 2010 with an average annual growth rate of 1.13%. Meanwhile, China and Japan exhibited 6.75% and 0.48% growth respectively in per capita energy consumption whereas North America and OECD (Organization of Economic Cooperation and Development) reported all most same consumption pattern in the same time period [4]. Therefore, Indian per capita energy consumption with 2010 as the baseline is 3.72 times less than global average, but its rate of growth is 2.47 times higher than global growth rate making it one of the fastest growing energy markets in the world. On cumulative basis, Indian primary energy consumption pie in the global chart has increased from 3.69% in 1990 to 5.62% in 2010 making it the second fastest energy consuming country after only to China [4,5]. Hence, it is very much expected that the energy requirements of India are supposed to increase many folds to reach the global average level in the years to come. In the decade 2000-2010, the Indian GDP growth rate was a robust 6.8% per annum [6], which shows that increasing energy consumption is an indicator of healthy economic growth [7].

As highlighted above, India is growing at a faster rate and consuming more energy than it ever did in her long millennia old civilization. India needs an abundant and sustainable energy supply in the foreseeable future to maintain the economic growth momentum and progressive social transformation without jeopardizing environment. But unfortunately, it is not able to diversify its sources of energy whose sustainability as well as environmental effect are the factors of great concern. This can be explained by the heavy reliability of Indian energy sector on exhaustible energy resources such as fossil fuels.
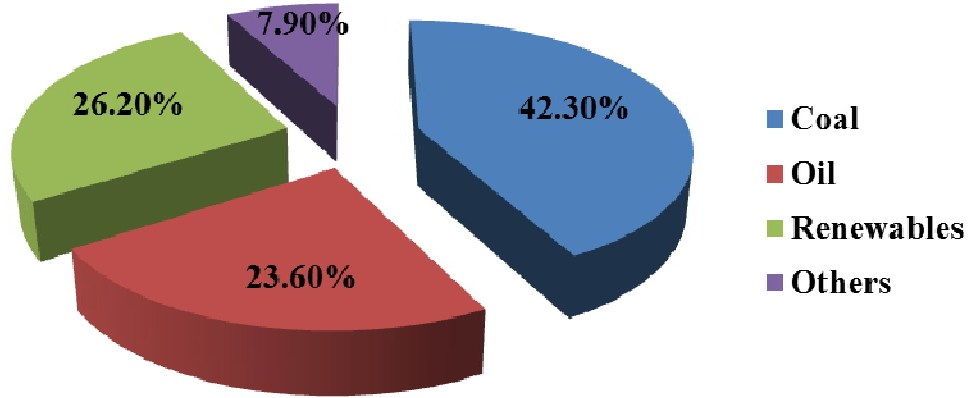
Fig.1.2: Sector wise contribution to primary energy consumption in India for the year 2009[8]

Fig.1.2 explains that out of the total primary energy requirement of India, 42.3% is met through coal, 23.6% through oil, 26.2% through renewable and rest through others [8].Contribution of non-renewable sources like coal and oil towards total primary energy requirement in India has alarmingly increased [8] since last ten years partly due to installation of a large number of Mega thermal power projects running on coal, natural gas or oil and an exponential increase in terms of numbers as well as variations of automobile fleet that was made available for a billion plus market. Although, coal is mostly indigenous, oil is not. Without any substantial increase in domestic crude oil production over the years and lack of diversification in energy sources compounded with rapid economic growth led to increased import of crude oil.
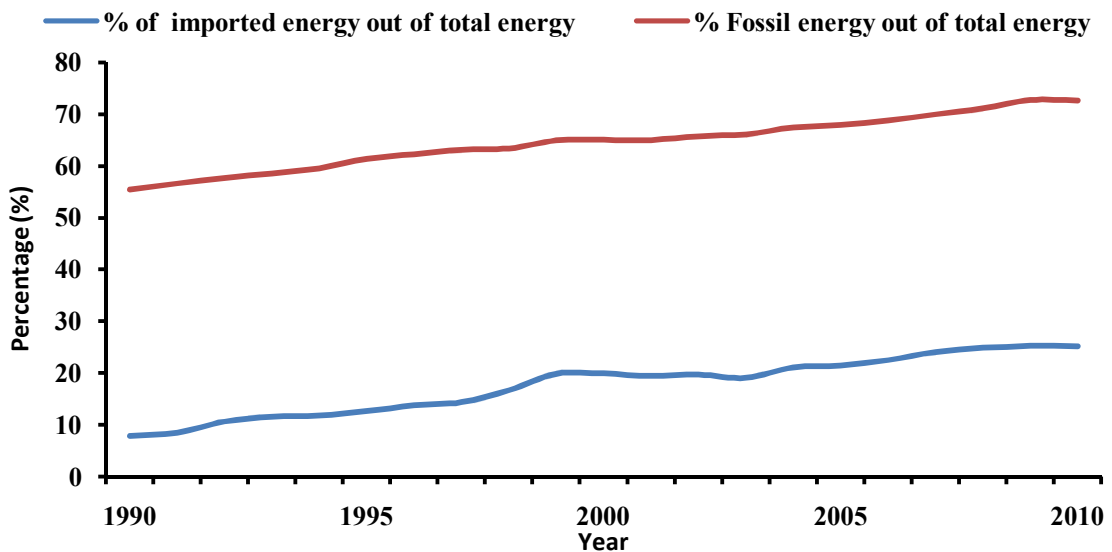
Fig.1.3: % Imported energy and % Fossil energy out of total energy in the period 1990-2010 [4]

Fig.1.3 indicates the World Bank data which states that the fossil fuel derived energy in the basket of total energy has increased from 55.37% in the year 1990 to 72.66% in the year 2010. Similarly, contribution of imported energy in the pie of total energy has increased from 7.86% in 1990 to 25.12% in 2010 clearly indicating the increasing dependence of India on imported energy sources.
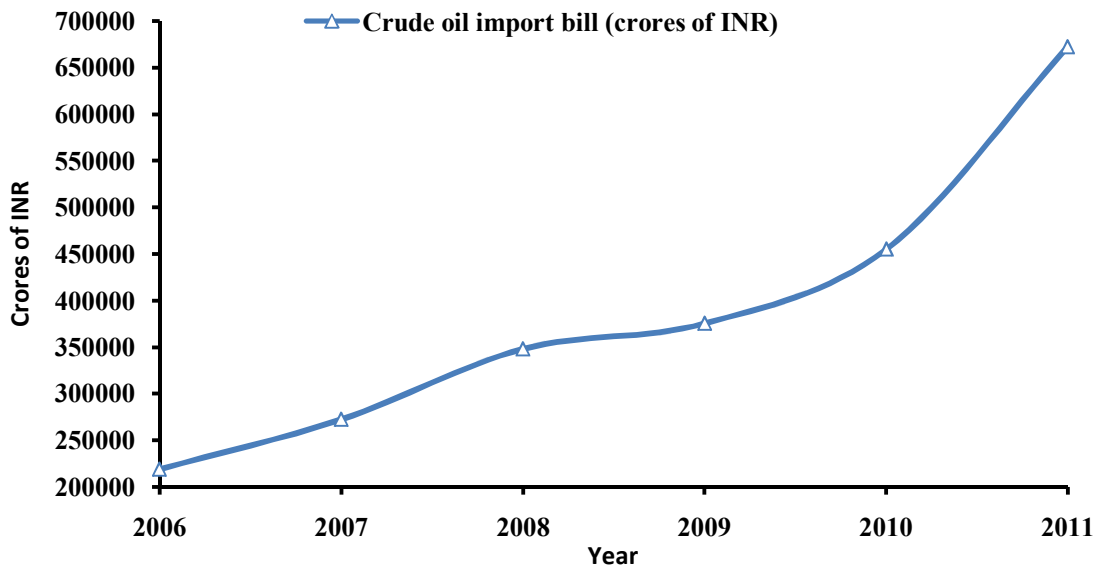
Fig.1.4: Crude oil import bill in Crores of Indian rupees (INR) during the period 2006 to 2010[9]

Fig.1.4 indicates an exponentially increasing trend of crude oil import bill from 2006 to 2011. India does not have large reserves of crude oil and imported 171.72 million tons (which is nearly 76% of its total oil requirement) of crude oil worth 6722.20 billion Indian rupees in 2011[9,10]. This heavy dependence of India on non-renewable resources results in faster resource depletion, environmental degradation and a huge economic burden for import of expensive fossil fuels resulting in widening trade deficit [11]. In the light of the above facts and discussions, the following conclusions can be made.

➢ India is an energy starving nation.
➢ Due to rapid economic growth of the last decade and projected high growth rate in the coming couple of decades at least, it will continue to consume more and more energy.
➢ Present energy sources are mostly non-renewable and increasingly import driven.
➢ Self-reliability in energy front and rapid exploration of renewable sources of energy is the pre-requisite for a sustainable, inclusive and vibrant India in the years to come.

1.2 ENERGY USAGE AND ENVIRONMENT

As discussed earlier, the impact of use of renewable resources of energy on environment is minimal. For example electrical power generation from solar energy does not hamper environment, but if the same electricity is generated from coal fired thermal power plants then it will lead to emission of poisonous gases like carbon monoxide (CO), sulphur oxides (SO_x) and nitrogen oxides (NO_x) along with fly ash slurry and several other water, soil and air pollutants resulting in environmental degradation.

It is evident from our previous discussions that our present energy consumption pattern both at national and global level is predominantly dependent on non-renewable resources in general and fossil fuels (coal, oil, natural gas etc.) in specific. This reliability leads to environmental degradation. OECD (Organization for Economic Co-operation and Development) environmental directorate, Paris, France has developed a set of key environmental indicators in 2008. Table.1.1 indicates that most of the key environmental indicators determined by OECD environmental directorate are heavily affected by the present energy consumption pattern worldwide and specifically in India.

Table.1.1: Effect of present energy consumption pattern on key environmental indicators [12]

Sl No.	Key Indicator	Factors responsible	*Present energy consumption effect
1	Climate Change	CO_2 and GHG emission intensities.	High
2	Ozone Layer	Ozone depleting substances.	Medium
3	Air Quality	SO_x and NO_x emission intensities.	High
4	Waste Generation	Municipal waste generation intensities.	High
5	Freshwater Quality	Waste water treatment connection rates.	Medium
6	Freshwater Resources	Intensity of use of water resources.	Medium
7	Forest Resources	Intensity of use of forest resources.	Medium
8	Fish Resources	Intensity of use of fish resources.	Low
9	Energy Resources	Intensity of energy use.	High
10	Biodiversity	Threatened species.	Low

* It may be noted that the present energy consumption pattern worldwide has strenuous impact on most of the key environmental indicators.

Therefore it can be concluded that in order to save the environment, either of the following must be done.

➢ Reduction in energy consumption.
➢ A shift in the present sources of energy from more polluting to less polluting and from non-renewable to renewable sources.

As bulk of the world population today are devoid of basic amenities of life, hence for inclusive, sustainable growth and progressive social transformation the latter option must be implemented.

1.3 DIESEL ENGINES AND NEED OF ALTERNATIVE FUEL

Projections for the 30-year period from 1990 to 2020 indicate that vehicle travel, and consequently fossil-fuel demand, will almost triple and the resulting emissions will pose a serious problem. The main reason for increased pollution levels, in spite of the stringent emission standards that have been enforced, is the increased demand for energy in all sectors and most significantly the increased use of internal combustion engines for mobility and power [13,14].As elaborated in the previous sections, a major chunk of imported crude oil derivatives are used as fuel in internal combustion engines. The most popular petroleum fuels are gasoline and diesel used as motor fuels in spark ignition and compression ignition engines respectively. Amongst them, diesel engines have proven their utility in the transportation and power sectors due to their higher efficiency and ruggedness and hence play a pivotal role in rural as well as urban Indian economy [15]. With respect to usage diesel engines are largely favored across a wide spectrum of activities like automotive application, small and decentralized power generation, prime mover for farm and agricultural machineries, small scale industrial prime mover and so on. Therefore, in Indian context, diesel consumption is always disproportionately higher than gasoline. Fig.1.5 shows the consumption of motor gasoline and high speed diesel oil during the period 2005 to 2012. It may be observed that diesel to gasoline consumption ratio was 4.80 in 2005 which was dropped to 4.31 in 2012. This indicated that the consumption of gasoline is increasing at a faster rate than the consumption of diesel, still diesel consumption in India is nearly four and half times higher than gasoline.
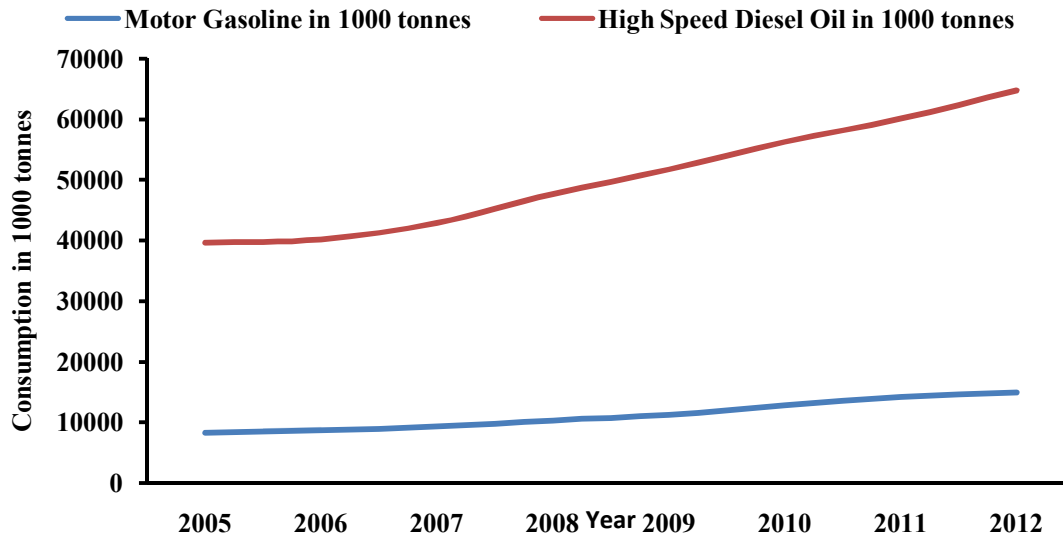
Fig.1.5: Consumption of gasoline and diesel during the period 2005 to 2012[9]

Therefore, even a partial substitution of mineral diesel by any renewable and carbon neutral alternative fuel can have significant positive effect on economy and environment in terms of reduction in carbon footprints and dependence on imported crude oil. In the light of the apprehensions about long-term availability of petroleum diesel, stringent environmental norms and environmental impacts due to extensive use in fast growing Indian economy have mandated the search for a renewable alternative of diesel fuel [16].

1.4 VEGETABLE OIL: AS ALTERNATIVE FUEL FOR DIESEL ENGINES

Vegetable oils are the plant origin biofuels generally obtained from resins and plant seeds. Because of being a part of carbon cycle, the vegetable oils are carbon neutral. Moreover, these oils are extensively found all over the country with special penetration in rural areas. Certain characteristics like renewable background, higher lubricity, high cetane rating, low sulfur content, non-toxic nature, bio-degradability, superior anti-corrosion properties etc. make these fuels a promising alternative one for diesel engine application [17,18,19,20]. However, there are certain constraints regarding usage of vegetable oils in diesel engines as well. The major problem with vegetable oils has been their higher viscosity than diesel. The higher viscosity is attributed towards the high molar masses of oils and the presence of unsaturated fatty acids. At high engine temperatures the polymerization of unsaturated fatty acids followed by cross-linking leads to formation of very large agglomerations and consequent gumming. When direct injection engines are allowed to run

with vegetable oils, injectors become choked after a few hours The higher viscosities cause poor fuel atomization which leads to incomplete fuel combustion and carbon deposition on the injector and valve seat, resulting in serious engine fouling.. Due to incomplete combustion, partially burnt vegetable oil runs down the cylinder walls and dilutes the lubricating oil and thickens the lubricating oil [17]. Therefore, vegetable oils are not recommended for direct diesel engine application. However, there are several methods like dilution, pyrolysis, transesterification and engine hardware modification in which vegetable oil can be used in diesel engines. Amongst these methods, transesterification has been established as the best method to use vegetable oils in diesel engines. Transesterification is a chemical process in which the triglycerides of the vegetable oil are converted in to mono-alkyl esters and glycerol in presence of a catalyst. The vegetable oil alkyl esters are popularly known as biodiesel and have properties very similar to mineral diesel. Transesterification process in details is discussed in the subsequent sections.

1.5 BIOFUEL POLICY: GOVERNMENT OF INDIA

In the light of the need regarding diversification in energy supply as discussed earlier, Indian Government has taken a lot of initiative in the front of wind and solar energy harnessing projects. However, the formal National Policy on Biofuels to explore the non-edible vegetable oils and other bio-origin oils as alternative fuels was approved by Government of India in December 2009. It encouraged the use of alternative fuels to supplement transport fuels (petrol and diesel for vehicles) and proposed a target of 20 percent biofuel blending (both bio-diesel and bio-ethanol) by 2017. In this context, the government launched the National Bio-diesel Mission (NBM) identifying *Jatropha curcas* (Fig.1.6) as the most suitable tree-borne oilseed for bio-diesel production. The Planning Commission of India had set an ambitious target of covering 11.2 to 13.4 million hectares of land under Jatropha cultivation by the end of the 11th Five-Year Plan [20]. The central government and several state governments are providing fiscal incentives for supporting plantations of Jatropha and other non-edible oilseeds. Several public institutions, state biofuel boards, state agricultural universities and cooperative sectors are also supporting the biofuel mission in different capacities [21].However; Government of India had two major constraints in its biofuel policy. Firstly, only non-edible vegetable oils were allowed to be used as fuel crops

as India is not self-sufficient in edible oil production, rather it imported 40% of its totally edible oil requirements in 2012 [22]. Secondly, only those non-edible oil species which can grow in waste and barren lands with drought conditions are preferred as diversion of arable lands for energy crop production may impinge food production.

Fig.1.6: Jatropha curcas (This figure is provided as additional information)

On the lines of the above constraints, government's ambitious plan of producing sufficient biodiesel to meet its mandate of 20 percent diesel blending by 2012 was not realized. Excessive dependence on Jatropha curcas to produce biodiesel, lack of sufficient feedstocks, absence of exploration of other suitable oilseeds for biodiesel production and lack of comprehensive research and development activities have been some of the major stumbling blocks cited officially by Government agencies for the above mentioned failure [23,24,25].

As cited in the previous paragraph, lack of sufficient feedstocks and excessive dependence on Jatropha curcas were some of the reasons for the initial set back of NBM. Therefore, exploration of other potential non-edible oil feedstocks for biodiesel production and an integrated research and development approach to address the multifaceted dimensions of biodiesel production and usage may supplement Government's biofuel policy and also increase the feedstock availability substantially. In this context, the present research work deals with one such less popular non-edible vegetable oil feedstock known as "Calophyllum Inophyllum" to evaluate its potential as an alternative diesel engine fuel.

1.6 "CALOPHYLLUM INOPHYLLUM": AN ALTERNATIVE DIESELFUEL

Calophyllum is a perennial angiosperm. Its full botanical name is "*Calophyllum Inophyllum*"[26]. It is also known as hone oil. In Indian east coast, it is locally referred as "Polanga" or "Kamani" (Fig.1.7). It is a non-edible oil seed belonging to the *Clusiaceae* family.

Fig.1.7: (a)-Green Calophyllum seeds with stem and leaves, (b)-Ripe fruit (left), cracked shell showing seed kernel inside(middle), and dry seed (right), (c)-Dry seeds, (d) Calophyllum flowers

It is a large and medium sized, evergreen sub-maritime tree which grows best in deep soil or on exposed sea sands. The rainfall requirement is 750–5000mm/yr. This plant has multiple origins including East Africa, India, South-East Asia and Australia [27,28,29,30]. The tree supports a dense canopy of glossy, green and lustrous elliptical leaves and branched stem. The growth rate of the tree is 1m (3.3ft) in height per year on good sites. Its leaves are heavy and glossy,10–20 cm (4–8in.) long and 6–9cm (2.4–3.6in.) wide, light green when young and dark green when older. Fruits are spherical drupes and arranged in clusters. The fruit is at first pinkish-green later turning bright green and when ripe, it turns dark gray-brown and wrinkled. The tree yields 100–200 fruits/kg. In each fruit, one large brown seed2–4cm (0.8–1.6in.) in diameter is found. The single, large seed is surrounded by a shell (endocarp) and a thin, 3–5 mm layer of pulp. Oil yield per unit land area has been reported at 2000kg/ha. The oil is tinted green, thick, and woodsy or nutty smelling [29,30]. The seed oil has very high oil content (65–75%) [30,31,32]. The exact production details of Calophyllum were not available. However, looking at its omnipresence throughout the Indian cost line, it

seems that its natural production potential is no less than Jatropha curcas. High oil content, extensive availability, non-edible nature, low water requirement, growth on non-arable lands etc. makes this oil seed highly suitable for fuel applications in diesel engines.

In the light of the above exhaustive discussion, it may be concluded that Indian economy and energy consumption pattern is growing rapidly over the years. To maintain this growth momentum, long term energy security by diversification of energy supply and environmental sustainability are the major ingredients. Development and usage of carbon neutral and renewable alternative fuels to substitute mineral diesel is one of the critical need of the hour. Recognizing the same, the Indian Government lunched national policy on biofuels in 2009. Subsequently, national biodiesel mission was launched by recognizing Jatropha curcas as the most suitable oil seed for fuel applications. However, the target of 20% substitution by 2012 was not realized due to mostly lack of feedstock availability. In this context, the present study tries to explore another potential non-edible vegetable oil feedstock for fuel application which can supplement Government's biofuel policy and increase feedstock availability substantially. The vegetable oil species known as "Calophyllum Inophyllum" has extensive presence throughout the Indian cost line and an integrated research and development approach to evaluate the potential of this oil seed to be a true alternative of mineral diesel is to be assessed.

2.1 INTRODUCTION

As discussed in the earlier section, an integrated research and development approach has to be implemented to assess the potential of "Calophyllum Inophyllum" as alternative diesel fuel. Therefore, the existing quantum of research work in the domains like optimization of biodiesel production from vegetable oil sources, physico-chemical and fuel property characterisation, application in engines to evaluate performance, emission and combustion, numerical studies using computational fluid dynamics and model validation etc. need to be studied as review of literature. In this context, a comprehensive literature review of various national and International journals was carried out. Some of the important outcomes are summarized below.

2.2 REVIEW OF AVAILABLE LITERATURE

2.2.1 Biodiesel Production from Vegetable oils, Characterisation and Optimization

Atadashi et.al. [33] explored the production of fatty acid methyl esters or biodiesel from high free fatty acid containing feedstocks like some non-edible vegetable oils, animal fats etc. to bring their properties close to mineral diesel. The results concluded that the properties of the biodiesel produced closely matched the corresponding ASTM standards and cost of production was reported to be 25% less compared to refined low FFA feedstocks.

Chen et. al. [34] studied the feasibility of biodiesel production from "Tung" (Vernicia montana) oil with respect to the transesterification yield and biodiesel properties. The findings indicated high cold filter plugging point of 11^OC, 94.9 wt.% of ester content and oxidation stability of 0.3 hours at 110^OC for the biodiesel sample produced. Moreover, the tung oil biodiesel exhibited high density of 903 kg/m^{3}at 15 ^{O}C, kinematic viscosity of 7.84 mm^2/s at 40 ^{O}C, and iodine value of 161.1 g I$_2$/100 g. The properties of the tung oil biodiesel were found to be improved by blending with canola and palm oil biodiesels to satisfy the biodiesel specifications.

Usta et. al. [35] evaluated tobacco seed oil as a feedstock for biodiesel production. Various physicochemical and fuel properties of the tobacco biodiesel were examined and

compared with European Biodiesel Standard EN14214. The results showed oxidation stability and iodine number of the biodiesel were not within the standards limit. Oxidation stability was improved by six different anti-oxidants, out of which "pyrogallol" was found to be the most effective. Poor iodine number was improved by blending it with biodiesel containing more unsaturated fatty acids. The resultant reduction in cold flow plugging point was addressed by adding "octadecene-1-maleic anhydride copolymer" as cold flow property improver.

Teixeira da Silva de La Salles et.al. [36] studied the production and physico-chemical characterisation of biodiesel from the fruits of the Syagrus coronate (Mart.) Becc., popularly known in Brazil as "licuri" or "ouricuri". The oil was transesterified using conventional catalysts and methanol, to obtain biodiesel. The properties of the biodiesel produced were comparable with standards.

Silitonga et. al. [37] investigated biodiesel characterization and production from Ceiba pentandra seed oil. The production was conducted by two step acid–base transesterification. The results found that properties of C. pentandra methyl ester fall within the recommended biodiesel standards (ASTM D6751and EN 14214). Beside, this study also suggested biodiesel–diesel blending to improve the properties such as viscosity, density, flash point, calorific value and oxidation stability.

Lin et. al. [38] carried out a three stage transesterification process to produce biodiesel from crude rice bran oil (RBO) The influence of variables on conversion efficiency to methyl ester, i.e., methanol/RBO molar ratio, catalyst amount, reaction temperature and reaction time, was studied. The content of methyl ester was analysed by chromatographic analysis. Through orthogonal analysis of parameters in a four-factor and three-level test, the optimum reaction conditions for the transesterification were obtained: methanol/ RBO molar ratio 6:1, usage amount of KOH 0.9% w/w, reaction temperature 60 ^{O}C and reaction time 60 minutes. Fuel properties of RBO biodiesel were studied and compared according to ASTM D6751-02 and DIN V51606 standards for biodiesel. Most fuel properties complied with the limits prescribed in the aforementioned standards.

Wang et. al. [39] investigated Siberian apricot (Prunus sibirica L.) seed kernel oil as a promising non-conventional feedstock for preparation of biodiesel. The oil has high oil content (50.18 ± 3.92%), low acid value (0.46 mg/g), low water content (0.17%) and high

percentage of oleic acid (65.23 ± 4.97%) and linoleic acid (28.92 ± 4.62%). The measured fuel properties of the Siberian apricot biodiesel, except cetane number and oxidative stability, were conformed to EN 14214-08, ASTM D6751-10 and GB/T 20828-07 standards, especially the cold flow properties were excellent (Cold filter plugging point -14°C).

Wang et. al. [40] studied feasibility of biodiesel production from Datura stramonium L. oil (DSO). The research work explored an optimum yield of 87% using a two-step catalysed reaction conditions. Furthermore, the fuel properties of DSO biodiesel were determined and evaluated. Compared with Jatropha curcas L. (JC) and beef tallow (BT) biodiesel, DSO biodiesel possessed the best kinematic viscosity (4.33 mm^2/s) and cold filter plug point (-5°C).

Benjumea et. al. [41] measured some basic properties of several palm oil biodiesel–diesel fuel blends according to the corresponding ASTM standards. In order to predict these properties, mixing rules were evaluated as a function of the volume fraction of biodiesel in the blend. Kay's mixing rule was used for predicting density, heating value, three different points of the distillation curve (T10, T50 and T90), cloud point and calculated cetane index, while an Arrhenius mixing rule was used for viscosity. The absolute average deviations (AAD) obtained was low, demonstrating the suitability of the used mixing rules. It was found that the calculated cetane index of palm oil biodiesel obtained using ASTM D4737 was in better agreement with the reported cetane number than the one corresponding to the ASTM D976.

Berman et.al. **[42]** investigated the specifications in ASTM D6751 and D7467 which are related to the fatty acid composition of pure castor methyl esters (B100) and its blend with petro-diesel in a 10% vol ratio (B10). Kinematic viscosity and distillation temperature of B100 (15.17 mm^2/s and 398.7 °C respectively) were the only two properties which did not meet the appropriate standard limits. In contrast, B10 met all the specifications. Still, ASTM D7467 required that the pure biodiesel meets the requirements of ASTM D6751. This can limit the use of a wide range of feedstocks, including castor, as alternative fuel, especially due to the fact that in practice vehicles normally use low level blends of biodiesel and petrodiesel.

Harrison et. al. [43] examined the effect of varying levels of eicosapentaenoic acid(EPA) and docosahexaenoic acid (DHA) on algal methyl ester fuel properties. Oxidative

stability, Cetane Number, density, viscosity, bulk modulus, cloud point and cold filter plugging point were measured for algal methyl esters produced from various microalgae feedstocks as well as model algal methyl ester compounds formulated to match the fatty acid composition of Nannochloropsis species, Nannochloropsis oculata and Isochrysis galbana subjected to varying levels of removal of EPA and DHA. The results suggest that removal of 50 to 80% of the long chain-polyunsaturated fatty acids (LC-PUFA) from Nannochloropsis-based methyl esters would be sufficient for meeting existing specifications for oxidative stability. However, higher levels of LC-PUFA removal from Nannochloropsis-based methyl esters would be required to produce fuels with acceptable Cetane Number. The removal of EPA and DHA was shown to have a detrimental effect on cold flow properties since the algal methyl esters are also high in fully saturated fatty acid content.

Chakraborty et. al. [44] carried out an investigation to evaluate the prospect of terminalia oil for biodiesel production with reference to some relevant properties. The fatty acid profile of oil extracted from terminalia was found comparable with similar seed oils attempted for biodiesel production in this region. Terminalia oil contained 32.8% palmitic acid, 31.3% oleic acid, and 28.8% linoleic acid. The calorific value and kinematic viscosity of terminalia oil were 37.50 MJ/kg and 25.60 cSt, respectively. The calorific value and cetane number of terminalia FAME were within the acceptable limit of the EN 14214 standard. However, the flashpoint of terminalia FAME (90 °C) was relatively lower than the minimum required standard. Overall, the properties of biodiesel obtained from terminalia seed conform to the existing biodiesel standard.

Chammoun et, al. [45] identified Oilseed radish (Raphanus sativus) as a potential cool season cover and energy crop for the southern United States. The fatty acid profile of this oil showed high levels of erucic acid (C22:1), which has been linked to health issues. The extracted oil was converted to fatty acid methyl esters (biodiesel) via transesterification. Fuel properties were analysed including fatty acid profile, free and total glycerol, acid number, sulphur content, water content and cold filter plugging point (CFPP). Fuel properties of the biodiesel were found to meet or exceed ASTM standards for use in on-road vehicles.

Chu et.al. [46] produced biodiesel from A. pedunculata conformed to EN14214, ASTM D6751, and GB/T20828 standards, except for those cetane number and oxidative stability. Cold flow and transportation safety properties were excellent (cold filter plugging

point 11°C, flashpoint 169°C). Additives and antioxidants would be required to meet cetane number and oxidative stability specifications. The addition of 500 ppm tert-butylhydroquinone resulted in a higher induction period (6.7 h), bringing oxidative stability into compliance with all three biodiesel standards.

Kaya et.al. [47] extracted the peanut (Arachis hypogea L.) seed oil from the seeds of the peanut that grown in SEA natolia of Turkey. Oil was obtained in 50 wt/wt.%, by solvent extraction. Peanut (A. hypogea L.) seed oil was investigated as an alternative feedstock for the production of a biodiesel fuel. Biodiesel was prepared from peanut by transesterification of the crude oil with methanol in the presence of NaOH as catalyst. Maximum oil to ester conversion was 89%. The viscosity of biodiesel oil was nearer to that of petroleum diesel and the calorific value was about 6% less than that of diesel. Peanut seed oil has about 8.3% less heating value than that of diesel oil due to the oxygen content in their molecules. The important properties of peanut oil and its methyl ester (biodiesel) such as density, kinematic viscosity, flash point, iodine number, neutralization number, pour point, cloud point, cetane number are found out and compared to those of no. 2 petroleum diesel, ASTM and EN biodiesel standards. The comparison showed that the methyl ester has relatively closer fuel properties to diesel than that of raw peanut seed oil.

Atapour et.al. [48] used frying oil as a low cost feedstock for biodiesel production by alkali-catalysed transesterification. The design of experiments was performed using a double 5-level-4-factor central composite design coupled with response surface methodology in order to study the effect of factors on the yield of biodiesel and optimizing the reaction conditions. The factors studied were: reaction temperature, molar ratio of methanol to oil, catalyst concentration, reaction time and catalyst type (NaOH and KOH). A quadratic model was suggested for the prediction of the ester yield. The p value for the model fell below 0.01 (F-value of 27.55). Also, the R^2 value of the model was 0.8831 which indicated the acceptable accuracy of the model. The optimum conditions were obtained as follows: reaction temperature of 65 ∘C, methanol to oil molar ratio of 9, NaOH concentration of 0.72% w/w, reaction time of 45 min and NaOH as the more effective catalyst. In these conditions the predicted and observed ester yields were 93.56% and 92.05%, respectively, which experimentally verified the accuracy of the model. The fuel properties of the biodiesel produced under optimum conditions, including density, kinetic viscosity, flash point, cloud

and pour points were measured according to ASTM standard methods and found to be within specifications of EN 14214 and ASTM 6751 biodiesel standards.

Ilham et. al. [49] demonstrated that, supercritical dimethyl carbonate method successfully converted triglycerides as well as fatty acids to fatty acid methyl esters (FAME) with glycerol carbonate, a higher value by-product compared to the conventional glycerol. The FAME was high in yield, comparable with supercritical methanol method, and satisfies the international standard for use as biodiesel fuel. In this study, therefore, optimization of supercritical dimethyl carbonate method was discussed to include all important key parameters such as reaction temperature, pressure, time, molar ratio of dimethyl carbonate to oil, the FAME yield, thermal decomposition, degree of denaturation, tocopherol content, oxidation stability and fuel properties. The optimum condition for supercritical dimethyl carbonate method was determined at 300°C/20 MPa/20 min/42:1 molar ratio of dimethyl carbonate to oil to have satisfactory yield of FAME at 97.4 wt%. Conclusively, this study showed the importance to address all those key parameters in order to produce high quality biodiesel from supercritical dimethyl carbonate method.

Kafuku et. al. [50] produced biodiesel using Croton megalocarpus oil as a non-edible feedstock. C. megalocarpus oil was obtained from north Tanzania. This study was aimed at optimizing the biodiesel production process parameters experimentally. The parameters involved in the optimization process were the amount of the catalyst, alcohol, temperature, agitation speed and reaction time. The optimum biodiesel conversion efficiency obtained was 88% at the optimal conditions of 1.0 wt.% amount of potassium hydroxide catalyst, 30 wt.% amount of methanol, 60°C reaction temperature, 400 rpm agitation rate and 60 min reaction time. The properties of croton biodiesel which were determined fell within the recommended biodiesel standards. Croton oil was found with a free fatty acid content of 1.68% which was below the 2% recommended for the application of the one step alkaline transesterification method. The most remarkable feature of croton biodiesel was its cold flow properties. This biodiesel yielded a cloud and pour point of -4°C and -9°C, respectively, while its kinematic viscosity lay within the recommended standard value.

Kilic et. al. [51] in this study investigated the optimization of biodiesel production from castor oil using full factorial design. The biodiesel production was carried out in a batch laboratory scale reactor by alkaline-catalysed transesterification process. Experimental

design was used in the evaluation of process variables. Effects of temperature, methanol/oil molar ratio and catalyst concentration were optimized according to the 23 full factorial central composite designs (CCD). For determining the influence of purification methods on biodiesel yield, different purification methods were applied to the product after transesterification reaction. Second order model was obtained to predict biodiesel yield as a function of these variables. According to the experimental results this process gave an average yield of biodiesel more than 90%.

Lee et. al. [52] employed CaO–MgO mixed oxide catalyst in transesterification of non-edible Jatropha curcas plant oil in biodiesel production. Response surface methodology (RSM) in conjunction with the central composite design (CCD) was employed to statistically evaluate and optimize the biodiesel production process. It was found that the production of biodiesel achieved an optimum level of93.55% biodiesel yield at the following reaction conditions: 1) Methanol/oil molar ratio: 38.67, 2) Reaction time: 3.44 h, 3) Catalyst amount: 3.70 wt.%, and 4) Reaction temperature: 115.87 °C. In economic point of view, transesterification of J. curcas plant oil using CaO–MgO mixed oxide catalyst required less energy which contributed to high production cost in biodiesel production.

Omar et. al. [53] investigated heterogeneous transesterification of waste cooking palm oil (WCPO) to biodiesel over Sr/ZrO_2 catalyst and the process optimization. Response surface methodology (RSM) was employed to study the relationships of methanol to oil molar ratio, catalyst loading, reaction time, and reaction temperature on methyl ester yield and free fatty acid conversion. The experiments were designed using central composite by applying24 full factorial designs with two centre points. Transesterification of WCPO produced79.7% maximum methyl ester yield at the optimum methanol to oil molar ratio ¼ 29:1, catalyst loading ¼ 2.7 wt.%, reaction time ¼ 87 min and reaction temperature ¼ 115.5°C.

Wu et. al. [54] carried out an optimization study on the production of biodiesel from camelina seed oil using alkaline transesterification. The optimization was based on sixteen well-planned orthogonal experiments (OA16 matrix). Four main process conditions in the transesterification reaction for obtaining the maximum biodiesel production yield (i.e. methanol quantity, reaction time, reaction temperature and catalyst concentration) were investigated. It was found that the order of significant factors for biodiesel production was

catalyst concentration > reaction time > reaction temperature > methanol to oil ratio. Based on the results of the range analysis and analysis of variance (ANOVA), the maximum biodiesel yield was found at a molar ratio of methanol to oil of 8:1, a reaction time of 70 min, a reaction temperature of 50°C, and a catalyst concentration of 1 wt.%. The product and FAME yields of biodiesel under optimal conditions reached 95.8% and 98.4%, respectively. The properties of the optimized biodiesel, including density, kinematic viscosity, acid value, etc., were determined and compared with those produced from other oil feedstocks. The optimized biodiesel from camelina oil met the relevant ASTMD6571 and EN 14214 biodiesel standards and could be used as a standard fuel in diesel engines.

Yucel[55] immobilized microbial lipase from T. lanuginosus onto polyglutaraldehyde-activated olive pomace powder. The support was used to produce biodiesel with pomace oil and methanol. Response Surface Methodology(RSM) in combination with Central Composite Design (CCD) was used to optimize the biodiesel production parameters. Reaction temperature, molar ratio of methanol to oil, biocatalyst content and reaction time were chosen as the variables and the response selected was the yield of pomace oil methyl ester in present work. A quadratic polynomial equation was obtained for pomace oil methyl ester yield by multiple regression analysis. The optimal conditions for the transesterification have been found to be: reaction temperature of 40 °C, alcohol/oil molar ratio of 5.3:1, biocatalyst content of 5.8% w/w and reaction time of24 h. The predicted pomace oil methyl ester yield was 92.87% under the optimal conditions. Verification experiment (91.81%) confirmed the validity of the predicted model. Biodiesel yield reached 93.73% by adding water (1% w/w) in reaction medium under the optimal conditions. Immobilized lipase was used to determine operational stability and it indicated that immobilized lipase was stable retaining more than 80% residual activity after being used repeatedly for 10 consecutive batches of pomace oil transesterification.

Yun et. al. [56] simulated a continuous enzyme-catalysed biodiesel pilot plant using waste cooking oil, with production capacity of 6482 ton/yr, by Aspen Plus. Detailed operating conditions and equipment designs were obtained. Five reactions were applied to represent the transesterification of the biodiesel production. The simulation results were in good agreement with the real data. Based on the simulation of the original process, five optimization processes, were proposed focusing on energy saving and methanol recovery.

Pinch technology was also used to develop heat exchange networks. Throughout the different optimizations, the quality of biodiesel was still kept at a high purity (>98.5%).

Uzun et. al. [57] carried out alkali-catalysed transesterification of waste frying oils (WFO) in various conditions to investigate the effects of catalyst concentration, reaction time, methanol/oil molar ratio, reaction temperature, catalyst type (hydroxides, methoxides and ethoxides), and purification type (such as washing with hot water, purification with silica gel and dowex) on the biodiesel yields. The optimum conditions were 0.5% wt. of NaOH, 30 min reaction time, 50°C reaction temperature, 7.5 methanol to oil ratio and purification with hot distilled water. 96% biodiesel yield with ~97% ester content was obtained within in these conditions, and the activation energy was found to be as 11741 J mol^{-1}. The determined specifications of obtained biodiesel according to ASTM D 6751 and EN 14214 standards were in accordance with the required limits.

As an outcome of exhaustive review of available literatures in the field of biodiesel production from vegetable oils, physico-chemical characterisation and process optimization the following major findings are obtained.

1. With some exceptions, most of the non-edible oils have high free fatty acid contents leading to a two stage transesterification process to produce biodiesel.
2. The energy consumption in two stage transesterification is higher. Therefore, optimization of process parameters is must in high FFA non-edible oil seeds for commercial scale production.
3. Response surface methodology using central composite design method was followed by many researchers as an effective process optimization technique in biodiesel production from a wide range of feedstocks.
4. However, most of the process optimization was confined to the final stage only with % yield as the response and not both the stages of transesterification.
5. In many reported cases the final biodiesel sample produced did not comply with the designated standards of ASTM/EN/ISO etc. resulting in further addition of additives and post-processing.

In the light of the above review, it may be stated that production of biodiesel from Calophyllum vegetable oil with optimized process parameters and the subsequent compliance

with the corresponding international standards may prove the suitability of this vegetable oil as a true alternative to mineral diesel.

2.2.2 Diesel Engine Trials and analysis of Results using Biodiesel as a fuel

Shivalakshmi et.al. **[58]** carried out an experimental investigation to evaluate the effect of using diethyl ether as additive to biodiesel on the combustion, performance and emission characteristics in an unmodified diesel engine at different loads and constant engine speed. The results indicated that peak cylinder pressure and heat release rate was higher for BD5 (5% (by vol.) diethyl ether blended biodiesel) than those of neat biodiesel. The carbon monoxide emissions especially at full load and smoke emissions at almost all engine loads decreased while oxides of nitrogen and hydrocarbon emissions increased for BD5 than those of neat biodiesel at almost all engine loads. The brake thermal efficiency of BD5 was higher as compared to biodiesel.

Shehata et. Al. [59] carried out experimental studies to evaluate the effect of biodiesel fuel on performance, emission and combustion characteristics of diesel engine with or without exhaust gas recirculation (EGR). Biodiesel fuels were prepared from cotton seed oil, palm oil and flax oil. Biodiesel fuels gave slightly less brake power (BP), brake thermal efficiency and slightly high brake specific fuel consumption (BSFC) and high fuel mass flow rate per cycle. Diesel fuel produced CO higher than biodiesel fuels due to less oxygen atoms in fuel molecules. Biodiesel fuels produced NO_X higher than diesel fuel due to high oxygen content in biodiesel fuels molecules and high cetane number. As EGR was increased, CO emission increased while NO_X decreased due to decrease in flame temperature and O_2 in fresh air charge. For biodiesel fuels, exhaust gas and oil temperature were higher than diesel fuel. However, wall temperature for diesel was higher than the biodiesel fuels. Biodiesel fuels gave peak cylinder pressure higher than diesel fuel. The position of peak cylinder pressure as arrangement as 11 crank angle degree (CAD) after top dead centre (ATDC) for flax, 12 CAD ATDC for cotton, 14 CAD ATDC for palm and 20 CAD ATDC for diesel fuel respectively.

Nabi et. al. [60] produced karanja methyl ester (KME), which was termed as BD by well-known transesterification process. The properties of B100 (B100) and its blends were determined mainly according to ASTM standard and some of them were as per EN14214

standard. The Fourier transform infrared (FTIR) analysis showed that the DF fuel contained mainly alkanes and alkens, while the B100 contained mainly esters. The gas chromatography (GC) of B100 revealed that a maximum of 97% methyl ester was produced from karanja oil. Engine experiment result showed that all BD blends reduced engine emissions including carbon monoxide (CO), smoke and engine noise, but increased oxides of nitrogen (NOx). Compared to DF, B100 reduced CO, and smoke emissions by 50 and 43%, while a 15% increase in NOx emission was observed with the B100. Compared to DF, engine noise with B100 was reduced by 2.5 dB.

Ganapathy et. al. [61] conducted experiments using full factorial design consisting of (33) with 27 runs for each fuel, diesel and Jatropha biodiesel. The effect of variation of above three parameters on brake specific fuel consumption(BSFC), brake thermal efficiency (BTE), peak cylinder pressure (P_{max}), maximum heat release rate (HRR_{max}), CO, HC, NO emissions and smoke density were investigated. It has been observed that advance in injection timing from factory settings caused reduction in BSFC, CO, HC and smoke levels and increase in BTE, P_{max}, HRR_{max} and NO emission with Jatropha biodiesel operation. However, retarded injection timing caused effects in the other way. At 15 N m load torque, 1800 rpm engine speed and 340crank angle degree (CAD) injection timing, the percentage reduction in BSFC, CO, HC and smoke levels were 5.1%, 2.5%, 1.2% and 1.5% respectively. Similarly the percentage increase in BTE, P_{max}, HRR_{max} and NO emission at this injection timing, load and speed were 5.3%, 1.8%, 26% and 20% respectively. The best injection timing for Jatropha biodiesel operation with minimum BSFC, CO, HC and smoke and with maximum BTE, P_{max} and HRR_{max} was found to be 340 CAD. Nevertheless, minimum NO emission yielded an optimum injection timing of 350 CAD.

Lapureta et. al. [62] collected and analysed the body of work written mainly in scientific journals about diesel engine emissions when using biodiesel fuels as opposed to conventional diesel fuels. Since the basis for comparison was to maintain engine performance, the first section was dedicated to the effect of biodiesel fuel on engine power, fuel consumption and thermal efficiency. The highest consensus was found to lie in an increase in fuel consumption in approximate proportion to the loss of heating value. In the subsequent sections, the engine emissions from biodiesel and diesel fuels were compared, paying special attention to the most concerning emissions: nitric oxides and particulate

matter, the latter not only in mass and composition but also in size distributions. In this case the highest consensus was found in the sharp reduction in particulate emissions.

Murlidharan et. al. [63] carried out experiments to estimate the performance, emission and combustion characteristics of a single cylinder; four stroke variable compression ratio multi fuel engine fuelled with waste cooking oil methyl ester and its blends with standard diesel. Tests has been conducted using the fuel blends of 20%, 40%, 60% and 80% biodiesel with standard diesel, with an engine speed of 1500 rpm, fixed compression ratio 21 and at different loading conditions. The performance parameters elucidated included brake thermal efficiency, specific fuel consumption, brake power, indicated mean effective pressure, mechanical efficiency and exhaust gas temperature. The exhaust gas emission was found to contain carbon monoxide, hydrocarbon, nitrogen oxides and carbon dioxide. The results of the experiment was compared and analysed with standard diesel and it confirmed considerable improvement in the performance parameters as well as exhaust emissions. The blends when used as fuel results in the reduction of carbon monoxide, hydrocarbon, carbon dioxide at the expense of nitrogen oxides emissions. It has found that the combustion characteristics of waste cooking oil methyl ester and its diesel blends closely followed those of standard diesel.

Mufijur et. al. [64] studied the feasibility of Jatropha as a potential biodiesel feedstock for Malaysia. Physico-chemical properties of Jatropha biodiesel and its blends with diesel followed by engine performance and emissions characteristics of B10, B20 and B0 were studied. The results showed that viscosities of B10 and B20 were closer to diesel. Moreover, only the oxidation stability of B10 and B20 met the European specifications (EN 590) of 20 h. Therefore, only B10 and B20 have been used to evaluate engine performance and emission. Compared to B0, the average reduction in brake power (BP) is 4.67% for B10 and 8.86% for B20. It was observed that brake specific fuel consumption (BSFC) increases as the percentage of biodiesel increase. Compared to B0, a reduction in hydrocarbon (HC) emission of 3.84% and 10.25% and carbon monoxide (CO) emission of 16% and 25% was reported using B10 and B20. However, the blends give higher nitrogen oxides (NOx) emission of 3% and 6% using B10 and B20. As a conclusion, B10 and B20 can be used in a diesel engine without any modifications.

Chen et. al. [65] blended Jatropha oil methyl esters (JMEs) produced from jatropha (Jatropha curcas) oil with diesel at various volumetric percentages to evaluate the variations in the fuel properties. Correlations between fuel properties, including the calorific heat, cold filter plugging point, density, kinematic viscosity, and oxidation stability of the JMEs–diesel blends, and the blending ratio of the JMEs was established. As a result, a blending ratio of the JMEs with diesel was recommended up to 40 vol. % in comparison with the relevant specifications for biodiesel–diesel blends. The combustion tests of the JMEs–diesel blends were performed in a diesel generator. Higher brake thermal efficiency and lower brake specific fuel consumption were clearly observed with higher output loading. The concentration of carbon dioxide and nitrogen monoxide in the exhaust gas increased with higher output loading while the concentration of oxygen and carbon monoxide decreased. The concentration of nitrogen oxide decreased with the addition of pyrogallol. Multiple linear correlations for combustion performance and pollutant emissions was established that were associated with system parameters, including output loading, the blending ratio, and the pyrogallol addition.

Canaci etl al. [66] predicted the engine performance and exhaust emissions for five different neural networks to define how the inputs affected the outputs using the biodiesel blends produced from waste frying palm oil. PBDF, B100, and biodiesel blends with PBDF, which are 50% (B50), 20% (B20) and 5% (B5), were used to measure the engine performance and exhaust emissions for different engine speeds at full load conditions. Using the artificial neural network (ANN) model, the performance and exhaust emissions of a diesel engine have been predicted for biodiesel blends. According to the results, the fifth network was sufficient for all the outputs. In the fifth network, fuel properties, engine speed, and environmental conditions were taken as the input parameters, while the values of flow rates, maximum injection pressure, emissions, engine load, maximum cylinder gas pressure, and thermal efficiency were used as the output parameters. For all the networks, the learning algorithm called back-propagation was applied for a single hidden layer. Scaled conjugate gradient (SCG) and Levenberg–Marquardt (LM) was used for the variants of the algorithm, and the formulations for outputs obtained from the weights were given in this study. The fifth network produced R^2 values of 0.99, and the mean % errors are smaller than five except for some emissions. Higher mean errors are obtained for the emissions such as CO, NOx and

UHC. The complexity of the burning process and the measurement errors in the experimental study can cause higher mean errors.

Chauhan et. al. [67] evaluated the performance parameters: brake thermal efficiency, brake specific fuel consumption, power output. As a part of combustion study, in-cylinder pressure, rate of pressure rise and heat release rates were evaluated. The emission parameters such as carbon monoxide, carbon dioxide, un-burnt hydrocarbon, oxides of nitrogen and smoke opacity with the different fuels were also measured and compared with base line results. The brake thermal efficiency of Jatropha methyl ester and its blends with diesel were lower than diesel and brake specific energy consumption was found to be higher. However, HC, CO and CO_2 and smoke were found to be lower with Jatropha biodiesel fuel. NO_x emissions on Jatropha biodiesel and its blend were higher than Diesel. The results from the experiments suggest that biodiesel derived from non-edible oil like Jatropha could be a good substitute to diesel fuel in diesel engine in the near future as far as decentralized energy production is concerned. In view of comparable engine performance and reduction in most of the engine emissions, it can be concluded and biodiesel derived from Jatropha and its blends could be used in a conventional diesel engine without any modification.

Chauhan et. al. [68] transesterified Karanja oil and found the properties within acceptable limits of relevant standards. The performance parameters evaluated in the present study included brake thermal efficiency of Karanja biodiesel with different compositions at 5%, 10%, 20%,30% and 100% with mineral Diesel. BTE was about 3-5% lower with Karanja biodiesel and its blends with respect to diesel. Also, emissions parameters such as carbon monoxide, carbon dioxide, UBHC (unburnt hydrocarbon), oxides of nitrogen and smoke opacity for different test fuels were also measured. UBHC,CO, CO_2 and smoke were lower with Karanja biodiesel fuel. However, NO_x emissions of Karanja biodiesel and its blend were higher than Diesel. The combustion analysis was done using peak cylinder pressure and heat release rate with respect to crank angle. The peak cylinder pressure and heat release rate was lower for Karanja biodiesel. The results from the experiments suggested that biodiesel from non-edible oil like Karanja and its blends with diesel could be a potential fuel for diesel engine and play a vital role in the near future especially for small and medium energy production.

Dhar et. al. [69] produced biodiesel from high free fatty acid neem oil using a two-step process i.e. etherification followed by transesterification. This biodiesel was characterized for its physical, chemical and thermal properties. Performance, emission and combustion characteristics of this biodiesel and its various blends with mineral diesel were compared with baseline data in a direct injection (DI) diesel engine. Brake specific fuel consumption for biodiesel and its blends was higher than mineral diesel and brake thermal efficiency of all biodiesel blends was found to be higher than mineral diesel. Brake specific CO and HC emissions for biodiesel fuelled engine were lower than mineral diesel but NO emissions were higher for biodiesel blends. Detailed combustion characterization revealed that combustion starts earlier for higher biodiesel blends however start of combustion was slightly delayed for lower blends of biodiesel in comparison with mineral diesel. Rate of heat release for all biodiesel blends were almost identical to mineral diesel. Combustion duration for biodiesel blends was found to be shorter than mineral diesel. Biodiesel produced from high FFA neem oil was found to be marginally inferior compared to mineral diesel.

Liaqat et. al. [70] used a total of three fuel samples, such as DF (100% diesel fuel), CB5 (5% coconut biodiesel and95% DF), and CB15 (15% CB and 85% DF). Engine performance test was carried out at 100% load, keeping throttle 100% wide open with variable speeds of 1500 to 2400 rpm at an interval of 100 rpm. Whereas, engine emission tests were carried out at 2200 rpm at 100% and 80% throttle position. As results of investigations, there was a reduction in torque and brake power, while increase in specific fuel consumption observed for biodiesel blended fuels over the entire speed range compared to net diesel fuel. In case of engine exhaust gas emissions, lower HC, CO and, higher CO_2 and NOx emissions was found for biodiesel blended fuels compared to diesel fuel. Moreover, reduction in sound level for both biodiesel blended fuels was observed when compared to diesel fuel.

Ozener et. al. [71] compared the combustion, performance and emission characteristics of conventional diesel fuel and biodiesel produced from soybean oil and its blends (B10, B20, B50). The tests were performed at steady-state conditions in a single-cylinder direct injection diesel engine over the entire rpm range (1200–3000 rpm). During the tests, the fuel consumption, pollutant emissions, exhaust temperature and in-cylinder pressures were measured. The experimental results, showed that, relative to diesel, biodiesel

had a 1–4% decrease in the torque and an approximately 2–9% increase in the brake-specific fuel consumption (BSFC) due to the lower heating value (LHV) of the biodiesel. However, biodiesel significantly reduced carbon monoxide (CO) (28–46%) and unburned total hydrocarbons (THCs), while the nitric oxides (NOx) (6.95–17.62%) and carbon dioxide (CO2) emissions increased slightly 1.46–5.03%. The combustion analyses showed that the addition of biodiesel to conventional diesel fuel decreased the ignition delay and reduced the premixed peak. These results indicated that biodiesel could be used without any engine modifications as an alternative and environmentally friendly fuel.

Selvam et. al. [72] experimentally investigated performance and exhaust emissions of direct injection diesel engine with methyl esters of beef tallow as neat biodiesel (B100) and its blend (B5, B25, B50 and B75) with diesel fuel. Engine performance parameters namely brake power, brake specific fuel consumption, brake thermal efficiency and exhaust emissions of CO, HC, NOx, and smoke density were determined for different loading conditions and at constant engine speed of 1500 rpm. The test result indicated that there was a slight decrease in brake thermal efficiency and increase in specific fuel consumption for all the blended fuels when compared to that of diesel fuel. The drastic reduction in carbon monoxide, unburned hydrocarbon and smoke density were recorded for all the blended fuels as well as with neat biodiesel. However, in the case of oxides of nitrogen, there was a slight increase for all the blended fuels and with neat biodiesel when compared to diesel fuel. On the whole, methyl esters of beef tallow and its blends with diesel fuel could be used as an alternative fuel for diesel indirect injection diesel engines without any significant engine modification.

Sahoo et. al. [73] filtered high viscous (72 cSt at 40°C) and high acid value (44 mg KOH/gm) polanga (Calophyllum Inophyllum) oil based mono esters (biodiesel) produced by triple stage transesterification process and blended with high speed diesel (HSD) and tested for their use as a substitute fuel of diesel in a single cylinder diesel engine. HSD and polanga oil methyl ester (POME) fuel blends (20%,40%, 60%, 80%, and 100%) were used for conducting the short-term engine performance tests at varying loads (0%, 20%, 40%, 60%, 80%,and 100%). Tests were carried out over entire range of engine operation at varying conditions of speed and load. The brake specific fuel consumption (BSFC) and brake thermal efficiency (BTE) were calculated from the recorded data. The engine performance

parameters such as fuel consumption, thermal efficiency, exhaust gas temperature and exhaust emissions (CO, CO2, HC, NO_x, and O_2) were recorded. The optimum engine operating condition based on lower brake specific fuel consumption and higher brake thermal efficiency was observed at 100% load for neat biodiesel. From emission point of view the neat POME was found to be the best fuel as it showed lesser exhaust emission as compared to HSD.

Raheman et. al. [74] presented the performance of biodiesel obtained from mahua oil and its blend with high speed diesel in a Ricardo E6 in this paper together with some of its fuel properties. These properties were found to be comparable to diesel and confirming to both the American and European standards. Engine performance (brake specific fuel consumption, brake thermal efficiency and exhaust gas temperature) and emissions (CO, smoke density and NO_x) were measured to evaluate and compute the behaviour of the diesel engine running on biodiesel. The reductions in exhaust emissions and brake specific fuel consumption together with increase brake power, brake thermal efficiency made the blend of biodiesel (B20) a suitable alternative fuel for diesel and thus could help in controlling air pollution.

Godiganur et. al. [75] ran a Cummins 6BTA 5.9 G2- 1,158 HP rated power, turbocharged, DI, water cooled diesel engine on diesel, methyl ester of mahua oil and its blends at constant speed of 1500 rpm under variable load conditions. The volumetric blending ratios of biodiesel with conventional diesel fuel were set at 0, 20, 40, 60, and 100. Engine performance (brake specific fuel consumption, brake specific energy consumption, thermal efficiency and exhaust gas temperature) and emissions (CO, HC and NO_x) were measured to evaluate and compute the behaviour of the diesel engine running on biodiesel. The results indicated that with the increase of biodiesel in the blends CO, HC reduced significantly, fuel consumption and NO_x emission of biodiesel increased slightly compared with diesel. Brake specific energy consumption decreased and thermal efficiency of engine slightly increased when operating on 20% biodiesel than that operating on diesel.

Rehman et. al. [76] carried out investigation in studying the fuel properties of karanja methyl ester (KME) and its blend with diesel from 20% to 80% by volume and in running a diesel engine with these fuels. Engine tests have been carried out with the aim of obtaining comparative measures of torque, power, specific fuel consumption and emissions such as

CO, smoke density and NO$_x$ to evaluate and compute the behaviour of the diesel engine running on the above-mentioned fuels. The reduction in exhaust emissions together with increase in torque, brake power, brake thermal e:ciency and reduction in brake-speci4c fuel consumption made the blends of karanja esteri4ed oil (B20 and B40) a suitable alternative fuel for diesel and could help in controlling air pollution.

Buyukkaya et. al. [77] investigated experimental tests to evaluate the performance, emission and combustion of a diesel engine using neat rapeseed oil and its blends of 5%, 20% and 70%, and standard diesel fuel separately. The results indicated that the use of biodiesel produced lower smoke opacity (up to 60%), and higher brake specific fuel consumption (BSFC) (up to 11%) compared to diesel fuel. The measured CO emissions of B5 andB100 fuels were found to be 9% and 32% lower than that of the diesel fuel, respectively. The BSFC of biodiesel at the maximum torque and rated power conditions were found to be 8.5% and 8% higher than that of the diesel fuel, respectively. From the combustion analysis, it was found that ignition delay was shorter for neat rapeseed oil and its blends tested compared to that of standard diesel. The combustion characteristics of rapeseed oil and its diesel blends closely followed those of standard diesel.

Qi et. al. [78] produced biodiesel from soybean crude oil by a method of alkaline-catalysed transesterification. The effects of biodiesel addition to diesel fuel on the performance, emissions and combustion characteristics of a naturally aspirated DI compression ignition engine were examined. Biodiesel was found to have different properties from diesel fuel. A minor increase in brake specific fuel consumption (BSFC) and decrease in brake thermal efficiency (BTE) for biodiesel and its blends were observed compared with diesel fuel. The significant improvement in reduction of carbon monoxide (CO) and smoke were found for biodiesel and its blends at high engine loads. Hydrocarbon (HC) had no evident variation for all tested fuels. Nitrogen oxides (NO$_x$) were slightly higher for biodiesel and its blends. Biodiesel and its blends exhibited similar combustion stages to diesel fuel. The use of transesterified soybean crude oil can be partially substituted for the diesel fuel at most operating conditions in terms of the performance parameters and emissions without any engine modification.

Qi et. al. [79] produced biodiesel from soybean crude oil by a method of alkaline catalysed transesterification. The important properties of biodiesel were compared with those

of diesel. Diesel and biodiesel were used as fuels in the compression ignition engine, and its performance, emissions and combustion characteristics of the engine were analysed. The results showed that biodiesel exhibited the similar combustion stages to that of diesel, however, biodiesel showed an earlier start of combustion. At lower engine loads, the peak cylinder pressure, the peak rate of pressure rise and the peak of heat release rate during premixed combustion phase were higher for biodiesel than for diesel. At higher engine loads, the peak cylinder pressure of biodiesel was almost similar to that of diesel, but the peak rate of pressure rise and the peak of heat release rate were lower for biodiesel. The power output of biodiesel was almost identical with that of diesel. The brake specific fuel consumption was higher for biodiesel due to its lower heating value. Biodiesel provided significant reduction in CO, HC, NO_x and smoke under speed characteristic at full engine load. Based on this study, biodiesel can be used as a substitute for diesel in diesel engine.

Sahoo et. al. [80] experimentally accessed the practical applications of biodiesel in a single cylinder diesel engine used in generating sets and the agricultural applications in India. Diesel; neat biodiesel from Jatropha, Karanja and Polanga; and their blends (20 and 50 by v%) were used for conducting combustion tests at varying loads (0, 50 and 100%).The engine combustion parameters such as peak pressure, time of occurrence of peak pressure, heat release rate and ignition delay were computed. Combustion analysis revealed that neat Polanga biodiesel that results in maximum peak cylinder pressure was the optimum fuel blend as far as the peak cylinder pressure was concerned. The ignition delays were consistently shorter for neat Jatropha biodiesel, varying between 5.9° and 4.2° crank angles lower than diesel with the difference increasing with the load. Similarly, ignition delays were shorter for neat Karanja and Polanga biodiesel when compared with diesel.

As an outcome of the elaborative review of existing technical literatures regarding the engine trial results of biodiesels derived from a wide range of vegetable oil feedstocks and its blends, the following conclusions are made.

1. Depending upon the feedstocks, some of the biodiesels showed improved brake thermal efficiency and reduced brake specific fuel consumption with increased biodiesel volume fraction in the test fuel where as some others exhibited exactly opposite trend. Therefore,

engine performance using biodiesel directly depends upon the property of the corresponding feedstock and the transesterification process.

2. Most of the literatures agreed on the common denominator that emissions of carbon monoxide and unburnt hydro carbons were reduced with biodiesel, whereas that of oxides of nitrogen increased. However, the same was not linear. In many cases even, reduction in oxides of nitrogen was reported.

3. All most all of the literatures indicated increased in-cylinder pressure for lower volume fraction of biodiesel in the test fuels irrespective of the feedstocks. This led to shorter combustion duration, increased in-cylinder temperature and lower exhausts temperatures reported in many cases. However, at higher volume fractions of biodiesel some literatures indicated reduction in peak in-cylinder pressure where some indicated minimal change in the peak in-cylinder pressure. Therefore, the combustion phenomena using biodiesel is highly sensitive to the nature of the feedstock and transesterification process which actually determines the fuel properties.

4. With increase in volume fraction of biodiesel, reduction in combustion heat release was reported in major cases. However, in some cases a marginal increase was reported at lower blends.

5. Increased heat release in the diffusion phase, smoother engine operation etc. are some of the major conclusions in most of the literatures.

In the light of the above reviews it may be concluded that comprehensive engine trials to evaluate performance, emissions and combustion studies on diesel engines fuelled with Calophyllum biodiesel is absent in the literature. Therefore, exhaustive engine trials using Calophyllum biodiesel at various proportions and the subsequent analysis may provide a clear picture regarding the suitability of the seed oil as an alternative fuel to diesel.

2.2.3 Numerical Simulation of in-cylinder biodiesel combustion using CFD

Bari et. al. [81] proposed that a Guide Vane Swirl and Tumble Device (GVSTD) be installed in front of the intake port to develop an organised turbulence to assist in the breakup of fuel molecules for improved mixing with air to expedite the combustion of viscous biodiesel. To investigate the effect of GVSTD to generate better in-cylinder air flow, ANSYS-CFX was used to run a 3D cold flow IC engine simulation. The model was validated with the experimental results of in-cylinder pressure from 0°CA to 540°CA and the results of in-cylinder airflow characteristics from simulations were compared with other related research works. In this research, three designs of the GVSTD with the height of the vanes varied at 0.25R, 0.50R and 0.75R, where R is the radius of the intake runner, were compared with the model without GVSTD to investigate its effect on the air flow inside the combustion chamber. The results showed that the 0.25R guide vanes created more turbulence, in-cylinder velocity, swirl and tumble in the injected fuel region than the other designs, which is needed to break up the fuel molecules to mix with air that will eventually improve the engine performance with biodiesel. The resistance to the air flow due to the vanes was also least for the 0.25R guide vanes.

Battistoni et. al. [82] carried out a comparison between the injection process with two fuels, a standard diesel fuel and a pure biodiesel, methyl ester of soybean oil. Multiphase cavitating flows inside injector nozzles were calculated by means of unsteady CFD simulations on moving grids from needle opening to closure, using an Eulerian–Eulerian two-fluid approach which takes into account bubble dynamics. Afterward, spray evolutions were also evaluated in a Lagrangian framework using results of the first computing step, mapped onto the whole exit area, for the initialization of the primary breakup model. Two nozzles with cylindrical and conical holes were studied and their behaviours were discussed in relation to fuel properties. Nozzle flow simulations highlighted that the extent of cavitations regions was not much affected by the fuel type, whereas it was strongly dependent on the nozzle shape. Biodiesel provides a slightly higher mass flow in highly cavitating nozzles. On the contrary using hole shaped nozzles (to reduce cavitations) diesel provided similar or slightly higher mass flow. Comparing the two fuels, the effects of different viscosities and densities play main role which explained these behaviours. Simulations of the spray evolution were also discussed highlighting the differences between

the use of fossil and biodiesel fuels in terms of spray penetration, atomization and cone-angle. Usage of diesel fuel in the conical convergent nozzle exhibited higher liquid penetration.

Bunce et. al. [83] carried out a study to determine the optimal engine decision-making for 100% soya-based biodiesel to accommodate fuel property differences via modulation of air–fuel ratio (AFR), exhaust gas recirculation (EGR) fraction, fuel rail pressure, and start of main fuel injection pulse at over 150 different random combinations, each at four very different operating locations. Applying the nominal diesel settings to biodiesel combustion resulted in increases in NO_x at three of the four locations (up to 44%) and fuel consumption (11–20%) over the nominal diesel levels accompanied by substantial reductions in particulate matter (over 80%). The biodiesel optimal settings were defined as the parameter settings that produced comparable or lower NO_x, particulate matter (PM), and peak rate of change of in-cylinder pressure (peak $dP/d\theta$, a metric for noise) with respect to nominal diesel levels, while minimizing brake specific fuel consumption (BSFC). At most of the operating locations, the optimal engine decision-making was clearly shifted to lower AFRs and higher EGR fractions in order to reduce the observed increases in NO_x at the nominal settings, and to more advanced timings in order to mitigate the observed increases in fuel consumption at the nominal settings. These optimal parameter combinations for biodiesel were able to reduce NO_x and noise levels below nominal diesel levels while largely maintaining the substantial PM reductions. These parameter combinations, however, had little (maximum 4% reduction) or no net impact on reducing the biodiesel fuel consumption penalty.

Luo et. al. [84] developed a skeletal mechanism with 115 species and 460 reactions for a tri-component biodiesel surrogate, which consists of methyl decanoate, methyl 9-decenoate and n-heptane to reduce computational costs for 3-D engine simulations. The detailed mechanism for biodiesel developed by Lawrence Livermore National Laboratory (LLNL) was employed as the starting mechanism. The rate constants for then-heptane and larger alkane subcomponents in the detailed mechanism were first updated. The detailed mechanism was then reduced with direct relation graph (DRG), isomer lumping, and DRG-aided sensitivity analysis (DRGASA), which was improved to achieve a larger extent of reduction. The reduction was performed for pressures from 1 to 100 atm and equivalence

ratios from 0.5 to 2 for both extinction and ignition applications. The initial temperatures for ignition were from 700 to 1800 K, covering the compression ignition (CI) engine conditions. Extensive validations were performed against 0-D simulations with the detailed mechanism and experimental data for spatially homogeneous systems, 1-D flame sand 3D-turbulent spray combustion. The skeletal mechanism was able to predict various combustion characteristics accurately such as ignition delay, flame lift-off length, and equivalence ratio at flame lift-off location under different ambient conditions. Compared with the detailed mechanism that consists of 3299 species and 10806 reactions, the skeletal mechanism features a reduction by a factor of around 30in size while still retaining good accuracy and comprehensiveness.

Ismail et. al. [85] established emissions formation process and its interaction with the combustion event for fossil diesel and the methyl esters of coconut (CME), palm (PME) and soy (SME) across three different engine conditions. Here, the OpenFOAM open source CFD codes were utilised to simulate the in-cylinder events. The ignition delay (ID) period and the timing of peak pressure were accurately predicted to within±0.2° crank angle for all the test cases. The maximum error between the experimental and computed peak pressure values across the test range was limited to below 4.5%. The change in the fuel type from fossil diesel to biodiesel altered the physical and the chemical delays, both of which affect the overall ID period. As a result, variations in the combustion behaviour and hence the emission characteristics were observed. Neat CME was found to produce both NO_x and soot reduction across all the engine loads tested. The most significant reduction in soot level was achieved at high load operation, while greatest NO_x reduction was recorded under low load condition when neat or B50 blends of the test biodiesel fuels were used. The best operating condition to result in simultaneous soot and NOx reduction through the use of biodiesel was at mid load condition with an engine speed of 2000 rev/min.

Ismail et. al. [86] developed a reduced chemical kinetics mechanism and validated under zero-dimension and multi-dimensional engine simulations for a range of engine operating conditions and types of biodiesel fuel. The mechanism was first constructed by reducing a detailed MB/MB2D mechanism consisting of301 species and 1516 reactions to 77 species and 212 reactions. The ignition delay periods and temporal evolutions of important species were in good agreement with those produced using detailed kinetics. The reduced

mechanism was then combined with a skeletal modified n-heptane mechanism to account for actual biodiesel energy content and molecular structure when fuel blends were introduced. Two additional global reactions were also included to cater for the change in ratio between saturated and unsaturated methyl esters in the fuels. The combined mechanism (BOS-V2) consisted of 113 species and 399 reactions with integrated nitrogen oxides (NO_x) reaction kinetics. This mechanism was then further validated using OpenFOAM for the computational fluid dynamics (CFD) engine simulations. Here, neat and B50 blends of coconut, palm and soy methyl esters were used. Good agreements in ignition delay, peak pressure, pressure trace, heat-release profile and emission trends were achieved between experimental and predicted data for all the tested fuels and engine operating conditions. The results showed that the proposed mechanism gave reliable predictions of in-cylinder combustion and emission processes.

Ng et. al. [87] investigated the combustion characteristics and emissions formation processes of biodiesel fuels in a light-duty diesel engine. A compact reaction mechanism with 80 species and 303 reactions was used to account for the effects of chemical kinetics. Here, the mechanism was capable of emulating biodiesel–diesel mixture of different blending levels and biodiesel produced from different feedstock. The integrated CFD-kinetic model was validated against a test matrix which covers the entire saturated–unsaturated methyl ester range typical of biodiesel fuels, as well as the biodiesel–diesel blending levels. The simulated cases were then validated for in-cylinder pressure profiles and peak pressure values/timings. Errors in the peak pressure values did not exceed 1%, while the variations in peak pressure timings were kept within 1.5 crank angle degrees (CAD). For this reported work, in-cylinder formation mechanisms of nitrogen monoxide (NO) and soot from the combustion of biodiesel fuels such as coconut methyl ester (CME), palm methyl ester (PME) and soybean methyl ester (SME) were simulated and compared against that of the baseline diesel fuel. It was established here that an increase in the degree of unsaturation in biodiesel fuels had detrimental effects on engine-out NO and soot concentrations. Biodiesel fuel with greater unsaturation level such as SME was having the predisposition to produce greater thermal NO due to larger regions of high temperature achieved during combustion. Besides, the highly unsaturated SME had greater tendencies to produce acetylene which were precursors for prompt NO and soot, leading to higher engine-out emissions of these pollutants.

In all, this study has demonstrated the feasibility of integrating a compact multi-component surrogate fuel mechanism with CFD to elucidate the in-cylinder combustion and emissions characteristics of biodiesel fuels.

Ng. et. al. [88] proposed a compact combined biodiesel–diesel (CBD) reaction mechanism for diesel engine simulations through the combination of three component mechanisms using a chemical class-based approach. The proposed mechanism comprised the reaction mechanisms of methyl crotonate (MC),methyl butanoate (MB) and n-heptane which were the surrogate fuel models of unsaturated fatty acid methyl ester, saturated fatty acid methyl ester and straight chain hydrocarbon (HC), respectively. The MC and MB mechanisms were adopted to represent biodiesel fuels, while n-heptane was utilised to characterise the combustion of fossil diesel. Here, the MC and MB mechanisms were reduced before integrating with a compact n-heptane mechanism. CHEMKIN-PRO was used as the solver for the zero-dimensional, closed homogenous reactor with a constant volume in this study. In the first phase, the mechanisms of MC and MB were methodologically reduced. The MC mechanism by Gail et al. with 301 species and1516 reactions was reduced to 47 species and 210 reactions, while the MB mechanism by Brakora et al. with41 species and 150 reactions was reduced to 33 species and 105 reactions. The mechanisms were reduced from a combination of methods, including peak molar concentration analysis, reaction flux analysis and the removal of individual species. In the second phase, the reduced MC and MB mechanisms were combined with the n-heptane mechanism by Pang et al. with 46 species and 112 reactions. Upon the combination of the component mechanisms, parametric adjustments to the Arrhenius rate constants of pertinent chemical reactions were performed for better ignition delay (ID) prediction. The final mechanism developed comprised 80 species and 299 reactions. The compact-sized CBD mechanism was validated against 234 test conditions ranging from initial temperatures of 750–1350 K, pressures of 40–60 barand equivalence ratios of 0.4–1.5. The mechanism was generally found to accurately predict the timing and duration of ID for the combustion of each surrogate fuel.

Pang et. al. [89] developed a reduced chemical mechanism of surrogate diesel fuel for diesel engine simulations. The aim here was to employ an appropriate reduction scheme to create a compact yet sufficiently comprehensive model which can accurately account for

in-cylinder diesel combustion and soot precursor formation processes. The Combustion Engine Research Center (CERC) mechanism of Chalmers University of Technology was used as the base mechanism since this is the most extensively validated and applied mechanism. The reduction scheme involved firstly identifying and then eliminating unimportant species/reactions in the ignition and soot precursor formation processes through the computed production rates and temperature sensitivity coefficients using CHEMKIN-PRO software. Subsequently, reactions were assimilated based on the quasi-steady state assumption (QSSA). The final reduced mechanism, which consisted of 109 elementary reactions with 44 species, was first validated under 48 shock tube conditions. Ignition delay (ID) periods predicted by the reduced and base CERC mechanisms were found to be in good agreement, although percentage errors of up to 20% were observed. Further validation was performed by incorporating the reduced mechanism into multi-dimensional CFD code, ANSYS FLUENT through a plug-in chemistry solver, CHEMKIN-CFD. Here, simulation results of combustion characteristics and soot production profiles were compared against data from an experimental study on a heavy-duty, direct injection diesel engine. Simulated peak pressures in cases with short and long ID periods were identical to those recorded from experiments and the maximum ID offset was maintained to within 1 crank angle degree. Spatial and temporal evolutions of in-cylinder soot were also captured successfully in both cases. Significant qualitative relationship between input parameters and soot evolution was elucidated from this study. The implementation of the reduced mechanism achieved a 38% reduction in computational runtime when compared with that of the base mechanism.

On the basis of the aforementioned literature review regarding numerical simulations and the use of computational fluid dynamics tools, in biodiesel application in diesel engines, the following major conclusions are drawn.

1. Numerical studies on biodiesel combustion in diesel engines are at its infancy as only limited research literature was available.

2. OpenFoam and ANSYS were the most used CFD software for such type of study.

3. The "CHEMKIN" chemical kinetics model for species and reaction in combustion process were adopted and validated in many cases.

4. Pressure profiles, temperature profiles and emissions were the most studied combustion phenomena in numerical studies.

Computer simulations to determine various engine trial parameters are a new thrust area in research as it provides wider flexibility than the actual experimental trials. Therefore, development of a suitable combustion model using computational fluid dynamics tool ANSYS14 ICEM and its validation with the actual combustion results of diesel and Calophyllum biodiesel may further widen the research knowledge and acceptability of the proposed Calophyllum Methyl Ester as a potential alternative to mineral diesel.

2.3 PROBLEM STATEMENT

In the light of the exhaustive and valuable literature review and the subsequent analysis, the problem statement for the present research was devised. It was clear that the most popular usage of vegetable oils in diesel engine was the conversion to methyl esters or biodiesel to address the high viscosity of vegetable oils. The conversion popularly known as transesterification may be a single step or two step processes depending upon the FFA of the vegetable oil. In most of the cases of non-edible vegetable oils the FFA was higher than 2% resulting in an acid catalysed esterification followed by a base catalysed transesterification process. As two steps transesterification is energy intensive, therefore optimization of various process parameters like catalyst concentration, reaction time, reaction temperature, molar ratio etc. is essential for commercially competitive production. The biodiesel so obtained should be thoroughly characterised as per the various ASTM/EN/ISO standards. If some of the properties are not consistent with standards as reported in many literatures, some additives may be added to improve theses essential standard properties. Then the final biodiesel so prepared would be used as a fuel in diesel engines in neat form as well as blends of various proportions in diesel. The performance, emissions and combustion behaviour of diesel engine fuelled with these set of test fuels validate the suitability of these fuels. Numerical studies on biodiesel combustion in diesel engines and its validation from the experimental results are a new thrust area of research. Setting up a geometrical model consistent with the actual engine set up and its simulation using computational fluid dynamics tools provides a wider flexibility in engine studies and fuel effects. On the basis of these valuable information, the following objectives were envisaged for the present research work.

1. Looking at the high FFA of Calophyllum vegetable oil, the two stage transesterification was to be done with process optimization in both the stages. The process parameters like catalyst concentration, reaction time and reaction temperature to be taken as factors in the experimental design. For the acid catalysed stage, %FFA and for the base catalysed stage, %yield of biodiesel were to be considered as the response. Based on the designed test matrix the experiments would be carried out and the results would be analysed in design of experiment software 8.0.7.1.

2. Bulk quantity Calophyllum Methyl Ester will be produced using the optimized parameters obtained in the step1. Various physico-chemical and fuel properties of CME would be evaluated and compared with various standards like ASTM/EN/ISO etc.

3. A comprehensive engine trial will be carried out to assess the performance, emissions and combustion behaviors of actual diesel engine fuelled with CME and its blends and its comparison with the baseline diesel operation.

4. A three dimensional geometrical model consistent with the actual engine set up will be designed using design modeler and to be simulated in the ICEM module of ANSYS 14 software. The simulation results will be compared to the experimental results for validation of the computational model.

SYSTEM DEVELOPMENT AND METHODOLOGY

3.1 INTRODUCTION

This chapter deals with the systematic execution of the four steps mentioned in the problem statement section. It includes the production of biodiesel from Calophyllum vegetable oil and its optimization using response surface methodology, preparation of various blends of CME and diesel, comprehensive physico-chemical characterisation, development of engine test rig, development of heat release model and other engine parameters like performance and emission, procedures for engine trial, development of computational model using ANSYS 14 ICEM etc. They are discussed briefly as follows.

3.2 PRODUCIOTION OPTIMIZATION OF CALOPHYLLUM BIODIESEL

Calophyllum oil was extracted from good quality seeds using a screw press. The oil so obtained was pressure filtered and heated at 120°C for 20 minutes to remove moisture. The oil was then preserved in an airtight screw cap bottle. Plate 3.1 shows neat Calophyllum vegetable oil and the seeds. The FFA of the oil was found to be 23.52%.

Plate3.1: Calophyllum seeds and vegetable oil

3.2.1 Transesterification for Production of Biodiesel

Biodiesel is normally produced by the transesterification of the waste vegetable oil, algal oil or animal fat as a feedstock. The most commonly used alcohol is methanol or ethanol to produce methyl esters or ethyl esters. It is generally referred as fatty acid methyl esters (FAME) or fatty acid ethyl esters (FAEE) [91]. Nowadays, there are four different methods available to reduce the viscosity of vegetable oil, which is detrimental to engine hardware, such as blending of oil with petroleum diesel, pyrolysis (Thermal Cracking), emulsification and transesterification as discussed earlier [92]. The diesel combustion engines to be modified to avoid carbon deposition, when the vegetable oil is used directly or mixed along with petroleum diesel [93,94]. The pyrolysis and emulsification methods are producing heavy carbon deposits, in complete combustion, increase of lubricating oil viscosity and undesirable side-products such as aliphatic and aromatic compounds and carboxylic acids [94]. Recently, transesterification has been reported as the most common way to produce biodiesel from vegetable or algal oil with alcohol usually methanol or ethanol, in presence of an acid or base catalyst [95]. The general scheme of the transesterification reaction for FAME and FAEE is presented in equation (3.1), (3.2), where R is a mixture of fatty acid chains [96].

$$
\begin{array}{l}
CH_2-O-CO-R_1 \\
| \\
CH-O-CO-R_2 + 3CH_3OH \quad \overset{Catalyst}{\longleftrightarrow} \\
| \\
CH_2-O-CO-R_3 \\
\text{Triglyceride} \qquad \text{methanol}
\end{array}
\qquad
\begin{array}{l}
CH_2-OH \quad R_1-COOCH_3 \\
| \\
CH-OH + R_2-COOCH_3 \\
| \\
CH_2-OH \quad R_3-COOCH_3 \\
\text{Glycerol} \quad \text{methylester}
\end{array}
$$

(3.1)

$$
\begin{array}{l}
CH_2-O-CO-R_1 \\
| \\
CH-O-CO-R_2 + 3C_2H_5OH \quad \overset{Catalyst}{\longleftrightarrow} \\
| \\
CH_2-O-CO-R_3 \\
\text{Triglyceride} \qquad \text{ethanol}
\end{array}
\qquad
\begin{array}{l}
CH_2-OH \quad R_1-COOC_2H_5 \\
| \\
CH-OH + R_2-COOC_2H_5 \\
| \\
CH_2-OH \quad R_3-COOC_2H_5 \\
\text{Glycerol} \quad \text{ethylester}
\end{array}
$$

(3.2)
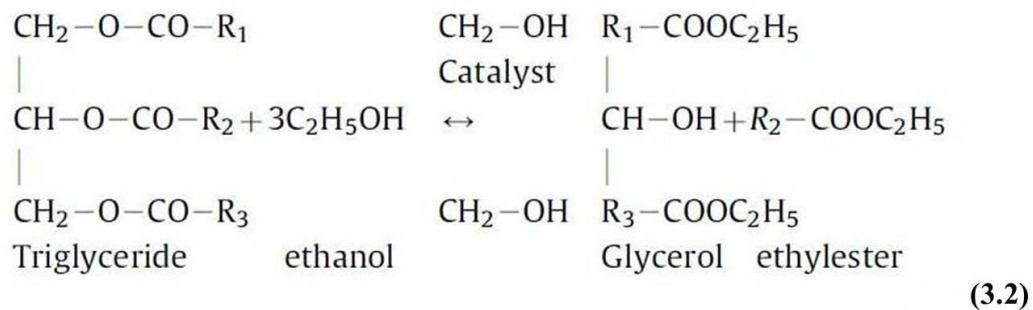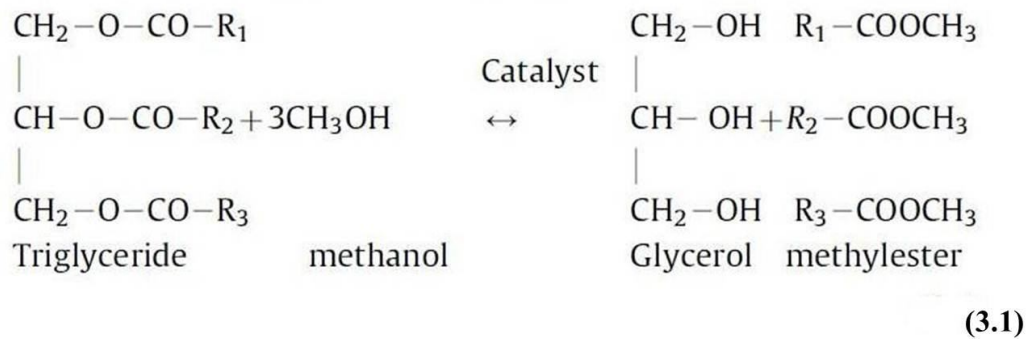
However, there are certain feedstocks where the content of free fatty acids in the vegetable oil is very high. The free fatty acids do not react with methanol in presence of an alkaline catalyst. However, the FFA can react with alcohol to form ester (biodiesel)by an acid-catalysed esterification reaction [97]. This reaction is very useful for handling oils or fats with high FFA, as shown in the equation (3.3) below:

$$R_1-COOH + \underset{(alcohol)}{ROH} \xrightarrow{H^+} \underset{(fatty\ acid\ ester)}{R-O-CO-R_1} + \underset{(water)}{H_2O} \quad \textbf{(3.3)}$$
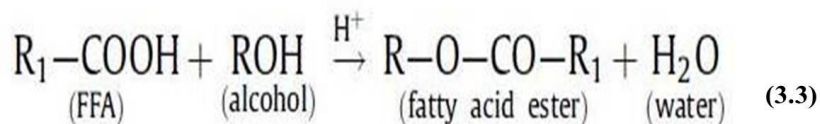
Normally sulphuric acid is considered as the suitable catalyst for this reaction, however a good range of acids may be considered for the same purpose. Therefore, vegetable oil feedstocks with more than 2% free fatty acid contents are generally transesterified in two stages. In the first stage the FFA is reacted with the alcohol in presence of acid catalyst and when the FFA is reduced below 2%, then it is transesterified in presence of alkaline catalyst.

As mentioned in the previous section, the FFA of Calophyllum vegetable oil was as high as 23.52%. Therefore, it has to pass through a two stage transesterification process to produce biodiesel. Such type of reactions is generally very much time consuming and consumes large amount of catalyst. Therefore, an optimization of process parameters like catalyst concentration, reaction time etc. shall lead to commercially competitive production of biodiesel from Calophyllum feasible.

3.2.2 Biodiesel production optimization from Calophyllum vegetable oil using response surface methodology

Application of statistical and mathematical models in designing scientific experiment is a long tradition but in recent times the development of sophisticated analytical and mathematical model based software has been appreciated by researchers in different fields. Response Surface Methodology (RSM) in experimental design has increasingly attracted the attention of many researchers. This is due to its advantages primarily in reducing the number of experiments and understanding the pattern in which the measured response is affected by the corresponding changes in variables [98]. The main advantage of RSM is that the design enables the improvement of the product from predicted property values and its ability to predict the interactions of more than two or more factors and their individual and collective

contribution to the measured response. The most widely used RSM model is the Central Composite Rotatable Design (CCRD).

A Response Surface Methodology was employed using a Central Composite Rotatable Design model. This was a second order model that included full factorial points, axial points and augmented central points. The three level-five factors CCD was designed to study the effects of each factor (catalyst concentration, Temperature and Time) as well as the multiples of the factor-factor interactions at constant molar ratio of 1:6. A summary of the RSM design using a box is given in Fig.3.1.
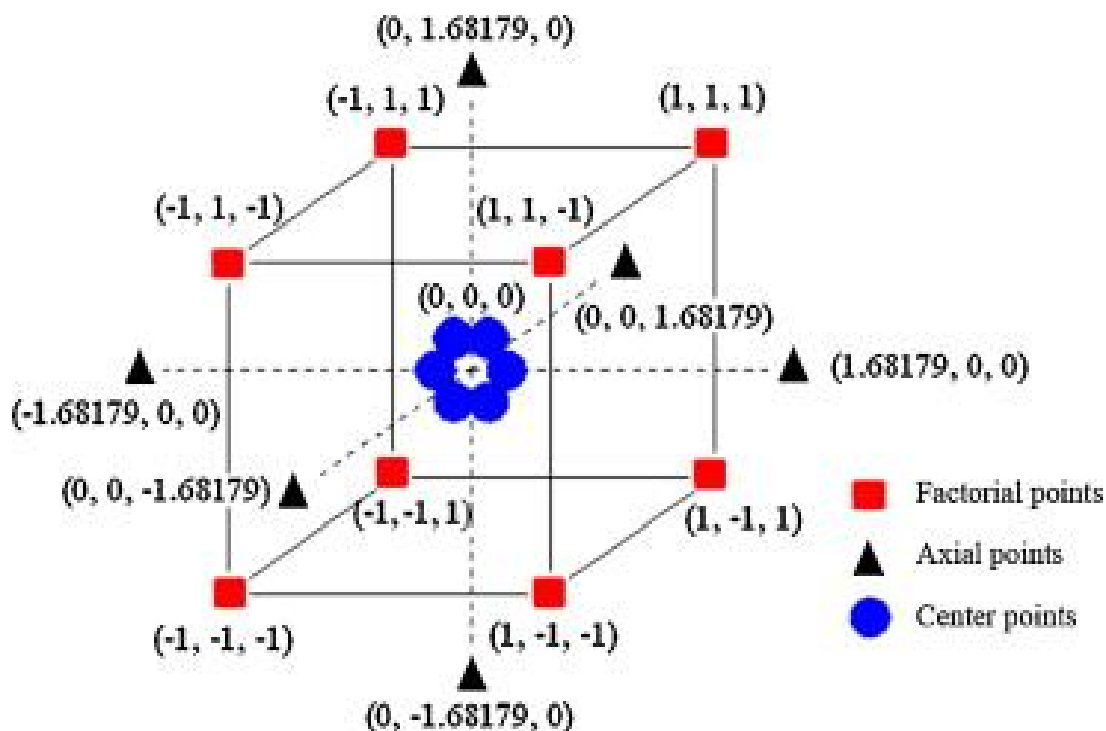
Fig.3.1: Box representation of RSM

As intended earlier, both the stages of transesterification i.e. acid catalysed and base catalysed, would be optimized. The independent variables were chosen from the preliminary studies conducted earlier which identified the most important factors affecting the esterification/transesterification reactions of the Calophyllum vegetable oils. For the esterification stage, concentration of catalyst (Paratoluene sulfonic acid-PTSA in this case), reaction time and reaction temperature were considered as the critical process parameters, whereas for the alkaline stage, concentration of potassium hydroxide (KOH), reaction time and reaction temperature were considered as the parameters of importance. The design

variables and levels are presented in the table 3.1 for the esterification stage and table 3.2 for the transesterification stage. The factors are coded as X1, X2 and X3 corresponding to catalyst concentration, temperature and time of the reaction respectively in the design. The levels were indicated as $-\beta, -\acute{\alpha}, 0, +\beta$ and $+\acute{\alpha}$ corresponding to the value of the lowest range to the highest range in increasing order for the corresponding factors.

Table.3.1: Factors and levels for the esterification stage

Factors	Code	Levels				
		$-\beta$	$-\acute{\alpha}$	0	$+\beta$	$+\acute{\alpha}$
Catalyst conc. (% wt)	X_1	0.5	0.75	1.0	1.25	1.5
Temperature (^{0}C)	X_2	50	55	60	65	70
Reaction Time (Mins)	X_3	60	75	90	105	120

Table.3.2: Factors and levels for the transesterification stage

Factors	Code	Levels				
		$-\beta$	$-\acute{\alpha}$	0	$+\beta$	$+\acute{\alpha}$
Catalyst conc. (% wt)	X_1	0.5	0.75	1.0	1.25	1.5
Temperature (^{0}C)	X_2	50	55	60	65	70
Reaction Time (Mins)	X_3	60	90	120	150	180

A total of 20 experimental-set including eight factorial points fixed at each corner of the box, six axial points running beyond the boundaries of the box and six central points at the centre of the box to ensure reliability of the design were developed. Number of experimental set is calculated from the standard design of experiments formula given in equation (3.4).

$$N = 2k + 2k + No \qquad (3.4)$$

Where k is the number of independent variables = 3

No is the number of repetition of experiments at the central point for the design to be rotatable = 6. The test matrix based on table 3.1 and 3.2 were generated for both the stages using a design of experiment software 8.0.7.1 and the subsequent experiments were carried out at the laboratory facility. Plate 3.2 shows the transesterification process being carried out in the lab with various permutation and combinations of the factors as per the test matrix.
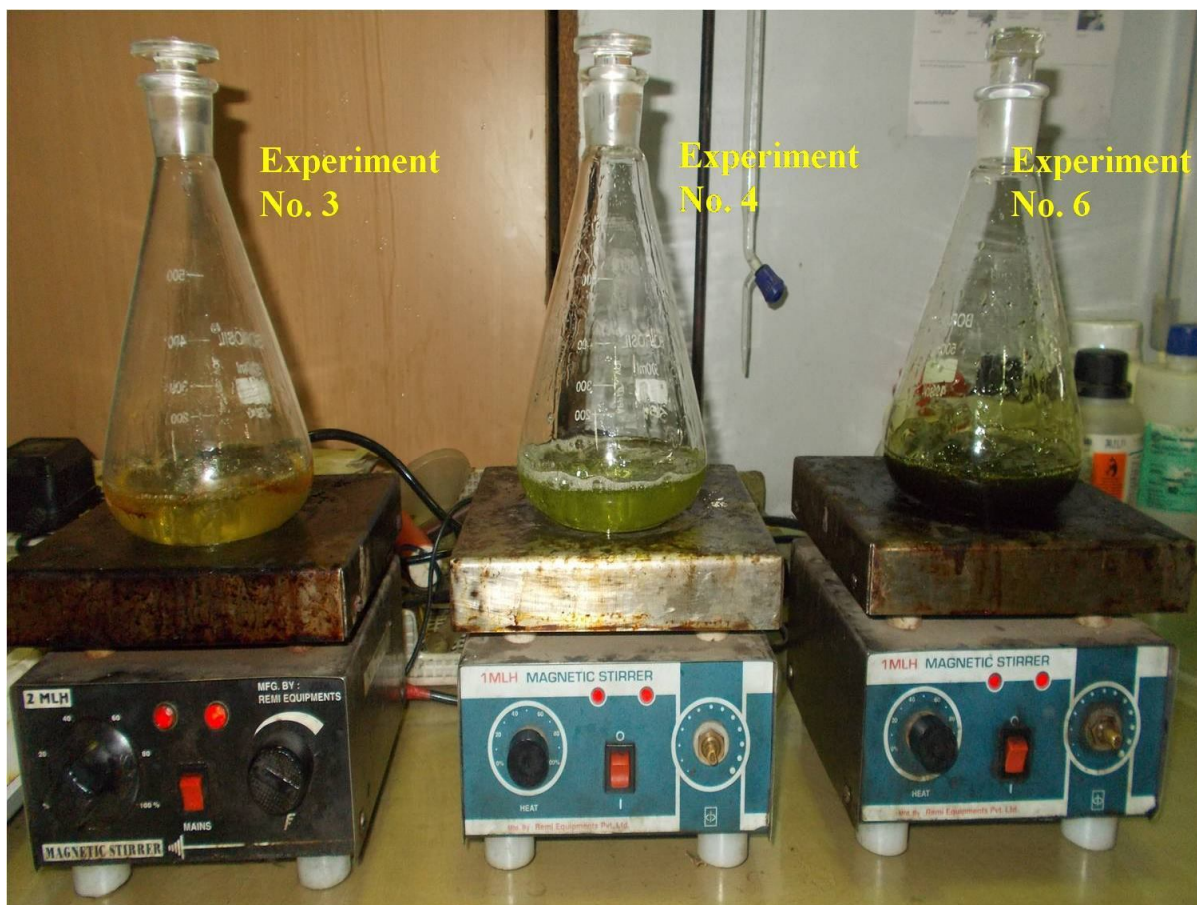
Plate 3.2: Transesterification experiments as per the test matrix

The results so obtained were fed to the design experiment software for further analysis. The analysis of variance (ANOVA) table and the response surfaces were obtained from the software. Details of the results and analysis are provided in the results section. However, the optimal conditions were found as follows.

For the esterification stage, an optimal FFA of 4.74% was achieved for 1.5% catalyst (PTSA) concentration, 65°C reaction temperature and 60 minutes reaction time. Similarly, in the transesterification stage, 0.88% concentration of catalyst (KOH), 62.75°C reaction temperature and 90 minutes of reaction time produced the optimum yield of 96.48% at constant methanol to oil molar ratio of 1:6. Based on this result, bulk quantity of Calophyllum biodiesel was prepared in a large capacity biodiesel reactor as shown in the plate 3.3. The reactor has a capacity of 10 Litres. One of the notable features of the reactor was its methanol recovery system which maintained the oil to methanol molar ratio precisely constant at 1:6 throughout the two stage transesterification process.
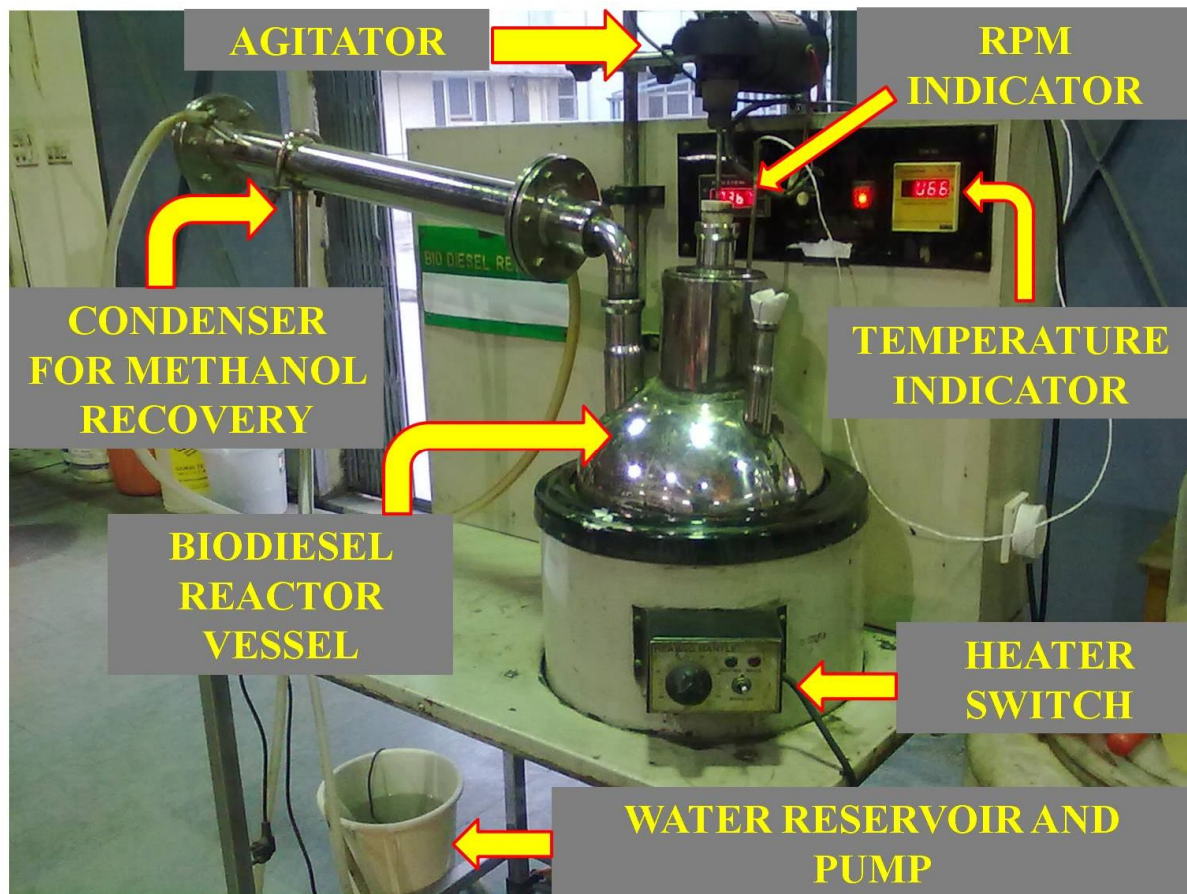
Plate 3.3: 10Liter Capacity Biodiesel Reactor

As mentioned above, the optimal FFA was 4.74% from the experimental design study. However, the literature indicated that it should be less than 2% for higher yield. Therefore, the esterification stage was carried out using the optimal parameters first to obtain 4.74% FFA in 60 minutes. After that Additional 20 minutes agitation provided the requisite less than 2% FFA. Subsequently, the oil was transesterified as per the optimal process parameters of 0.88% of KOH by original oil mass and nearly 63°C temperature for 90 minutes. The sample so obtained from the reactor was gravity separated for 12 hours to remove glycerol. However, the biodiesel sample so obtained contained impurities like methanol and KOH traces. For further purification the sample was washed with slightly hot distilled water for several times to remove any traces of methanol or catalysts. The water washing was stopped when the washed water became colourless. Then the oil was heated at 120°C for 25 minutes to remove the moisture.

Finally the Calophyllum methyl ester was obtained as a pale yellow and more or less transparent fluid. The gravity separation funnel and the final biodiesel sample are shown in Plate 3.4.
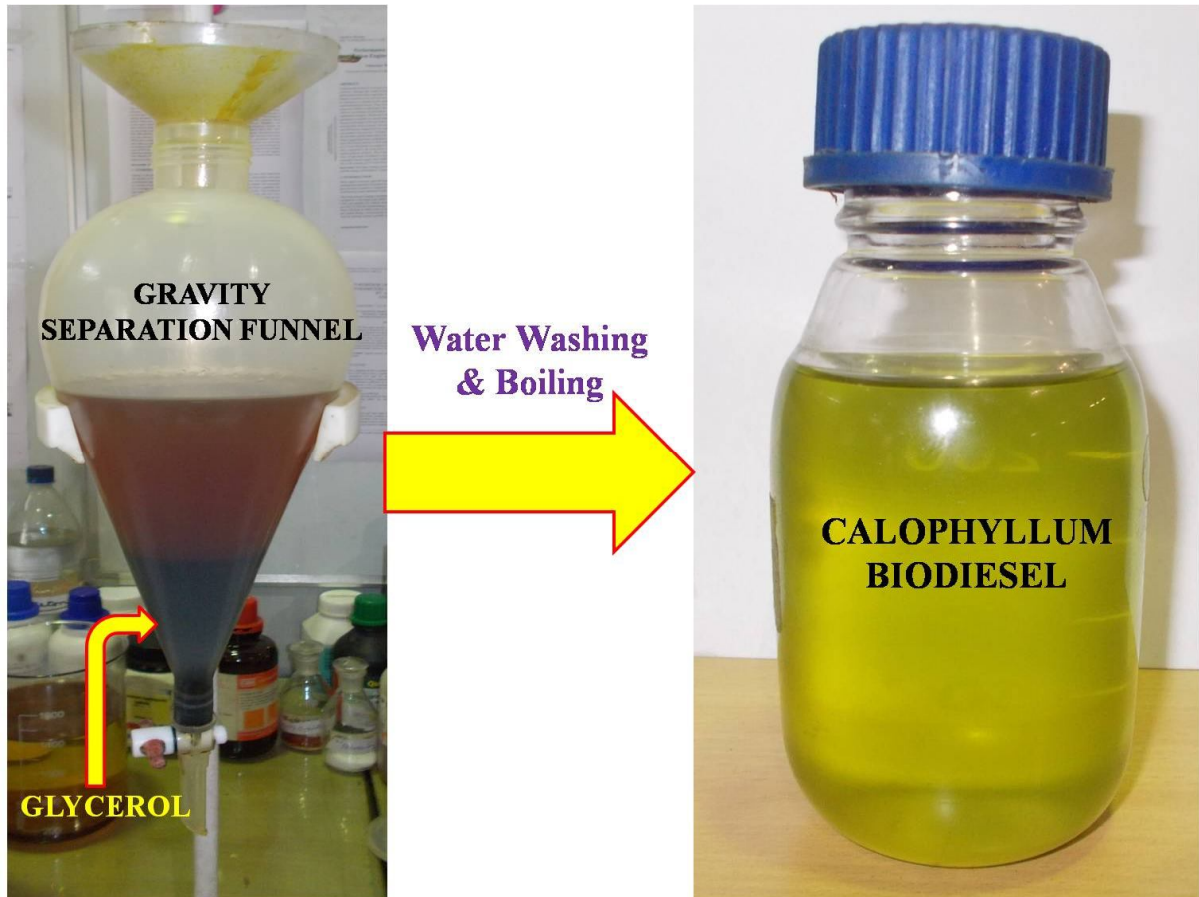
Plate 3.4: Mineral Diesel and Calophyllum Biodiesel

The biodiesel so obtained was completely miscible with mineral diesel. To check the miscibility various proportions of biodiesel was added to mineral diesel and monitored for 15 days. No signs of separation were observed. Therefore, the methyl ester of Calophyllum or the Calophyllum biodiesel is concluded to be completely miscible with mineral diesel.

3.3 PHYSICO-CHEMICAL CHARACTERISATION OF CALOPHYLLUM BIODIESEL

Determination of various physico-chemical and fuel properties of the Calophyllum methyl ester was essential for its standardisation as well as various calculations for engine trials. Moreover, the properties of blends of CME and diesel were also essential. Therefore, 11 test fuel samples of 500 cc each were prepared comprising of neat diesel, neat CME and various blends of CME and diesel. The blends were named as CME10, CME20, CME30, CME40, CME50, CME60, CME70, CME80, CME90 and CME100 with 10%, 20%, 30%, 40%, 50%, 60%, 70%, 80%, 90% and 100% volume wise substitution of diesel by CME respectively. Mineral diesel was named as the baseline. The properties of all these test fuel samples were evaluated in the laboratory as discussed below.

3.3.1 Density

A simple U tube oscillating true density meter is one of the simplest methods for the determination of density and specific gravity. The equipment used was "Antan Par Density Meter, Model DMA 4500 shown in Plate 3.5.

Plate 3.5: Antan Par Density Meter

In the present investigation the specific gravity of the test fuel samples was measured at a temperature of 15^0C in accordance with ASTM D-4052. Subsequently the temperature was varied from 30°C to 80°C with 10°C increment in each step and the density was measured for individual test fuels separately to evaluate the effect of temperature on density. The procedure for measurement of density and specific gravity was very simple. Initially the equipment was switched on by supplying electrical power. Then the test fuel pipeline was rinsed by injecting 10cc of toluene through the sample injection port. Subsequently 10cc of actual sample was fed to the injection port. It took approximately 5-7 minutes to give a precise value of density and specific gravity of the test fuel. The repeatability of the measurement was checked thrice and found satisfactory. Moreover, the average of the three measurements was taken as the final value for each sample.

3.3.2 Kinematic Viscosity

Plate 3.6 shows the kinematic viscometer taken for the measurement of viscosity.
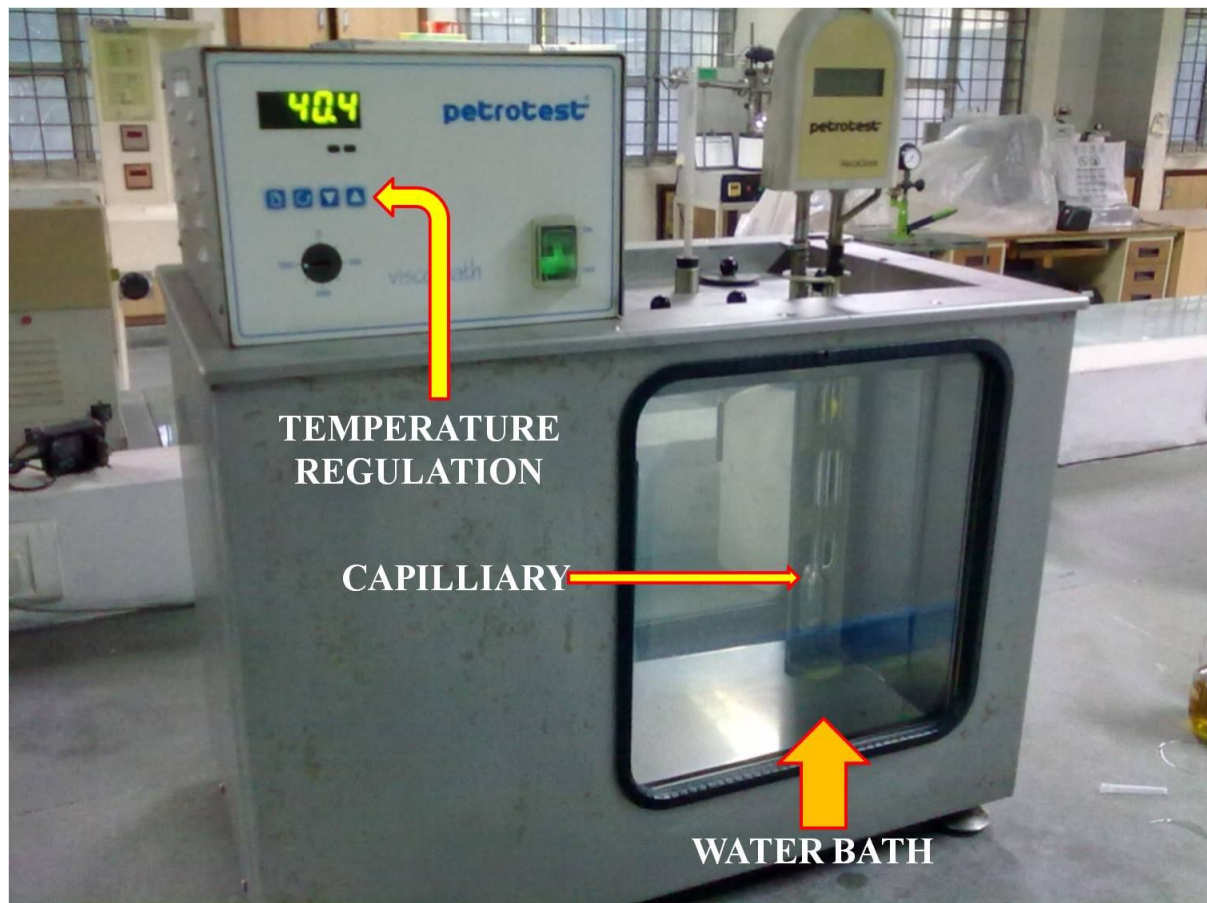
Plate 3.6: Petrotest Viscometer

The viscosity of the fuel affects atomization and fuel air mixing as discussed comprehensively in the earlier sections. Viscosity is also an important property associated with the lubricity. As many researchers indicated that biodiesel have superior lubricating properties than diesel, hence determination of viscosity and the effect of temperature on viscosity can provide a better understanding of Calophyllum biodiesel as a fuel cum lubricant. Viscosity measurements were conducted for different test fuels under consideration. Kinematic viscosity of liquid fuel samples were measured at 40^0C as per ASTM D-445. Subsequently, the temperature was varied between 30°C to 80°C with an increase of 10°C in each step to evaluate the effect of temperature on viscosity for individual test fuels. The equipment used was "Petrotest Viscometer. A suitable capillary tube was selected, and a measured quantity of sample was allowed to free flow through the capillary tube. Time was noted in passing of the fluid from the capillary tube having an upper level and lower level mark. Subsequently, kinematic viscosity was calculated by multiplying the capillary constant with the time measured in seconds (Equation 3.5). The final value was obtained in mm^2/s or centistokes abbreviated as cSt.

$$\nu = k * t \tag{3.5}$$

Where, $\quad \nu$ = Kinematic viscosity, mm^2/sec

$\quad$ k = Constant; mm^2/sec^2 (k= 0.005675 mm^2/sec^2)

$\quad$ t = Time, in second

3.3.3 Calorific Value

The Bomb calorimeter is the device usually used for the determination of calorific value. The calorific value is the amount of heat released by the combustion of unit quantity of fuel in the presence of oxygen in a bomb calorimeter. The calorific value of the fuel was determined with the Isothermal Bomb Calorimeter as per the specifications given in ASTM D240 standard. The calorimeter model used was Parr 6100 Oxygen Bomb Calorimeter. Electrodes were used to burn the sample of fuel in the bomb calorimeter. Bomb calorimeter is shown in Plate 3.7.
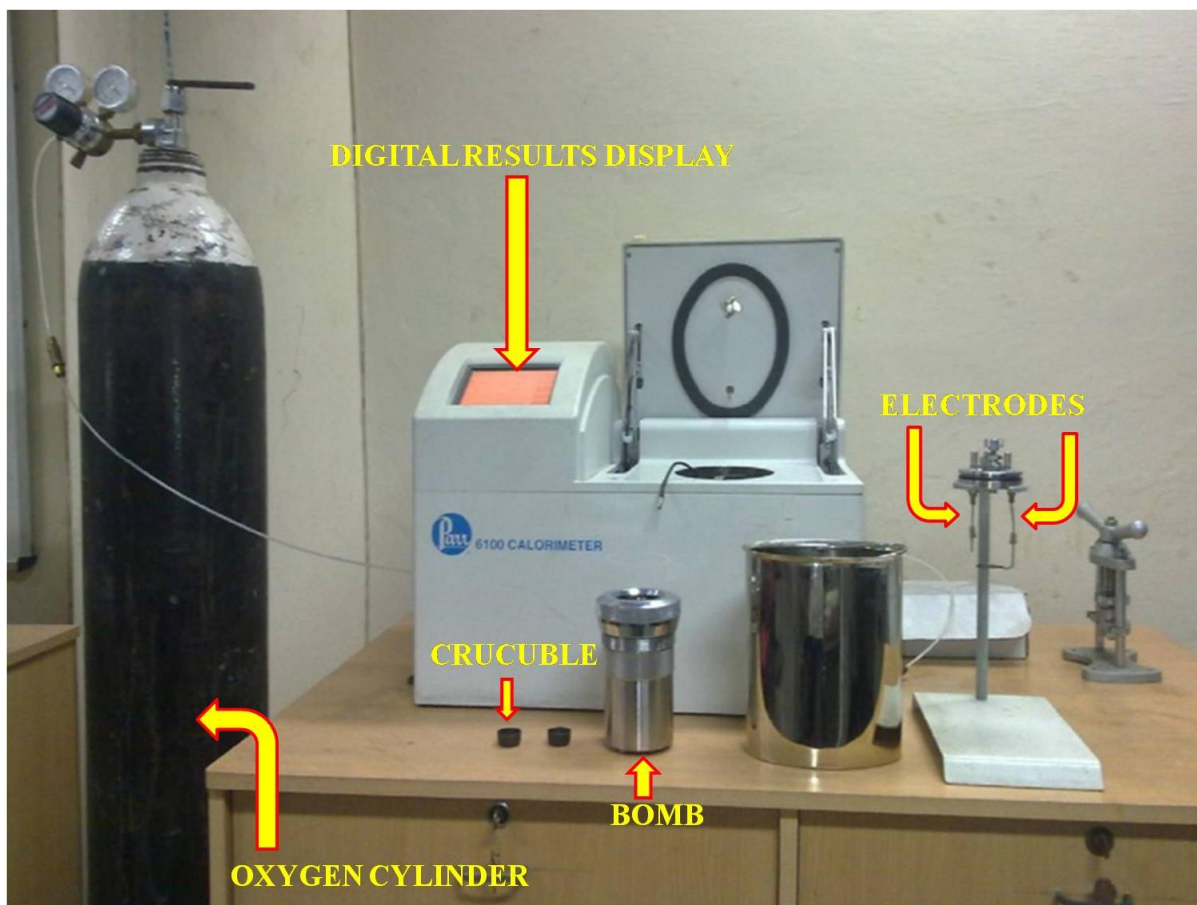
Plate 3.7: Parr 6100 Oxygen Bomb Calorimeter

3.3.4 Cold Flow Plugging Point

Cold Filter Plugging Point (CFPP) is defined as the minimum temperature at which the fuel filter does not allow the fuel to pass through it. At low operating temperature fuel may thicken and does not flow properly affecting the performance of fuel lines, fuel pumps and injectors. Cold filter plugging point of biodiesel reflects its cold weather performance. It defines the fuel's limit of filterability. The apparatus for CFPP measurement is shown in plate 3.8. The measurements were carried out as per the ASTM D6371 05(2010) standards. All the test samples were subjected to the CFPP test to evaluate the effect of increasing volume fractions of CME in the blend on the cold flow properties.
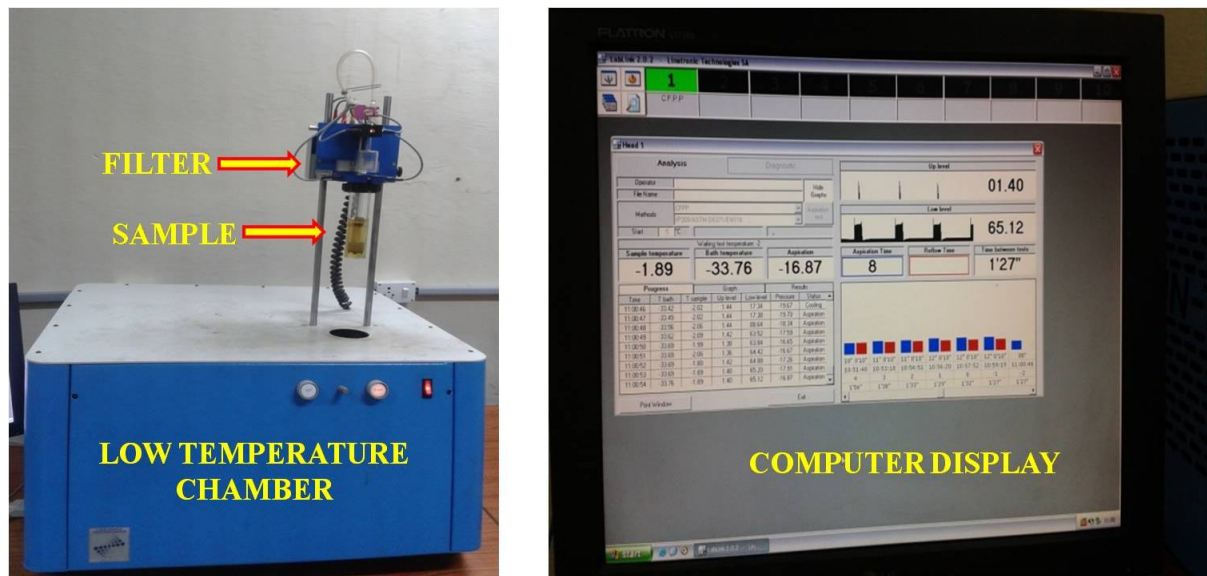
Plate 3.8: Cold flow plugging point apparatus

3.3.5 Oxidation Stability

Oxygen in the surrounding atmosphere causes a chemical reaction to take place within fuels overtime. This reaction, known as autoxidation, causes a fuel's composition to change, which in turn affects how a fuel is burned during combustion. During autoxidation, unsaturated fatty acids undergo radical reactions in which decomposition products are formed such as peroxides as the primary oxidation products and alcohols, carboxylic acids, and aldehydes as the secondary oxidation products. The time until occurrence of these secondary reaction products is referred to as the induction time or induction period, which is a good indicator for the fuel's oxidation stability. Biodiesel is known to oxidize faster than conventional diesel because it already contains a percentage of oxygen within itself. In the present investigation, the oxidation stability index (hours) was measured by the induction period of the sample due to electric conductance of the peroxides formed by bubbling oxygen from the water source system flowing at 10L/hour in the biodiesel Rancimat 873 shown in the Plate 3.9. The standard for the measurement was EN14112. The bath temperatures considered for the individual measurements was 110°C.
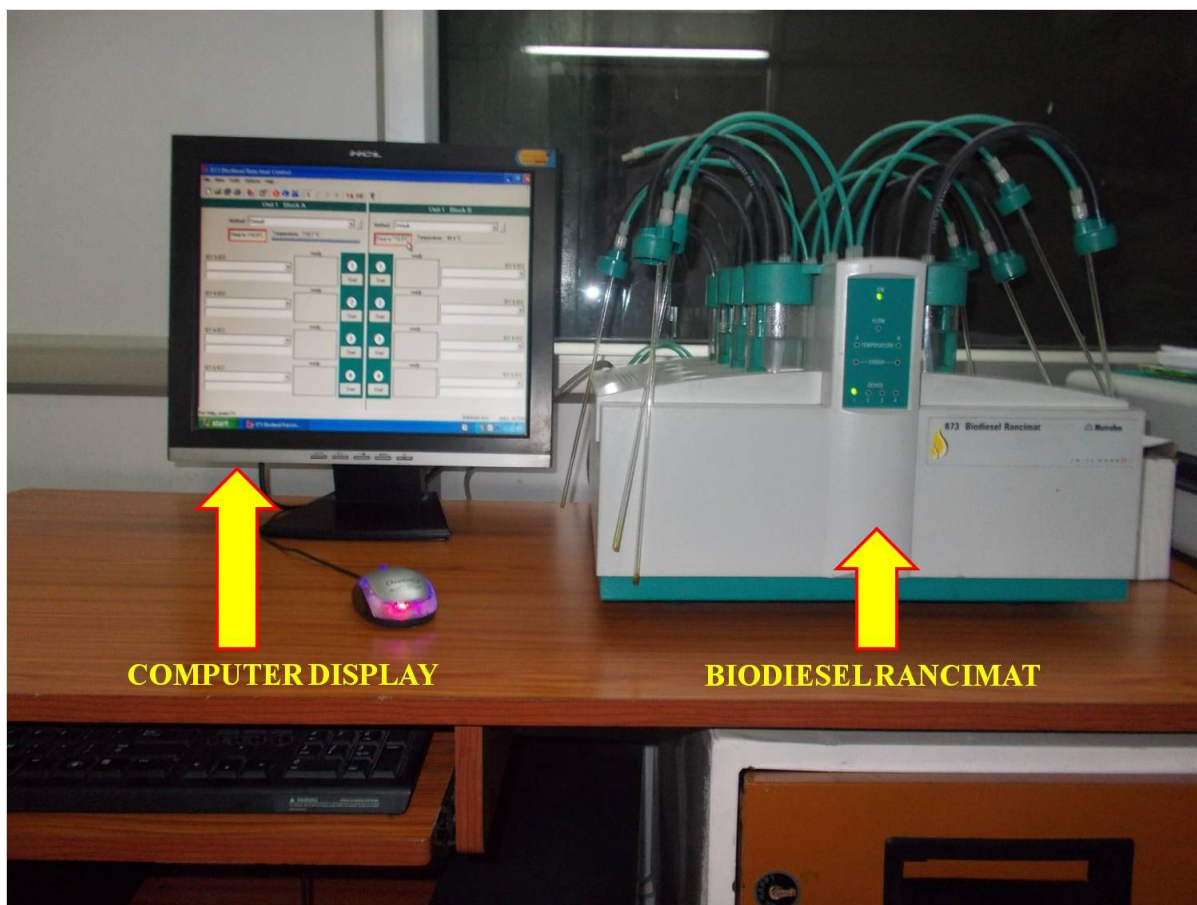
Plate 3.9: Biodiesel rancimat for measurement of oxidative stability

3.3.6 Gas Chromatography for Fatty Acid Profiles

The chromatography was conducted by injection of 20 µg of the CME into the equipment with a split/split-less injection port using flame ionization detector and N_2 as the carrier gas flowing at a rate of 8ml/min. The split ratio was 50:1 while the injection temperature was kept at 350^oC and sample elusion time of 45 minutes. This equipment was highly precise and provided the composition in terms of peaks on a chart paper. From the area of the individual peaks, the composition of CME was determined. Dilution of CME with methanol in 1:10 ratio provided better visibility of the peaks. The chromatography equipment is shown in the Plate 3.10.
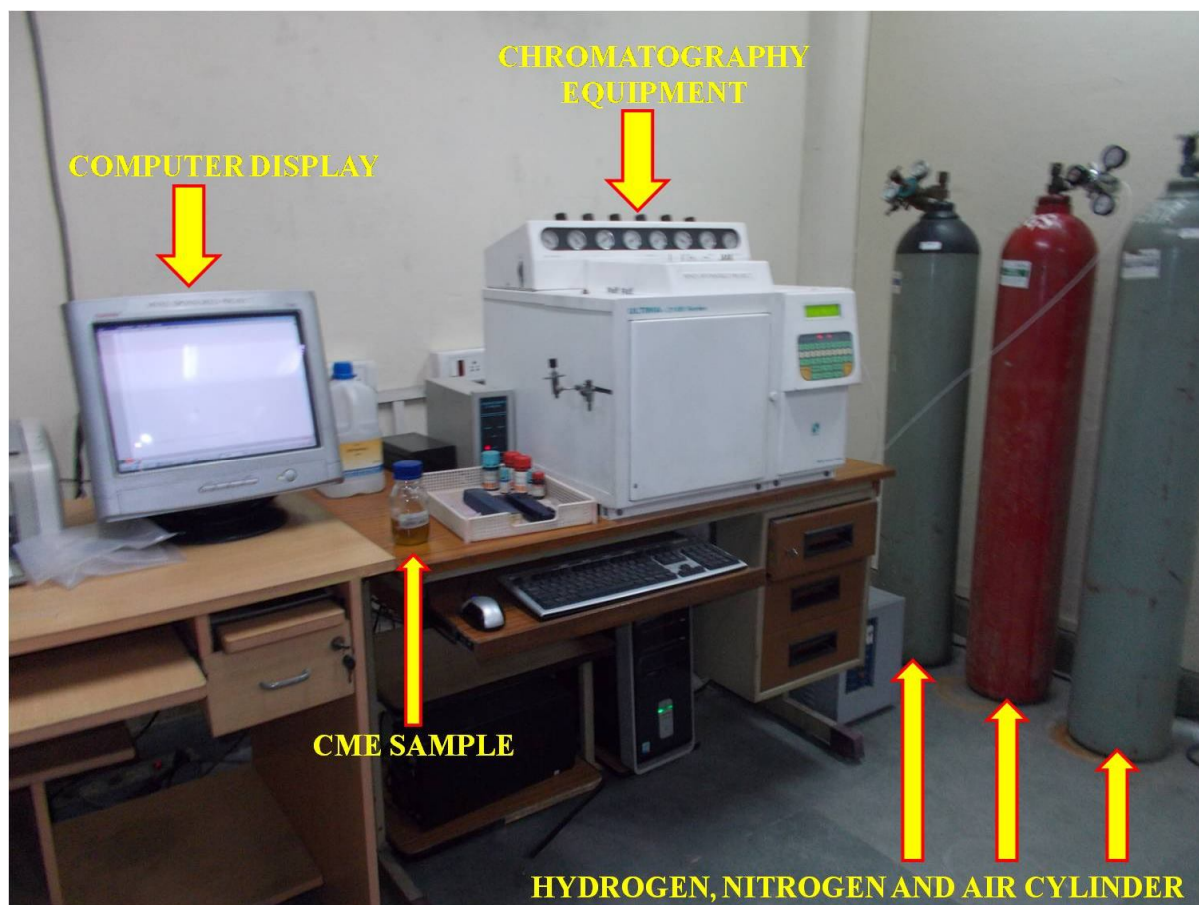
Plate 3.10: ULTIMA 2100 High Precision Liquid Chromatography Equipment

3.4 PREPARTION OF FUEL BLENDS FOR ENGINE TRIAL

As mentioned in the earlier sections, the National Biodiesel Mission envisaged 20% substitution of mineral diesel by biodiesel. The major reason of confining the biodiesel substitutions by 20% is the lack of feedstocks. Moreover, long term durability issues concerned with biodiesel usage in unmodified diesel engines are also one of the factors affecting the lower substitution targets of biodiesel. In this context, the present study considered 10%, 20%, 30% and 40% blends of CME in diesel. For better understanding the engine was also allowed to run on neat CME. Therefore, the test fuels for engine trial comprised of CME10, CME20, CME30, CME40 and CME100 along with the neat diesel.

The test fuel samples were prepared by volume wise substitution of diesel in the blend and the subsequent rigorous agitation using a high rpm hand blender. Plate 3.11 shows meat diesel and neat CME whereas various blends for the engine trial are shown in Plate 3.12
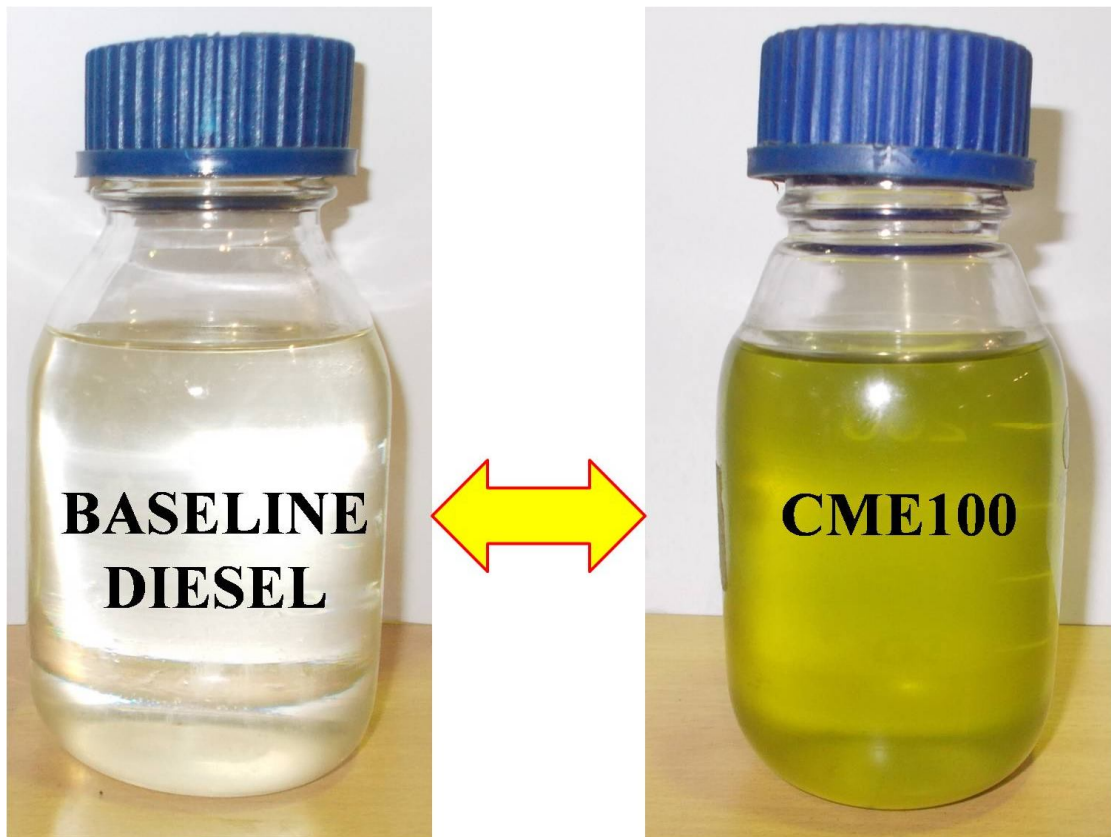
Plate 3.11: Neat diesel and neat Calophyllum Methyl Ester
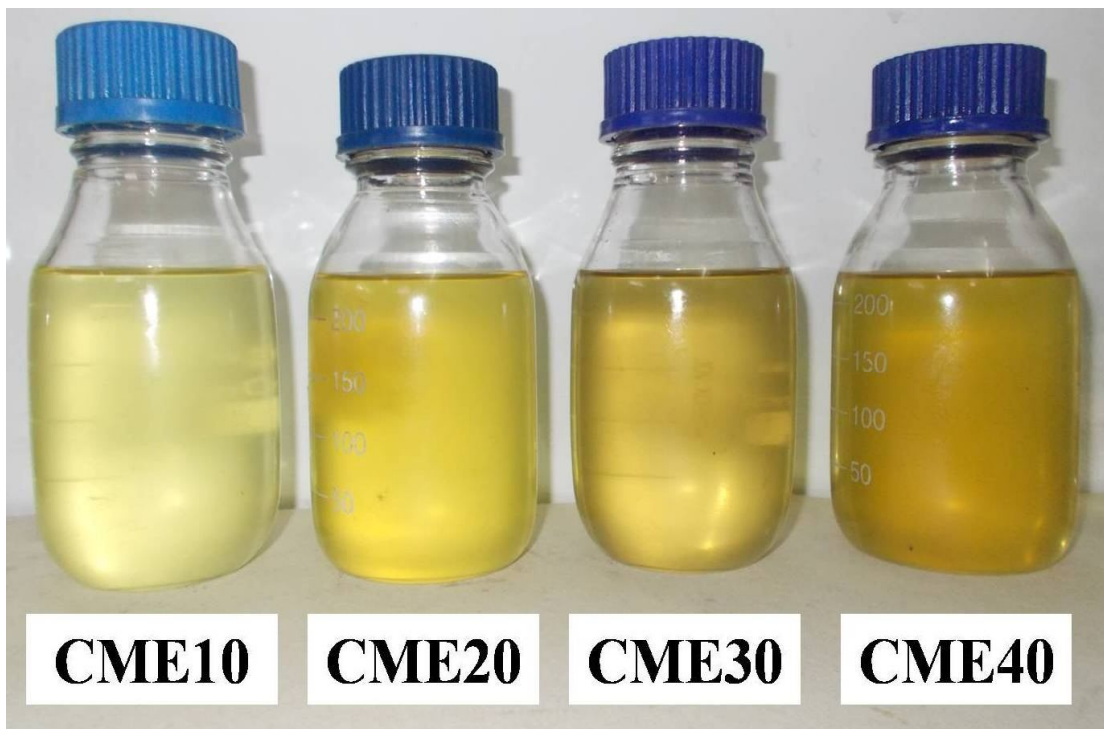
Plate 3.12: Various blends of Calophyllum biodiesel and diesel

3.5 SELECTION OF DIESEL ENGINE AND TEST RIG DEVELOPEMENT

3.5.1 Selection of Diesel Engine for Experimental trial

As indicated earlier, diesel engines play a vital role in Indian economy. Starting from small capacity single cylinder agricultural engines to heavy duty multi-cylinder railway locomotive and marine engines, they are widely used. However, in the present study a single cylinder and light duty diesel engine was chosen for experimental trials because of a number of reasons. Firstly, such types of engines are portable and hence can be used almost anywhere even in the remotest parts of the country where the conventional energy modes are not accessible. Secondly, these engines are an integral part of rural agrarian economy of India and thirdly there are at least two million such engines that actively running across the country making it one of the largest sources of decentralised power.

3.5.2 Development of Engine Test Rig

A single cylinder, four stroke, vertical, light duty, water cooled, diesel engine of Kirloskar make was chosen for the present engine trials. Such types of engines are generally used for agricultural activities or decentralised power generation purposes in India. Plate 3.13 shows the engine.

Plate 3.13: The Test Engine

The engine can be hand started using decompression lever and was provided with centrifugal speed governor. The cylinder was made of cast iron and fitted with a hardened high-phosphorus cast iron liner. The lubrication system used in this engine was of wet sump type, and oil was delivered to the crankshaft and the big end by means of a pump mounted on the front cover of the engine and driven from the crankshaft. The inlet and exhaust valves were operated by an overhead camshaft driven from the crankshaft through two pairs of bevel gears. The fuel pump was driven from the end of camshaft. The detailed specification of the engine is provided in table 3.3.

Table.3.3: Test Engine Specification

Make	Kirloskar
No. of cylinder	1
Strokes	4
Rated Power	3.5 kW@1500rpm
Cylinder diameter	87.5mm
Stroke length	110mm
Connecting rod length	234mm
Compression ratio	17.5:1
Orifice diameter	20mm
Dynamometer arm length	185mm
Inlet Valve Opening	4.5°BTDC
Inlet Valve Closing	35.5°ABDC
Exhaust Valve Opening	35.5°BBDC
Exhaust Valve Closing	4.5°ATDC
Fuel injection timing	23^0BTDC

The specification of the fuel injector is shown in table 3.4 and the injector with the spray cone is shown in Plate 3.14. Valve lift profile of the engine was essential for numerical studies to be discussed in the subsequent sections. Therefore, valve lift at each crank angle was generated for both inlet and exhaust valves. For this a scale was generated at the periphery of the dynamometer. The lift was measured by using a magnetic base dial gauge.

Table.3.4: Injector specification

Type	Bosch
No. of injector holes	3
Nozzle diameter	0.148 mm
Spray orientation angle	55°CA
Injection duration	18°CA
Full load diesel injection per cycle	32.8 mg
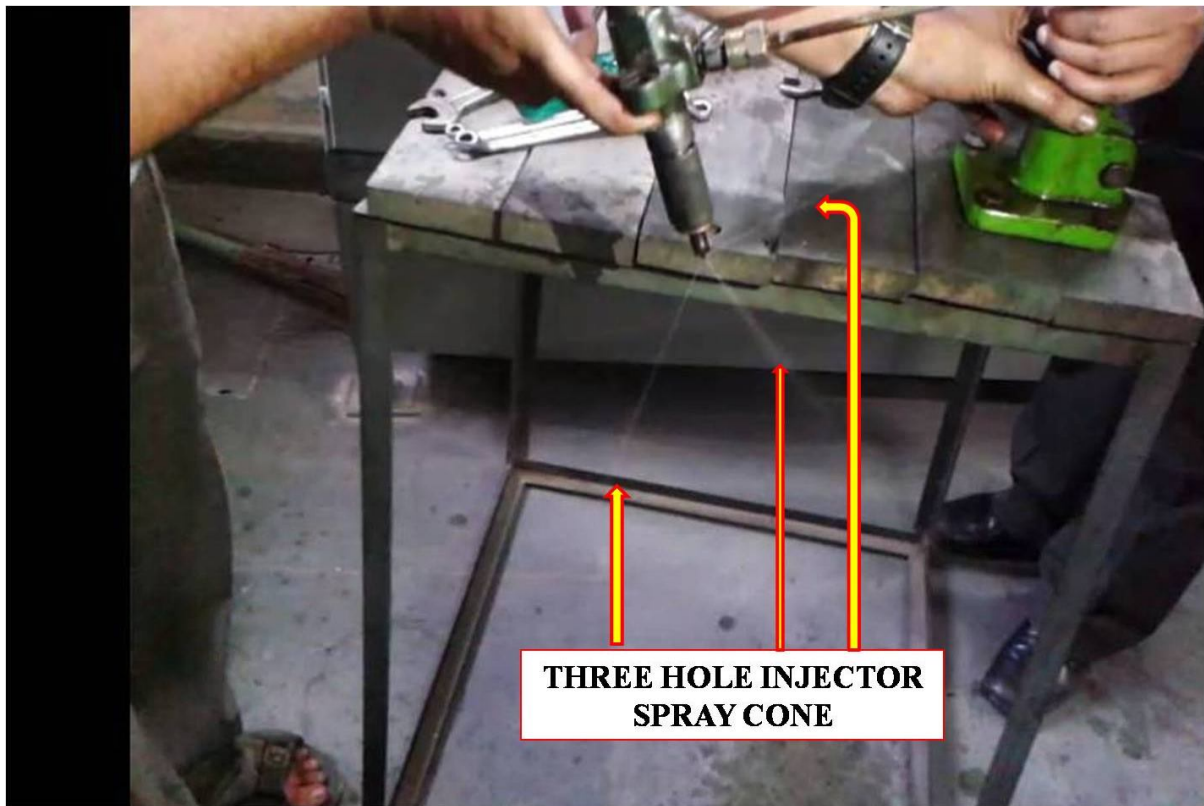
Plate 3.14: Three hole injector and the spray cone

For the provision of loading, a water cooled eddy current dynamometer of 7.5kW rating was coupled with the engine shaft. A high precision stain gauge type load cell was attached to the dynamometer to accurately transmit the engine loading. A magnetic pick up type rpm sensor was attached at the end of the dynamometer to measure rpm. The eddy current type dynamometer, the magnetic pick up type rpm sensor and the strain gauge type load cell are shown in Plate 3.15. The cooling water flow for the engine was 350 Liters/hour and that of the dynamometer was 75 Liters/hour. The flow of the cooling water was controlled by two numbers of rotameters, one for the engine and other for the dynamometer.
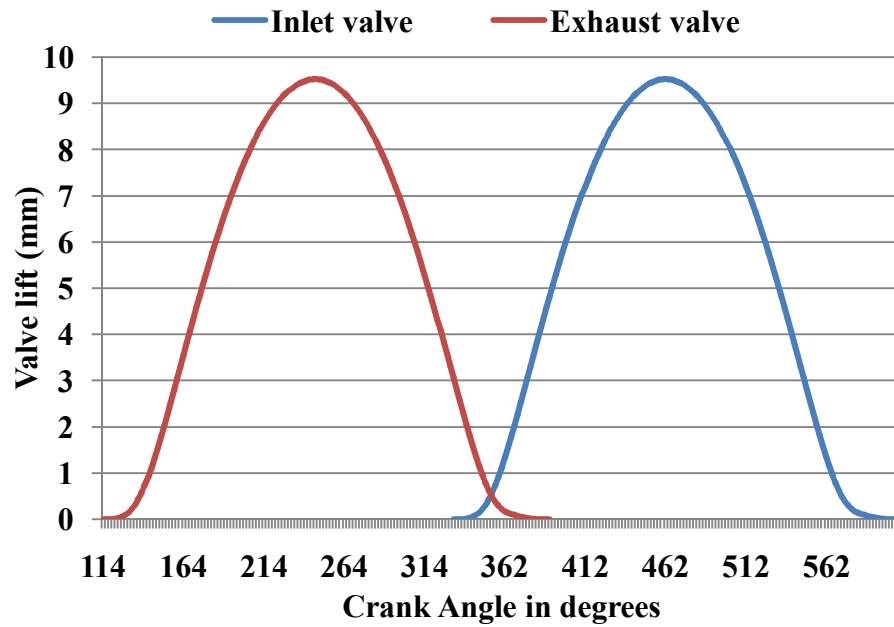
Fig.3.2: Valve lift profile
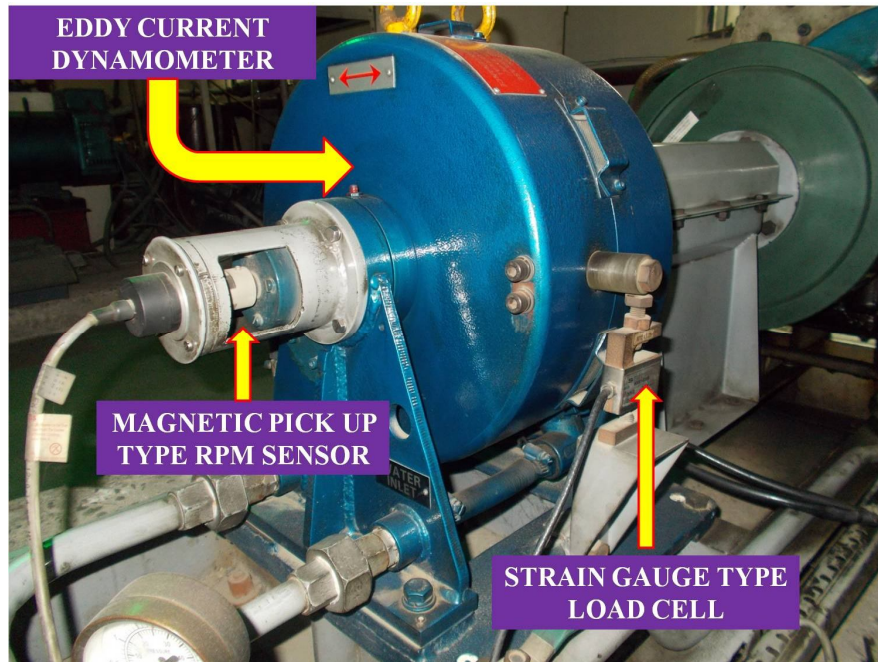
Plate 3.15: The eddy current type dynamometer with load and rpm sensor

Two sets of fuel tanks were provided for the engine set up. One tank was used for diesel and the other tank was meant for the blends of CME and diesel. The cyclic variation of combustion pressure and the corresponding crank angle was recorded using a "Kubeler" piezoelectric transducer, with a low noise cable, mounted into the engine head. The pressure

transmitter contained a piezoelectric sensor and charge amplifier. The maximum resolution of the pressure sensor was 1°CA. For exhaust gas temperature measurement, Chrome-Alumel K-Type thermocouples were employed close to the engine exhaust manifold. Air flow rate was measured using a mass airflow sensor. Fuel consumption rate was measured by 20cc burette and stop watch with level sensors. Fuel flow rate, air flow rate, load, rpm, pressure crank angle history and temperature data were fed to a centralized data acquisition system NI USB-6210, 16-bit. A personal computer with a software package "Enginesoft" was connected to the data acquisition system for online and subsequent offline analysis. Plate 3.16 shows the rotameters, the air flow and fuel flow sensors, the pressure transducer and the K-type thermocouple.
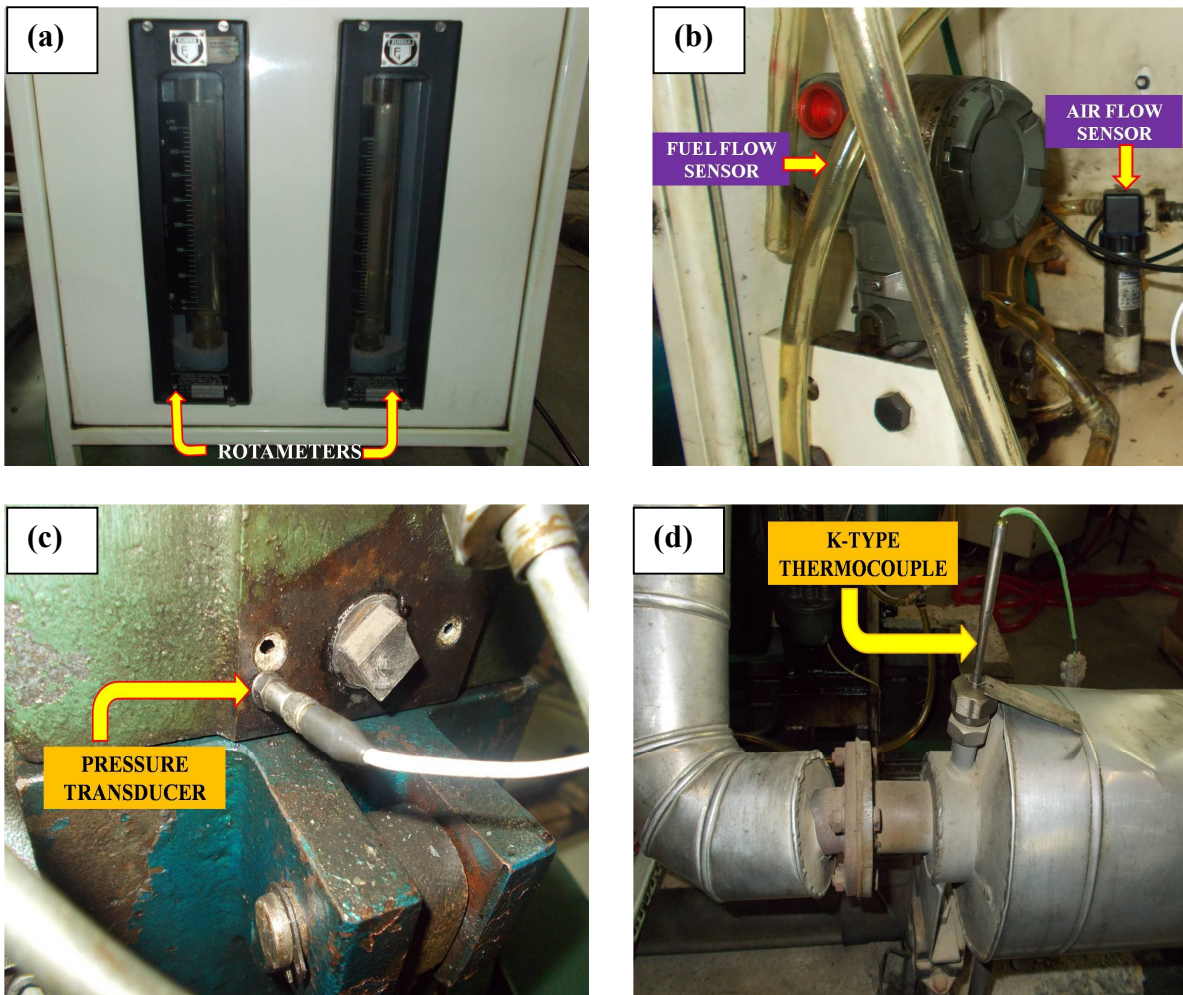
Plate 3.16: (a)-Rotamameters for water flow, (b)-Fuel and air flow sensors, (c)-Pressure transducer, (d)- K-type thermocouple

The control panel of the engine test rig comprised of the data acquisition system, burette for manual fuel measurement, orifice and "U" tube manometer for air measurement, sensor indicator for manual data access, load variation switch etc. The control panel was used for loading and unloading the engine. Besides, the air and fuel consumption data of the sensor was verified from the manual measurements. The data acquisition system inside the control panel received the signals and transmitted them to the computer. Plate 3.17and 3.18 shows the data acquisition system and the control panel.

Plate 3.17: The Data Acquisition System
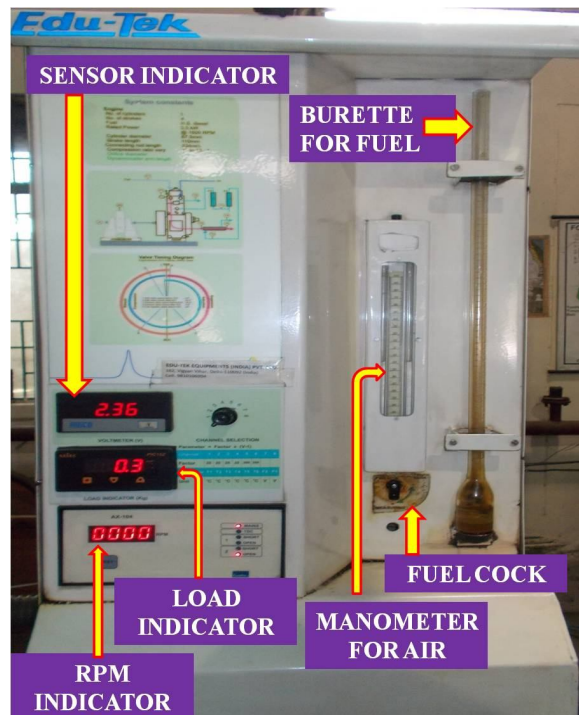
Plate 3.18: The Control Panel

The major pollutants appearing in the exhaust of a diesel engine are the oxides of nitrogen, smoke opacity, unburnt hydrocarbons, carbon monoxide, carbon dioxide, etc. For measuring the smoke opacity, AVL 437 smoke analyzer was utilized. This instrument gave reading in terms of percentage opacity. Of the light beam projected across a flowing stream of exhaust gases, a certain portion of light is absorbed or scattered by the suspended soot particles in the exhaust. The remaining portion of the light falls on a photocell, generating a photoelectric current, which is a measure of smoke density. The technical detailed specifications have been given in Appendix I. For measurement of UBHC, CO, CO_2 and NOx, AVL 4000 Light Di-Gas Analyzer was used. The detailed specification of AVL Di-gas Analyzer has been given in Appendix II. The gas analyzer and the smoke meter were connected to the engine exhaust by means of probes. Plate 3.19 shows the exhaust gas analyzer and the smoke meter.

Plate 3.19 Exhaust gas analyzer and smoke meter

The final experimental test setup consisted of the CI engine, engine cooling water system, the fuel supply and measurement system, air supply and measurement system, load variation and measurement system, rpm measurement system, in-cylinder pressure measurement system, emission measurement system, digital data acquisition system and computer. Fig.3.3 shows the engine test rig lay out comprising of individual components and their inter-connectivity.
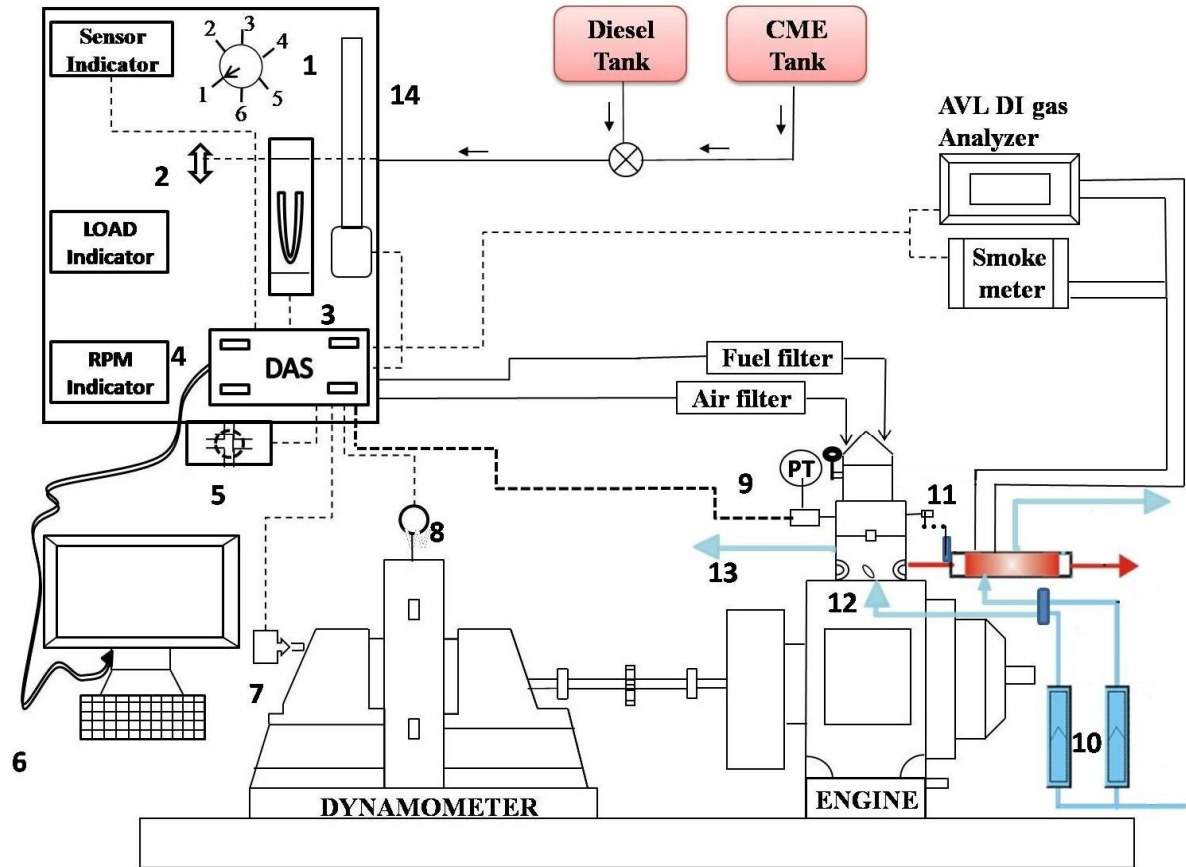
1- Sensor channel switch, 2-Fuel cock, 3-"U" tube manometer, 4- Data acquisition system, 5- Load variation switch, 6-Computer, 7-RPM sensor, 8-Strain gauge type load cell, 9-Pressure transducer, 10-Rotameters, 11- K-type thermocouple, 12- Inlet jacket water, 13-Exit jacket water, 14- Burette.

Fig.3.3: Layout of engine test rig

3.6 SELECTION OF ENGINE TEST PARAMETERS

The selections of appropriate test parameters are a vital part of engine research. The objectives of the present investigation is to determine the performance, emission and combustion characteristics of the diesel engine fuelled with CME and its blends followed by a comparison with the baseline data of diesel. The engine test was done as specified by IS: 10000. The main parameters desired from the engine were selected judiciously. Various engine test parameters are classified as the observed parameters and the calculated parameters.

Observed parameters are enlisted below.

1. Engine load.
2. Engine speed.
3. Fuel consumption rate.
4. Air flow rate.
5. In-cylinder pressure.
6. Emissions of CO, CO_2, NO_x, THC.
7. Exhaust temperature.
8. Smoke opacity.

Calculated parameters are given below.

1. Brake mean effective pressure (BMEP).
2. Brake thermal efficiency (BTE).
3. Brake specific energy consumption (BSEC).
4. Mass fraction burnt rate (MFB).
5. In-cylinder gas temperature (IGT).
6. Pressure rise rate (PRR).
7. Heat release rate (HRR).

Once the parameters were selected, the essential instruments required for sensing these parameters were installed at the appropriate points as described in the lay out diagram Fig. 3.18 in the experimental set-up.

3.7 MEASUREMENT METHODS AND CALCULATIONS

As already elaborated, the main components of the experimental setup are two fuel tanks (Diesel and CME), fuel consumption measuring unit, air flow rate measuring unit, eddy current dynamometer for loading arrangement, RPM meter, temperature indicator, in-cylinder pressure sensor and emissions measurement equipments. While carrying out the experiment the engine was always started with diesel and allowed to run for 30 minutes for warm up. For baseline diesel data, the observations were taken only after the prescribed 30 minutes were complete. For CME and its blends the fuel line was swapped, after the warm up period with neat diesel, allowing the CME blend tank to connect to the engine for taking observations. The load on the engine shaft was varied using the eddy current dynamometer.

3.7.1 Measurement of engine power and mean effective pressure

The brake power at the engine shaft was calculated by the formula in equation 3.6.

$$BP \ (kW) = \frac{2 \ X \ \pi \ X \ rpm \ X \ Load \ (Kg) X \ 9.81 \ X \ Dynamometer \ arm \ length \ (m)}{60 \ X \ 1000} \quad (3.6)$$

Similarly the brake mean effective pressure was calculated using the formula in equation 3.7.

$$BMEP \ (bar) = \frac{120 \ X \ BP \ (kW)}{L \ X \ A \ X \ N \ X \ 101.325} \quad (3.7)$$

Where L = Stroke length in meter.

A = Piston area in m^2

N = Engine rpm.

The rated power of the engine was 3.5 kW. However, after re-calibration it was found that the engine hardware was able to operate smoothly up to 4.7 kW at 1500 rpm. With the dynamometer arm length of 0.185 meter, it was calculated that 17.3 Kg corresponded to 100% of the engine load and 0.3Kg was equivalent to the zero load. Therefore, various loads applied to the engine were 0.3Kg, 3.7Kg, 7.1Kg, 10.8Kg, 14.5Kg and 17.3Kg corresponding to the loads of 0%, 20%, 40%, 60%, 80% and 100% of the calibrated load. All performance, emission and combustion data were recorded at each load for various test fuels.

On the basis of the above calculation, the brake power at 0%, 20%, 40%, 60%, 80% and 100% loads were 0.087kW, 1.056kW, 1.99kW, 3.01kW, 3.99kW and 4.71kW respectively where as the BMEP were calculated to be 0.13 bar, .53 bar, 2.88 bar, 4.36 bar, 5.77 bar and 6.82 bar in the same order.

3.7.2 Measurement of fuel flow

The fuel consumption of an engine is measured by determining the time required for consumption of a given volume of fuel. The mass of fuel consumed can be determined by multiplication of the volumetric fuel consumption to its density. In the present set up volumetric fuel consumption was measured using a fuel flow sensor inserted inside the control panel. The sensor signal was fed to the data acquisition system. The same data was available in "MSEXCEL" format from the "Enginesoft" software in the computer for offline

analysis. Moreover, the data was also available at the sensor indicator with the fourth channel slot. The sensor data in many cases was validated by manually taking the time for 20cc fuel consumptions in the burette by blocking the fuel cock. However, it was observed that the sensor data was more precise. The fuel flow sensor is already shown in the plate 3.14 (b).

Two important engine performance parameters i.e. brake thermal efficiency (BTE) and brake specific energy consumption (BSEC) were determined from the rate of fuel flow as shown below. Brake thermal efficiency is the ratio of brake power to the product of mass flow rate of fuel and its heating value. The BTE is calculated by the formula mentioned in equation 3.8.

$$\text{BTE (\%)} = \frac{BP\ (kW)}{mf\ X\ Qcv} \tag{3.8}$$

Where mf = Mass flow rate of fuel in (Kg/s)

Qcv = Calorific value of fuel (kJ/Kg)

Brake specific energy consumption is the amount of fuel energy consumed in order to generate one unit of shaft power. It is calculated by the standard formula mentioned in equation 3.9.

$$\text{BSEC (MJ/kWh)} = \frac{mf\ X\ Qcv\ X\ 3600}{BP(kW)} \tag{3.9}$$

3.7.3 Measurement of RPM

A magnetic pick up type rpm sensor was attached to the end of the dynamometer shaft which was toothed. This type of sensor consists of a permanent magnet, yoke, and coil. This sensor was mounted close to a toothed gear. As each tooth moved by the sensor, an AC voltage pulse was induced in the coil. Each tooth produced a pulse. As the gear rotated faster more pulses were produced. These impulse signals were fed digitally to the data acquisition system. The engine control module of the data acquisition system calculated the engine rpm which was subsequently displayed both in the control panel and the enginesoft database in the computer. The rpm sensor is already shown in plate 3.13.

3.7.4 Exhaust temperature and emission measurement

Chromel-Alumel K-type thermocouples were connected to a 6 channel digital panel meter to measure temperatures of exhaust gas. The meter was calibrated by a millivolt source up to 800° C. The sensor was placed close to the exhaust manifold of the engine. Plate 3.14 (d) showed the thermocouple position. The temperature data was observed both at the sensor indicator in the control panel as well as the enginesoft database.

As discussed above the gaseous pollutant emissions were measured using the gas analyzer and the smoke meter. The emission data was collected manually from the printed results of the analyzers as well as the enginesoft database from the computer.

3.7.5 Measurement of air flow

The air flow was measured using a turbine type flow meter installed inside the control panel. Plate 3.14 (b) shows the sensor in the previous sections. In principle, the tturbine flow meters use the mechanical energy of the fluid to rotate a "pinwheel" (rotor) in the flow stream. Blades on the rotor are angled to transform energy from the flow stream into rotational energy. The rotor shaft spins on bearings. When the fluid moves faster, the rotor spins proportionally faster. Blade movement is often detected magnetically, with each blade or embedded piece of metal generating a pulse. The transmitter processes the pulse signal to the data acquisition system that determines the flow of the fluid. The air flow data was available in the sensor indicator of the control panel and the enginesoft database. Moreover, there was another method available to validate the sensor data. It was based on the orifice and the air box method. The differential pressure across the orifice inserted in the air flow channel provides the air flow rate using the formula in equation 3.10.

$$\text{Mass of air (m)} = C_d \text{ X A X } \sqrt{(2gh_w\rho_w\rho_a)} \tag{3.10}$$

Where C_d = Co-efficient of discharge of orifice (0.6 in the present case).

A = Orifice area

g = Acceleration due to gravity

h_w = Height of water column

ρ_w/ρ_a = Density of water/air

However, it was observed that the sensor data were more precise.

3.7.6 In-cylinder pressure

As discussed in the earlier sections, the "Kubeler" piezoelectric transducer was used for in-cylinder pressure measurement. Plate 3.14 (c) shows the pressure transducer. The signals from the charge amplifier were fed to the data acquisition system where the engine control module converted the signals into digital data. The in-cylinder pressure data in terms of pressure – crank angle history was only obtained in the enginesoft database. In the present study the average of 91 cycles were considered for analysis of in-cylinder pressure crank angle data.

3.7.7 Characterisation of heat release rate

Evaluation of cyclic heat release is very much significant for combustion study. Various heat release models have been proposed by researchers for determining critical combustion parameters like heat release rate, pressure rise rate etc. In the present investigation, the heat release calculations described by Sorenson et al. [99] and Hanson et.al. [100] was referred. Although combustion in a CI, DI (compression-ignition, direct-injection) engine is quite heterogeneous, the contents of the combustion chamber are assumed to be homogeneous in the method suggested by Sorenson et.al. This type of heat release model is generally termed as zero-dimensional model in the literature. In contrast to the model proposed by Sorenson et.al., Hanson, have developed more complex, quasi-dimensional models, but it was only slightly more accurate than the zero-dimensional model. In the light of the above fact, the zero dimensional model proposed by Sorenson was considered for combustion characterisation.

The Sorenson's model is a thermodynamic model based upon energy conservation principle. Neglecting the heat loss through piston rings [101] the energy balance inside the engine may be written as

$$\frac{dQ}{d\theta} - \frac{dQw}{d\theta} = \frac{d(\text{mu})}{d\theta} + P\frac{dV}{d\theta} = mC_v\frac{dT}{d\theta} + P\frac{dV}{d\theta} \qquad (3.11)$$

Where $dQ/d\theta$ = Rate of net heat release inside the engine cylinder (J/°CA)

            $dQ_w/d\theta$ = Rate of heat transfer from the wall (J/°CA)

            m = Mass flow of the gas (Kg)

            u = Internal energy of the gas (J/Kg)

P = Cylinder pressure (bar)

V = Gas volume (m³)

θ = Crank angle (°)

T = Gas temperature (°K)

C_v = Specific heat at constant volume (J/Kg°K)

Now the ideal gas equation is given by PV = mRT   (3.12)

Where R = Universal gas constant

The derivative of universal gas equation with respect to crank angle is given by

$$P\frac{dV}{d\theta} + V\frac{dP}{d\theta} = mR\frac{dT}{d\theta}$$ (3.13)

Putting equation (3.13) in equation (3.111), the heat release rate is derived as follows.

$$\frac{dQ}{d\theta} = P\frac{Cp}{R}\frac{dV}{d\theta} + V.\frac{Cv}{R}\frac{dP}{d\theta} + mT\frac{dCv}{d\theta} + \frac{dQw}{d\theta}$$ (3.14)

Where C_p = Specific heat at constant pressure (J/Kg°K)

Equation (3.14) is further simplified for actual heat release calculation and is given below.

$$\frac{dQ}{d\theta} = \frac{1}{\gamma-1}(V\frac{dP}{d\theta} + \gamma P\frac{dV}{d\theta}) - \frac{dQw}{d\theta}$$ (3.15)

Where   γ = ratio of specific heats

In a four-stroke engine, crank angles are typically given with zero values at the TDC, (top dead center) between the intake and exhaust strokes. However, the important heat release events occur between SOI (start of injection, typically about 337°) and EVO (exhaust valve opening, typically about 500°). The trigonometric functions require their arguments in radians that are essential for gas volume calculations. The formula for calculating the arguments for the trigonometric functions, equation 3.16 was used.

$$\theta_{rad} = \frac{\pi(\theta - 360 + \text{Phase})}{180}$$ (3.16)

Where θ_{rad} = argument of trigonometric functions (radians)

          Phase = phase shift angle (°CA)

The piston displacement was needed in calculating the gas volume. It is provided in equation 3.17.

$$\frac{S}{R} = [1 - \cos(\theta_{rad})] + \frac{L}{R}\{1 - [\sqrt{1 - \frac{\sin(\theta rad)}{L/R}}]^2\}$$ (3.17)

Where S = piston displacement from TDC (m)

R = radius to crank pin (m)

L = connecting rod length (m)

Then the gas volume was calculated as in the equation 3.18

$$V = V_{cl} + S A_p \tag{3.18}$$

Where A_p = top area of piston (m^2) = π(bore)^2/4

bore = cylinder bore (m)

V_{cl} = clearance volume (m^3)

r = compression ratio

Stroke = piston stroke (m)

The combustion chamber wall area, needed for heat transfer calculations, was given in the equation 3.19.

$$A_{wall} = 2A_p + \pi \text{ (bore) } S \tag{3.19}$$

Equation 3.19 ignores the area associated with the piston cup, but the approximation has little effect on the heat release results. The heat release equation (3.15) requires the calculation of dP/dθ. It can be shown that the slope at the jth point of the curve defined by n sequential points is as shown in equation 3.19.

$$\frac{dPj}{d\theta} = \frac{n\Sigma(Pi\theta i) - \Sigma Pi\ \Sigma\theta i}{n\Sigma(\theta i)2 - (\Sigma\theta i)2} \tag{3.20}$$

Where n is an odd number and each summation is from [j − (n − 1)/2] to [j + (n − 1)/2]. When a shaft encoder is used to trigger pressure measurements, the points are equally spaced along the θ axis at spacing $\Delta\theta$. The choice of n is a compromise; a larger n helps to combat noise in the pressure data, but may also obscure real changes in the heat release curve. In the present case with $\Delta\theta$ = 1°, choice of n = 7 was found to fit the equation 3.15 over 4° of the pressure trace and was a suitable compromise. Equation 3.21 shows the pressure smoothing technique applied to the noise in pressure data.

$$P_{j+1} = P_j + \frac{dPj}{d\theta}\Delta\theta \tag{3.21}$$

Calculation of dV/dθ was accomplished as per the equation 3.22.

$$\frac{dVj}{d\theta} = V_j - V_{j-1} \tag{3.22}$$

In-cylinder gas temperature varies rapidly throughout the cycle. Consequently the value of γ varies with temperature. The ideal gas law was used to calculate the spatially averaged temperature in the combustion chamber as mentioned in the equation 3.23.

$$T_j = \frac{P_j V_j}{MR_g} \qquad (3.23)$$

Where $\qquad$ T_j = bulk gas temperature at point j (°K)

$\qquad\qquad\qquad$ R_g = idea gas constant = 8.314/29 = 0.287

$\qquad\qquad\qquad$ M = mass of charge, g = (1 + AF) mf

$\qquad\qquad\qquad$ AF = air/fuel ratio of engine

$\qquad\qquad\qquad$ m_f = mass of fuel injected into each engine cycle (g)

The value of γ varies with temperature and the calculation of γ from the bulk gas temperature is shown in equation 3.24.

$$\gamma = \left(1 - \frac{R_g}{C_p}\right)^{-1} \qquad (3.24)$$

According to Crowell [102], the value of C_p/R_g can be calculated from the equation 3.25

$$\frac{C_p}{R_g} = A_0 + A_1 T_j + A_2 T_j^2 + A_3 T_j^3 + A_4 T_j^4 \qquad (3.25)$$

Where $\qquad$ A_0 = 3.04473

$\qquad\qquad\qquad$ A_1 = 1.33805e-3

$\qquad\qquad\qquad$ A_2 = –4.88256e-7

$\qquad\qquad\qquad$ A_3 = 8.55475e-11

$\qquad\qquad\qquad$ A_4 = –5.70132e-15

The final term in equation 3.15 was $dQ_w/d\theta$, the term was calculated using the equation 3.26.

$$\frac{dQ_w}{d\theta} = \frac{hA_{wall}(T_w - T_j)}{24N} \qquad (3.26)$$

Where $\qquad$ $dQ_w/d\theta$ = rate of wall heat transfer (J/°CA)

$\qquad\qquad\qquad$ T_w = Effective wall temperature (°K)

$\qquad\qquad\qquad$ h = Convective heat transfer coefficient (J/s·m^2·°K)

$\qquad\qquad\qquad$ N = Engine speed (rpm)

The heat transfer calculations are not very sensitive to the wall temperature, T_w; a wall temperature of $T_w = 475°K$ has been found to give satisfactory results. Eichelberg [103] developed the following equation for convective heat transfer:

$$h = 0.00767 \, S_p^{0.333} \, (P_j T_j)^{0.5} \tag{3.27}$$

Where, S_p = mean piston speed, m/s = 2 R ω/π = 2 (stroke) N/60

          ω = crankshaft speed (rad/s)

3.7.8 Calculation of mass fraction burnt

Mass fraction burned (MFB) in each individual engine cycle is a normalized quantity with a scale of 0 to 1, describing the process of chemical energy release as a function of crank angle. The determination of MBF is commonly based on burn rate analysis – a procedure developed by Rassweiler and Withrow (published in 1938). It is still widely used because of its relative simplicity and computational efficiency, despite the approximate nature of this method [104].

The Rassweiler and Withrow procedure is based on the assumption that, during engine combustion, the pressure rise Δp_j (at crank angle increment) consists of two parts: pressure rise due combustion (Δpc_j) and pressure change due to volume change (Δpv_j).

Therefore, $\Delta p_j = \Delta pc_j + \Delta pv_j$ (3.28)

Assuming that the pressure rise Δpc_j is proportional to the heat added to the in-cylinder medium during the crank angle interval, the mass fraction burned at the end of the considered j^{th} interval may be calculated as [104]

$$MFB = \frac{mb \, (i)}{mb \, (total)} = \frac{\Sigma_0^i \Delta Pc}{\Sigma_0^N \Delta Pc} \tag{3.29}$$

Where N is the total number of crank angles in the in-cylinder pressure ~ crank angle data.

3.7.9 Calculation of other combustion parameters

A comprehensive spreadsheet in "MSEXCEL" was prepared using the concepts of section 3.7.7 and section 3.7.8. The rate of heat release for the test fuels were calculated using equation (3.15). The cumulative heat release was calculated by summing up the heat release per crank angle data throughout the cycle. The pressure rise rate for various test fuels were calculated from the spread sheet data base using equation (3.20) and (3.21). The bulk gas temperature was calculated using equation (3.23) and the mass fraction burnt was

calculated from equation (3.29). Calculation of wall heat transfer was based on equation (3.26) and the subsequent mathematical operations in the spreadsheet.

Ignition delay for the test fuels were calculated as the difference between the fuel injection angle and the crank angle corresponding to the MFB of 0.05. Similarly the total combustion duration for the test fuels was calculated as the difference between the crank angles corresponding to MFB of 0.10 to MFB of 0.95.

3.8 ACCURACIES AND UNCERTAINTIES OF THE EXPERIMENTAL RESULTS

Table 3.5 shows the accuracies and uncertainties associated with various measurements.

Table.3.5: Accuracies and uncertainties of measurements

S.N.	Measurements	Measurement Principle	Range	Accuracy
1	Engine load	Strain gauge type load cell	0-25 Kg	±0.1Kg
2	Speed	Magnetic pick up type	0-2000 rpm	±20 rpm
3	Time	Stop watch	--	±0.5%
4	Exhaust Temperature	K-type thermocouple	0-1000°C	±1^{0}C
5	Carbon monoxide	Non-dispersive infrared	0-10% vol.	±0.2%
6	Carbon dioxide	Non-dispersive infrared	0-20% vol.	±0.2%
7	Total hydrocarbons	Non-dispersive infrared	0-20,000 ppm	±2 ppm
8	Oxides of nitrogen	Electrochemical	0-4000 ppm	±15ppm
9	Smoke	Photochemical	0-100%	± 2%
10	Crank angle encoder	Optical	0-720 °CA	± 0.2^{0}CA
11	Pressure	Piezoelectric	0-200 bar	± 1 bar
	Calculated results			**Uncertainty**
12	Engine power	--	0-8 kW	±1.0%
13	Fuel consumption	Level sensor	--	±2.0%
14	Air consumption	Turbine flow type	--	±1.0%
15	BTE	--	--	±1.0%
16	BSEC	--	--	±1.5%
17	Heat release	Sorenson model	--	±5.0%
18	In-cylinder temp.	Ideal gas equation	Up to 3000°K	±5.0%

It may be observed that all of the measurements exhibited higher accuracy. The repeatability of all measurements were checked throughout the experimental trial and found sufficiently close. It may be noted that the various measurands like viscosity, density, calorific value, oxidative stability, chromatography etc. in the property characterisation were not subjected to the data accuracy. It was so because equipments like chromatography and oxidative stability were high precision and regularly calibrated equipments. Therefore, the % uncertainties in these equipments were very low. For viscosity, density, calorific value and cold flow plugging point the % uncertainty was less than 0.1%. The repeatability of these equipments were checked and found highly satisfactory.

3.9 PROCEDURES FOR ENGINE TRIAL

The engine was started at no load by pressing the exhaust valve with decompression lever and it was released suddenly when the engine was hand cranked at sufficient speed. After feed control was adjusted so that engine attained rated speed and was allowed to run (about 30 minutes) till the steady state condition was reached and the exhaust gas temperature corresponding to that load stabilized. The enginesoft software was connected to the data acquisition system and allowed to run. Automatic data entry system was activated and the resolutions of various sensors were set. All the sensors were allowed to perform at their minimum resolutions. For pressure crank angle history the average of 91 cycles were chosen for each load where as for performance and emission studies the average of 10 consecutive data was chosen to minimize error. To validate the sensors, and the electronic gadgets, the time for 20cc fuel consumption and the manometric readings of air consumption were taken repeatedly and averaged several times. The manual data so obtained was compared with the "enginesoft" data and found very close to each other. Similarly, data in the printed copies of emission analyzers were often compared with the emission data of the enginesoft database and found all most identical. All the performance, emission and combustion parameters were evaluated at each load thoroughly. Many times the trial was repeated to avoid any discrepancy in results. As mentioned earlier, for baseline data, diesel tank was used and thereafter for blends the CME tank was used by swapping the fuel line by the rotary valve. Every time the engine was started with diesel and stopped after running at least 20 minutes on diesel.

3.10 SETTING UP THE GEOMETRICAL MODEL FOR NUMERICAL STUDIES

3.10.1 Introduction

It may be observed that the in-cylinder experimental studies on diesel engine combustion are highly cumbersome and expensive. The limitations of the sensors and the uncertainties put a lot of restriction on the quality of results obtained. In this context, numerical simulations in the form of computational fluid dynamics (CFD) are usually conducted to obtain data not measurable using conventional experimental methods [105] such as in the present case, the determination of in-cylinder pressure at 0.1°CA differences. Moreover, the results of numerical simulation if properly validated against an actual experiment can provide real insight in to the underlying phenomena of fuel oxidation and emissions formation [89]. This enables significant time and cost saving [106], which assists in the rapid development of engines and combustion concepts [107,108].

From the discussion above, it is evident that integrated CFD based numerical simulation models holds great promise as a low cost, high fidelity approach to underpin combustion research of biodiesel fuel in diesel engine. Opportunities to further advance this lie in improving the accuracy and robustness of the models, as well as the computational runtime of the simulations. Locally and internationally, the level of activity is growing, as do the range of applications and extent of literature detailing on these. With that in mind, the main objective of the final part of the present research work is to generate a three dimensional geometrical model consistent with the test engine and its simulation using ANSYS 14 ICEM module with integrated chemical kinetic reaction mechanism for the CME fuelled light-duty diesel engine. The experimental data was used to validate the model. Only the results of neat CME operation was considered as a pilot study for numerical simulation.

3.10.2 Numerical simulation set up

A finite volume based commercial CFD software; ANSYS 14 operating on Windows 7, 64 bit operating system was used for the simulation study. The IC Engine module of the software was highly versatile with provisions for geometry generation, meshing and simulation. However, the geometry was generated using CATIA VR 16 and subsequently

imported to ANSYS for further analysis. Fig.3.4 shows the geometrical model in shaded and wire frame view in ANSYS 14. An exploded view in CATIA VR 16 was provided for better clarity. The model was tried with best spirit to be in line with the actual engine dimensions. However, some discrepancies may be there.
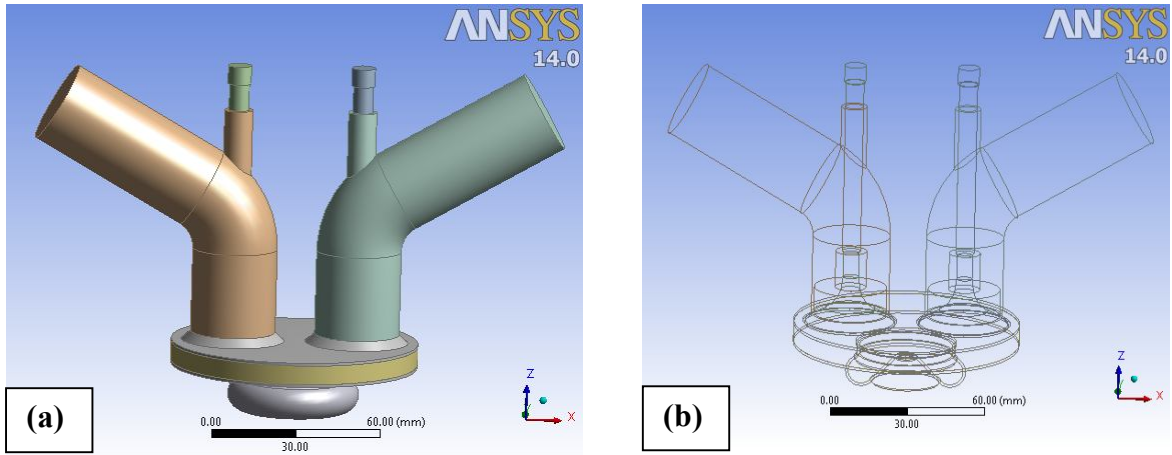
Fig. 3.4: Three dimensional shaded (a) and wire frame (b) view in ANSYS 14 geometry modeler
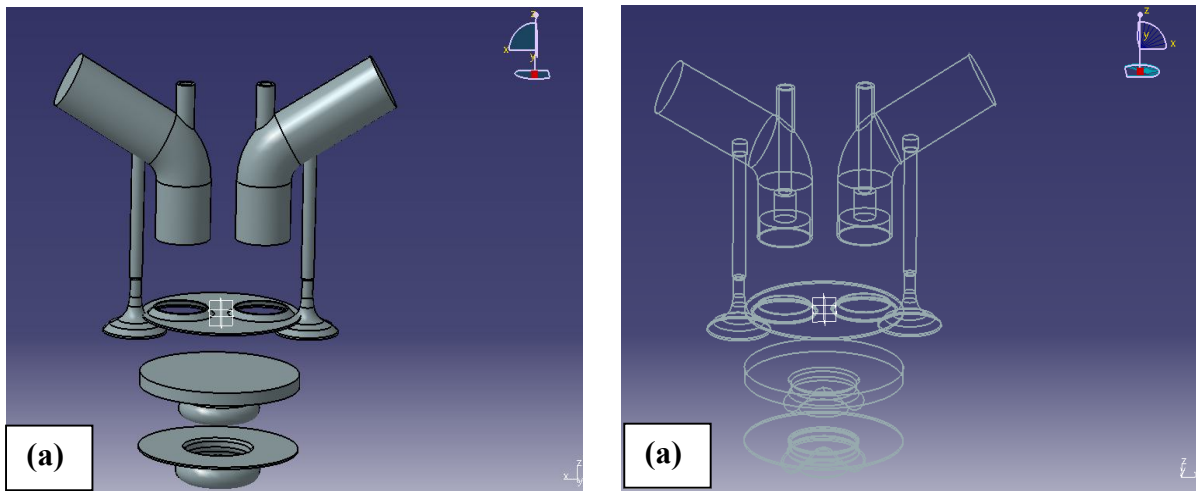
Fig. 3.5: Three dimensional exploded views shaded (a) and wire frame (b) in CATIA VR16

3.10.2 Mesh generation and grid independence study

The model for engine simulation was in consistent with the specifications of the light duty single cylinder diesel engine mentioned in the table 3.3 and table 3.4. The valve lift profile used in the simulation was consistent with Fig. 3.2 As shown in the plate 3.13, the

nozzle contained three symmetric holes placed 120° apart from each other. In a view of this 120° symmetrical sector mesh was used instead of the whole 360°. This reduced the computational time significantly. However, the interaction between the spray models was not visualised on account of the sector mesh. The 27, 832 cell mesh generated was adequate for the combustion simulation. The simulation only covered the closed portion of the engine cycle i.e. from the intake valve closure at 35.5°CA ABDC to the exhaust valve opening at 35.5°BBDC.

For the grid independence study, three different resolutions i.e. fine, medium and coarse of mesh were considered. The experimental firing case using CME100 was considered as the benchmark. Despite the variation in number of cells and the simulation time required, the three mesh resolutions indicated close pressure profiles. Key results of the grid independence study are shown in table 3.6.

Table.3.6: Grid independence study

S.N.	Mesh resolution	Fine	Medium	Coarse
1	Interval size (mm)	2	2.5	3.0
2	Number of cells	27832	12292	7868
Firing case with CME100				
3	Time for simulation (hours)	7.35	5.5	3.87
4	Peak pressure (bar)	63.9	62.5	62.1
6	% Difference with experimental CME100	0.58	-1.6	-2.2

The table 3.6 shows that the finer meshes provided the best matching with the experimental results. However, the medium and the coarse meshes were also very close to the experimental data. Besides, finer mesh consumed 25.17% and 47.34% higher simulation time as compared to the medium and coarse meshes respectively. In the present study finer mesh with 2mm interval size and 27,382 cells were considered for final mesh and combustion simulation. The use of fine mesh is justified here as higher number of cells is needed in firing cases to accurately capture the overall spray and combustion characteristics, which in turn dictates the accuracy of the simulated combustion and emissions processes. The meshed geometry is shown in Fig. 3.6.
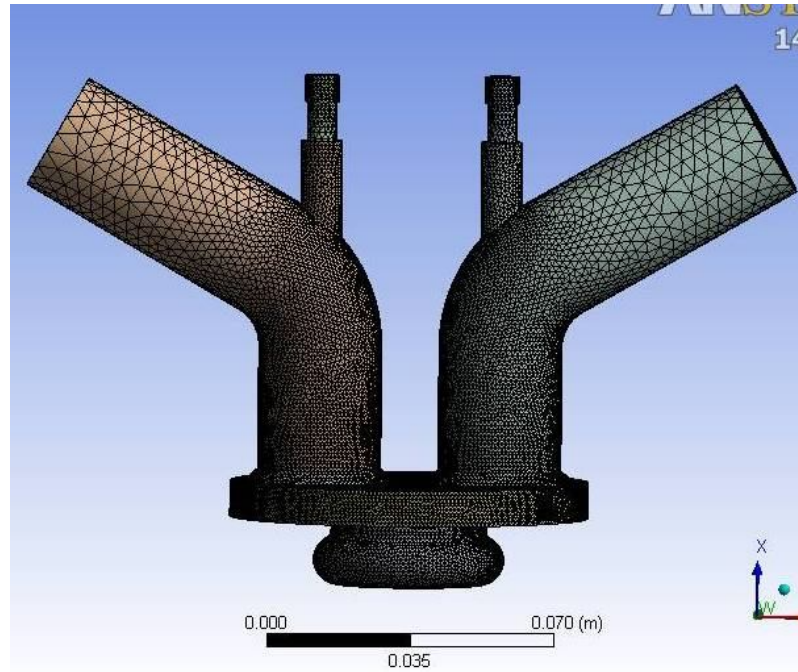
Fig. 3.6: Meshed geometry

3.11 SIMULATION OF THE MESHED GEOMETRICAL MODEL

3.11.1 Chemistry of the fuel

Compact biodiesel mechanism (CBD) comprises of the methyl crotonate (MC) and methyl butanate (MB) reaction mechanisms, which are the surrogate biofuel models of unsaturated and saturated fatty acid methyl esters, respectively [89]. The mechanism was able to account for oxidation, ignition and combustion of Calophyllum biodiesel. A thermal NO_x model was included in the combustion chemistry to represent the formation of NO [109]. It should be noted here that the fuel models used in the simulation were surrogate fuel models. As such, the fuel properties between the experimental and surrogate fuels differ significantly. In order to obtain properties similar to those of the experimental study, the MC and MB ratios in the simulated fuel should have been explicitly specified. However, the same was not done in the present case due to lack of expertise.

For the injection parameters, information related to the location of the injector and spray direction were obtained from in-cylinder measurements. The start and end of fuel injection were fixed at 23° BTDC and 5° BTDC, respectively. Fuel temperature was set as 285 K, while the injector nozzle diameter was 0.148 mm. The spray axis was retained at 45°

from the vertical axis, with a spray cone angle of approximately 55°. Initial injection velocity of the CME fuel droplets at the nozzle was made at 140 m/s. The injection profile for the simulation followed that of a square-wave injection rate shape for simplicity.

3.10.4 Various sub-models for numerical simulation

In modeling the spray breakup event, Wave model was implemented [85] with the values of model constants, B0 and B1 retained at 0.59 and 8 respectively for all the simulation cases. The selection of current B1 value was simply to produce reasonably good prediction on the ignition delay period, as well as the magnitudes and timings of peak pressure. As detailed experimental measurements for fuel penetration and droplet size distribution were not available for comparison, processes such as spray breakup and penetration were assumed to be appropriately simulated as long as combustion and emissions profiles were predicted accurately. The droplet collision model in this study followed the O'Rourke algorithm for particle tracking which stochastically estimated the frequency of the droplet collisions and their possible outcomes such as bouncing, coalescence or grazing. Discrete phase wall boundary conditions to describe events such as spray jets impingement on piston surface and cylinder walls were set here as wall film. Droplets can splash, rebound or stick on the surface and spread out to form a thin layer of film, and this depends on the respective Weber number. In-cylinder turbulence was modeled using the Re-normalization Group (RNG) k–e model, while Unsteady Laminar Flamelet model was implemented as the turbulence–chemistry interaction model. Reaction rates were calculated based on the Arrhenius equations as prescribed by the CBD mechanism. Effects of chemical kinetics were described by a relatively simple one-dimensional laminar flamelet, which translated to greater savings in computational runtime as compared to the typical computationally expensive reactor models. All the required sub-models used in the present simulation are listed in the table 3.7.

Table.3.7: Implemented sub-models for simulation

S.N.	Sub model name	Type
1	Turbulence model	RNG k-ε
2	Turbulence chemistry	Unsteady laminar flamelet
3	Discrete phase wall boundary	Wall film
4	Drag law	Dynamic drag
5	Droplet collision	Chemkin
6	Spray break up	Wave break up
7	Ignition and combustion	CBD
8	NO_x	Thermal NO

3.10.5 Model Validation

For the validation of the integrated numerical model, the experimental combustion data of CME 100 was compared with the simulation data. The ignition delay period, peak in-cylinder pressure and general shape of pressure profiles were used as validation criteria. The combustion data of experimental and the simulated regimes matched satisfactorily with each other. The details of pressure profile matching are provided in the results section.

RESULTS AND DISCUSSION

In the present investigation, the various results obtained were categorized as the production optimization of CME, physico-chemical characterization of CME and its blends, Performance, emission and combustion characteristics of diesel engine fuelled with various test fuels, results of the numerical simulation and model validation.

4.1 OPTIMIZATION RESULTS FROM CENTRAL COMPOSITE DESIGN

4.1.1 Optimal results for esterification

As discussed in the previous section, the reaction time, reaction temperature and concentration of catalyst (PTSA) was considered as the factors and the %FFA as the response in the esterification stage.

Table 4.1: Analysis of Variance for esterification

Source	Sum of Squares	Df	Mean square	F value	p-value	Remarks
Model	14.52	7	2.07	24.54	< 0.0001	Significant
A- Catalyst Conc.	7.33	1	7.33	86.79	< 0.0001	Significant
B-Temperature	0.58	1	0.58	6.83	0.0227	Significant
C- Time	0.10	1	0.10	1.21	0.2929	Not-significant
AB	0.042	1	0.042	0.50	0.4940	Not-significant
B2	3.78	1	3.78	44.74	< 0.0001	Significant
C2	0.44	1	0.44	5.20	0.0416	Significant
AB2	1.14	1	1.14	13.47	0.0032	Significant
Residual	1.01	12	0.085	1.01	0.00421	Significant
Lack of fit	1.01	7	0.14	1.01	0.3221	Not significant
Pure error	0.000	5	0.000			
Corr Total	15.53	19				

20 Numbers of experiments were performed with various permutation and combinations of the factors as indicated by the test matrix generated from the design experiment software. The results so obtained in the experiments were fed to the software again and the analysis of variance (ANOVA) table was generated as shown table 4.1. Good co-relational results were obtained with a reduced quadratic model. It may be observed that with a p value of <0.0001, the model was statistically significant. On simpler terms the quadratic model could effectively predict, with minimal error, the actual %FFA during large scale esterification of the oil [110]. In addition, the catalyst concentration and the reaction temperature were also statistically significant to the % FFA reduction while time was found to be in-significant. However, it was the popular perception that reaction time is a significant factor in the esterification process. The lack of significance in the present case may be explained by the fact that the reaction time range for the design was maintained at 60 minutes to 120 minutes based upon the pre-design assessment. However, it was later on realized that most of the esterification process was complete within 60 minutes leading to the insignificance of time beyond 60 minutes for the esterification process. This model was further validated by the F-value of 24.54 that implies the model is significant on a general note that these values are used in evaluating the null hypothesis of the experiment and useful in validating the hypothesis. Other features include the R-Squared value of 0.9347 indicating that the model can explain the effects up to about 93% while the remaining 7% cannot be explained by the model. The Adeq. Precision value defined as a function of noise to signal ratio. The value obtained was 20.83 suggesting that the model has an adequate signal and can be employed on the response surface to be navigated. The statistical values of the esterification are shown in the table 4.2. In summary, the model was a good model because the fitness and accuracy of a model depends on the degrees of freedom, the lack of fitness must be non-significance and the R-squared values should be closer to 1 [111] all of which are satisfied. These three factors (catalyst concentration, time and temperature) are referred to as the main effect while the effects of the combination of factors is regarded as the interactive/compounding effects in different categories of first term, second term, third term and so on. According to the results, first order compounding terms B^2 and C^2 showed statistical significance while A^2 showed in-significance on the response. Other factor combinations also showed some degrees of significance in the model terms.

Table.4.2: Statistical values of the esterification of Calophyllum vegetable oil

Stdandard Deviation	0.29	R-Squared	0.9347
Mean	3.70	Adj. R-Squared	0.8966
C.V %	7.87	Pred. R-Squared	0.6852
PRESS	4.89	Adeq. Precision	20.831

The model was used to develop an equation that can easily predict the coded and the un-coded values of the model terms that affects the response. The equation generated for the un-coded values of the model is given below as (4.1).

$$Y = \beta_0 + \sum_{i=1}^{3} \beta_i x_i + \sum_{i=1}^{3} \beta_{ii} x_i^2 + \sum \sum_{i<j=1}^{3} \beta_{ij} x_i x_j \qquad (4.1)$$

Where X_i and X_j are the un-coded independent variables β_o is the intercept, β_i, β_{ii} and β_{ij} represent the linear, quadratic and interaction constant coefficients respectively while Y is the response (Yield).

The equation for the coded values is provided as (4.2)

$$FFA = 4.16 - 1.14A - 0.21B - 0.087C - 0.072AB - 0.51B^2 - 0.17C^2 + 0.59A\ B^2. \qquad (4.2)$$

The equation developed above is showing the contributions of all the factors either synergistic or antagonistic effects on the response. The positive signs in front of each medel term show that it is contributing positively to the response while a negative sign implies that the response is suffered due to the effect of that model term. Additionally, the value before the model term defines the coefficient of the model term in the quadratic equation. The final un-coded equation for the quadratic second order model is presented as equation (4.3).

$$FFA = -55.05 + 40.79C + 2.01Tp + 0.03Tm - 1.42C*Tp - 0.01Tm^2 - 1.93Tp^2 + 0.01C*Tm^2$$

$$(4.3)$$

Where C = Catalyst (PTSA) concentration in % of oil mass.

T_p=Reaction temperature in °C

T_m=Reaction time in minutes

The probability of finding the optimal point of the actual and the predicted yield is represented by the normal probability plots of residuals [112]. In this study, the normal plot of the residuals indicated the uniform normal distribution of error within the limits of the

experiments showing the close linearity of the plots. It was observed from the Fig.4.1that there occur partial groupings of the experiments concentrating along the range of -1 to +1 on the normal probability against internally studentized residuals plot possible due to presence of the central point around this region.
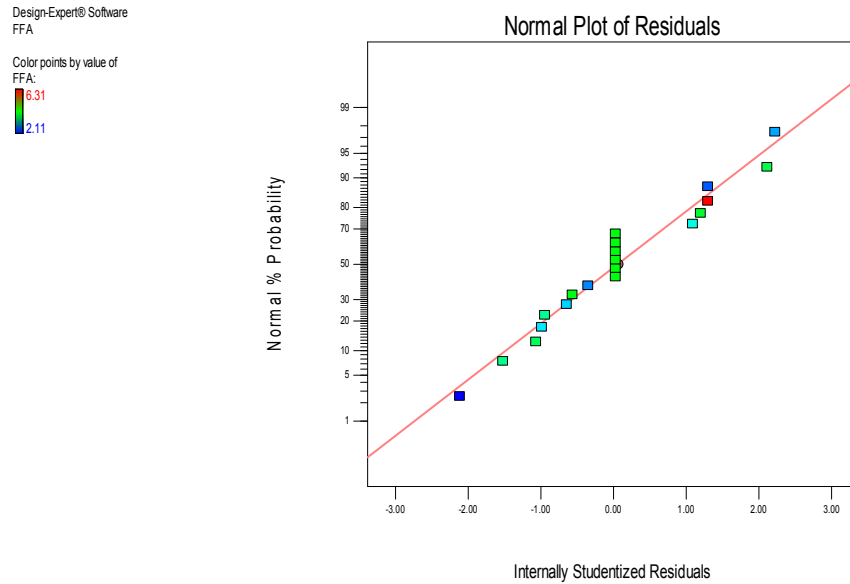
Fig. 4.1: Normal probability plot of residuals
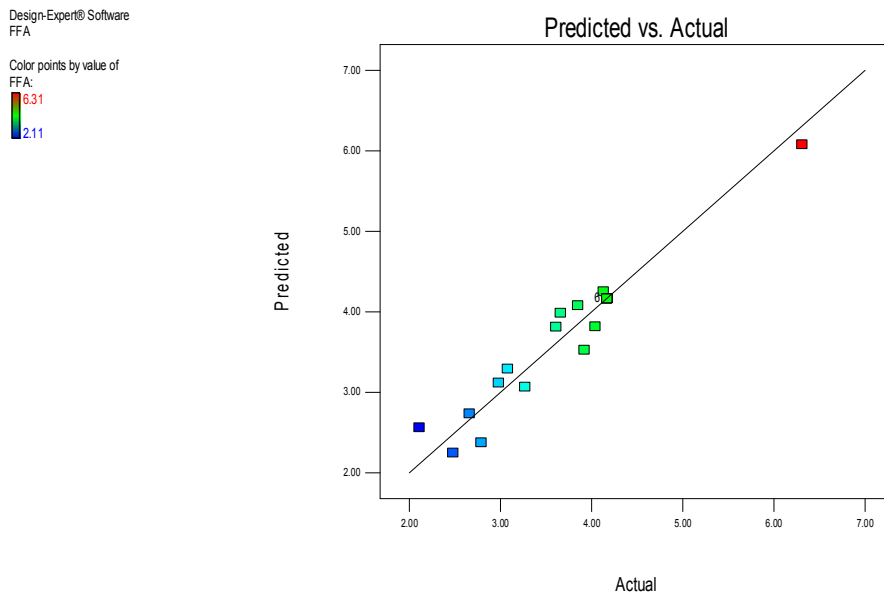
Fig. 4.2: Predicted and observed values of the designs

Fig.4.2 shows the predicted and the observed values of the design. It may be clearly seen that the predicted and the observed values are grouped pretty close to each other and concentrating around a medium range. In the light of the above discussions it may be stated that the model can effectively predict the %FFA for large sized transesterification with minimal error.

The experimental and predicted values corresponding to various permutation and combinations of process parameters as per the design test matrix is shown in table 4.3.

Table.4.3 Predicted and observed values of FFA

Experiment No	Coded Level			Predicted % FFA	Observed% FFA
	X_1	X_2	X_3		
1	-1	-1	-1	4.25	4.13
2	-1	-1	+1	3.29	3.08
3	-1	+1	-1	3.98	3.66
4	-1	+1	+1	2.73	2.66
5	+1	-1	-1	4.08	3.85
6	+1	+1	-1	3.12	2.98
7	+1	+1	+1	3.81	3.61
8	0	0	-0.5	2.56	2.11
9	0	0	+0.5	6.08	6.31
10	0	-0.5	0	2.25	2.48
11	0	+0.5	0	3.07	3.27
12	-0.5	0	0	2.37	2.79
13	+0.5	0	0	3.82	4.04
14	0	0	0	3.53	3.92
15	0	0	0	4.16	4.17
16	0	0	0	4.16	4.17
17	0	0	0	4.16	4.17
18	0	0	0	4.16	4.17
19	0	0	0	4.16	4.17
20	0	0	0	4.16	4.17

*For the coded level table 3.1 may be referred.

It may be observed that the predicted and the observed %FFA was very close in all the cases validating the previous assumption that the model was a good fit one. Now the three dimensional surface was plotted using the model in design experiment software. The response surface graph represents the main and interactive effects of the factors on the response (% FFA). The plot is shown in Fig. 4.3.

It could be seen from the graph that the catalyst concentration and the temperature were the most important factors affecting the response. The graph shows how the increase in both catalyst concentrations and temperature reduced the % FFA of the oil while the FFA was found to be higher than 5.4% likely due to the antagonistic effects of the factors on the yield as indicated in the equation (4.3).
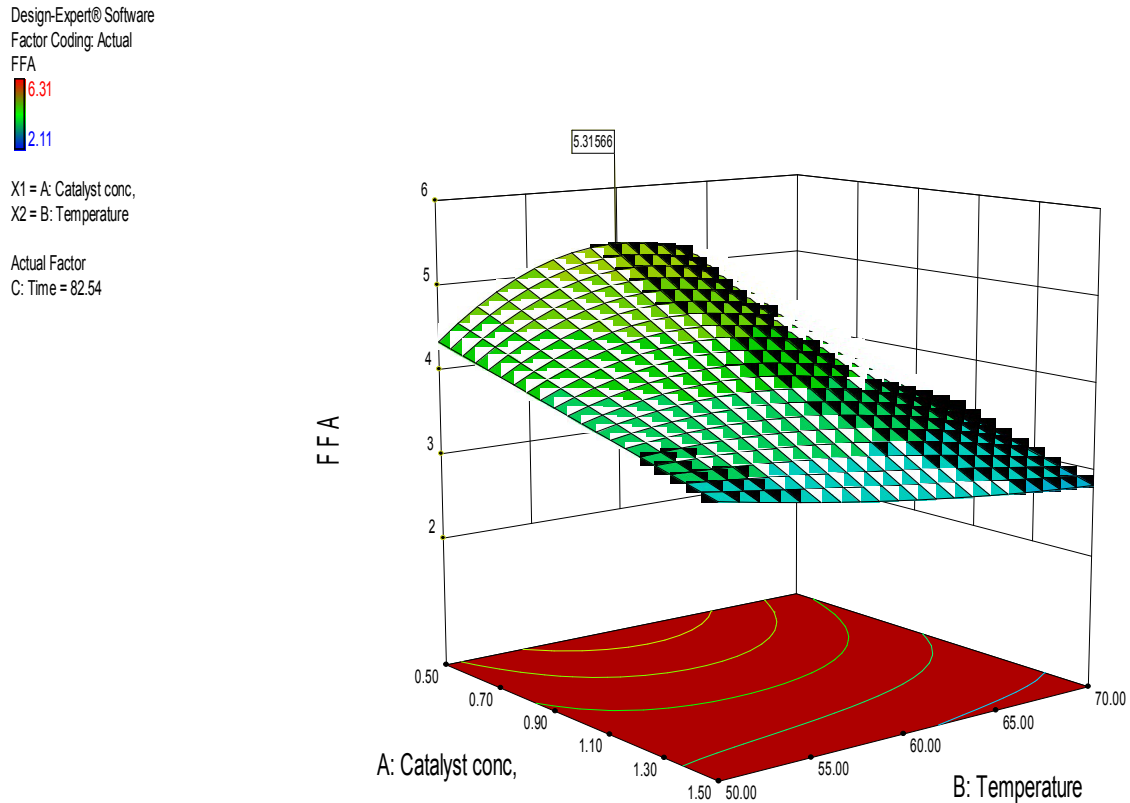
Fig. 4.3: Response surface for esterification

An optimal FFA of 4.74% was predicted by the model with catalysts concentration of 1.5%, reaction temperature of 65°C and reaction time of 60 munities. This suggested that the catalyst concentration was not enough to reduce completely the FFA value below the required 2% recommended for transesterification. However, looking at the initial FFA of 23.52% the reduction was found to be encouraging.

4.1.1 Optimal results for transesterification

A similar design of experiment was used for the transesterification of the oil to biodiesel. In this case, the catalyst concentration (% wt of KOH), the reaction and the reaction time were considered as independent variables keeping the methanol to oil molar ratio and the stirring speed constant. 20 Numbers of experiments were performed with various permutation and combinations of the factors as indicated by the test matrix generated from the design experiment software. The results so obtained in the experiments were fed to the software again and the analysis of variance (ANOVA) table was generated as shown table 4.4.

Table 4.4: Analysis of Variance for transesterification

Source	Sum of squares	Df	Mean square	F-value	p-value prob >F	Remarks
Model	1063.83	11	96.71	44.62	< 0.0001	Significant
A-Catalyst Conc.	262.66	1	262.66	121.19	< 0.0001	Significant
B- Temperature	113.34	1	113.34	52.29	< 0.0001	Significant
C-Time	9.95	1	9.95	4.59	< 0.0006	Significant
AB	154.00	1	154.00	71.06	< 0.0001	Significant
AC	58.75	1	58.75	27.11	< 0.0008	Significant
BC	116.59	1	116.69	53.79	< 0.0001	Significant
A2	163.69	1	163.69	75.53	< 0.0001	Significant
B2	27.54	1	27.54	12.70	0.0074	Significant
ABC	53.87	1	53.87	24.86	0.0011	Significant
A2C	37.04	1	37.04	17.09	0.0033	Significant
AB2	331.81	1	331.81	153.10	< 0.0001	Significant
Residual	17.34	8	2.17			
Lack of fit	7.47	7	2.49	1.26	0.3815	Not- Significant
Pure Error	9.87	5	1.97			

The table highlighted the degrees of accuracy of the data and statistical reliability of the results. The model was found to be significant with p-value<0.0001, F-value 44.62 and lack of fit as not-significant. However, the model that fit to the data was a cubic model instead of a quadratic one obtained in the previous stage. Besides, this model treated the reaction time as a significant parameter unlike that affect the process. Table 4.5 shows the statistical values of the transesterification stage.

Table 4.5: Statistical values for transesterification

Std. Dev.	1.47	r-squared	0.9840
Mean	92.05	Adj. R-squared	0.9619
C.V %	1.60	Pred R-Squared	0.6277
Press	402.53	Adeq. Precision	25.045

The final equation for the yield and the effects of the individual as well as the interactive effects of the factors on the yield is given below as equation (4.4).

$$\text{Yield} = +95.28-6.81A+2.88B+1.33C-4.39\,AB+2.71AC+3.82BC-3.35A^2-1.38\quad B^2-2.60ABC-3.34A^2C+10.01AB^2 \tag{4.4}$$

The final uncoded values for the percentage yield as a function of the independent variables is given as equation (4.5).

$$\text{Yield}= 601.41+659.71C+25.03T_p-1.19T_m\;23.85C*T_p+1.05C*T_m+0.01*T_p*T_m+13.33C^2-0.21*T_p^2-8.65C*T_p*T_m-0.22C^2*T_m+0.20C*T_p^2 \tag{4.5}$$

Where C = Catalyst (KOH) concentration in % of oil mass.

T_p = Reaction temperature in °C

T_m = Reaction time in minutes

The predicted and actual values were correlated by the graph showing the precision as well as the normal distribution of the data as a function of the percentage yields for both actual and predicted. The plot between the predicetd and the actual values are provided in the Fig. 4.4. The three dimensional response surface for the tranesterification stage is provided in the Fig. 4.5.
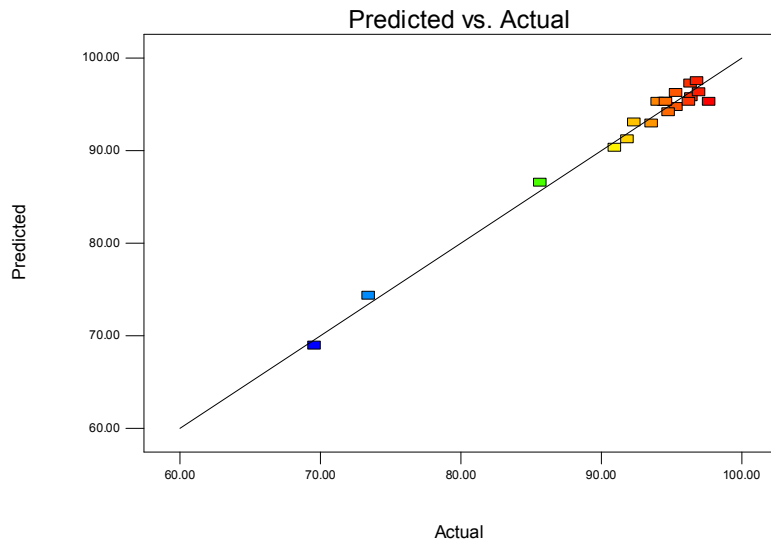
Fig. 4.4: Predicted and observed values of the designs
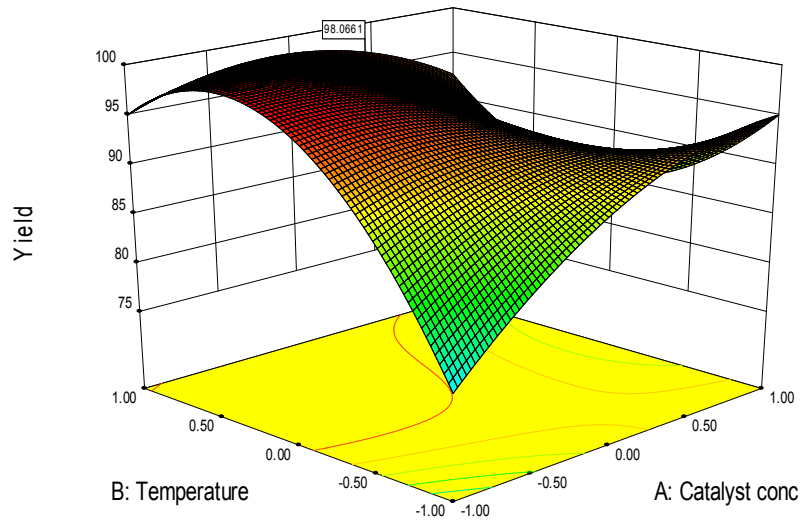
Fig. 4.5: Response surface for transesterification

The response surface graph in the Fig.4.5 shows the effects of the reaction temperature and the catalyst concentration as it affect the yield is presented in the graph. It indicates the synegistic effects of the independent variables as can be clearly seen on the graph. Low catalyst concentration and low reaction temperature negatively affected the yield while the increase in temperature increases the yield to a pointcloser to the bioling point of

methanol before a slight decrease in the yield was observed. The increase in biodiesel yield at higher temperature is due to the fact that viscosity of oils decreases at high temperature and results in an increased reaction rate and shortened reaction time, thereby, increasing the biodiesel yield it also increases with increase in reaction time at low catalyst concentration [112]. The same trend was observed for catalyst concentration as the increase in the catalyst resulted in the increase in the yield but was also found to decrease slightly with the highest catalyst concentration. This could be attributed to the formation of much glycerol that results in persistant washing . For the transesterification of the Calophyllum oil to biodiesel, the optimal yield was predicted as 96.48% under the reaction conditions of 0.88% catalyst (KOH) concentration reacting at temperature of $62.75^{\circ}C$ for the reaction time of 90 minutes with constant stirring speed and a oil to methanol molar ratio of 1:6.

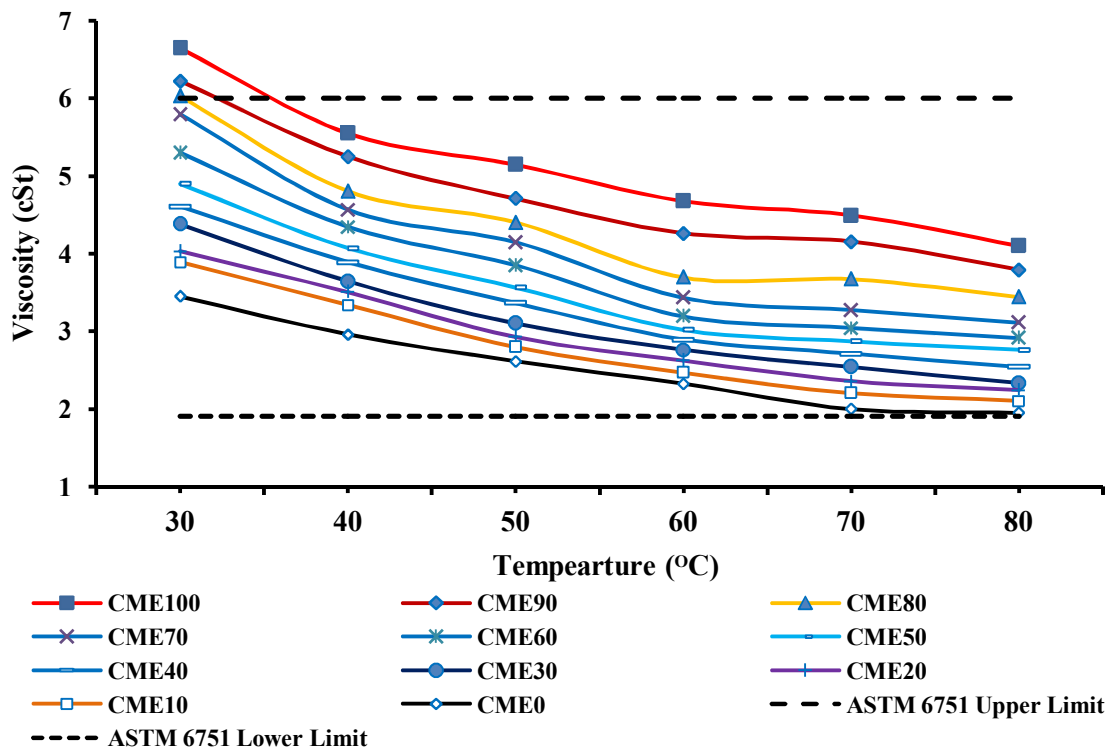## 4.2 RESULTS OF PHYSICO-CHEMICAL CHARACTERISATION

4.2.1 Viscosity

Fig. 4.6: Variation of viscosity with temperature for various test fuels

The viscosity was measured using the Petrotest viscometer as discussed in the earlier sections. Fig.4.6 shows the variation of viscosity of CME and its blends with temperature. CME100 exhibited kinematic viscosity of 5.55 cSt at 40°C temperature which was lower than the ASTM 6751 limit of 6 cSt. Therefore, the viscosity of CME was within the ASTM standard limit. Further, all the blends of CME and diesel, within the entire experimental range of 30°C to 80°C temperature, exhibited viscosities within the prescribed limit of ASTM 6751. The variation of kinematic viscosity with temperature was found to be nearly 38% for CME100. However, for lower blends viscosity variation with temperature was nominal. At 40°C diesel showed 2.956cSt of viscosity whereas CME100 was having nearly twice the value. Therefore, atomization, vaporisation and air-fuel mixing characteristics of CME are supposed to be inferior as compared to mineral diesel.

4.2.2 Density

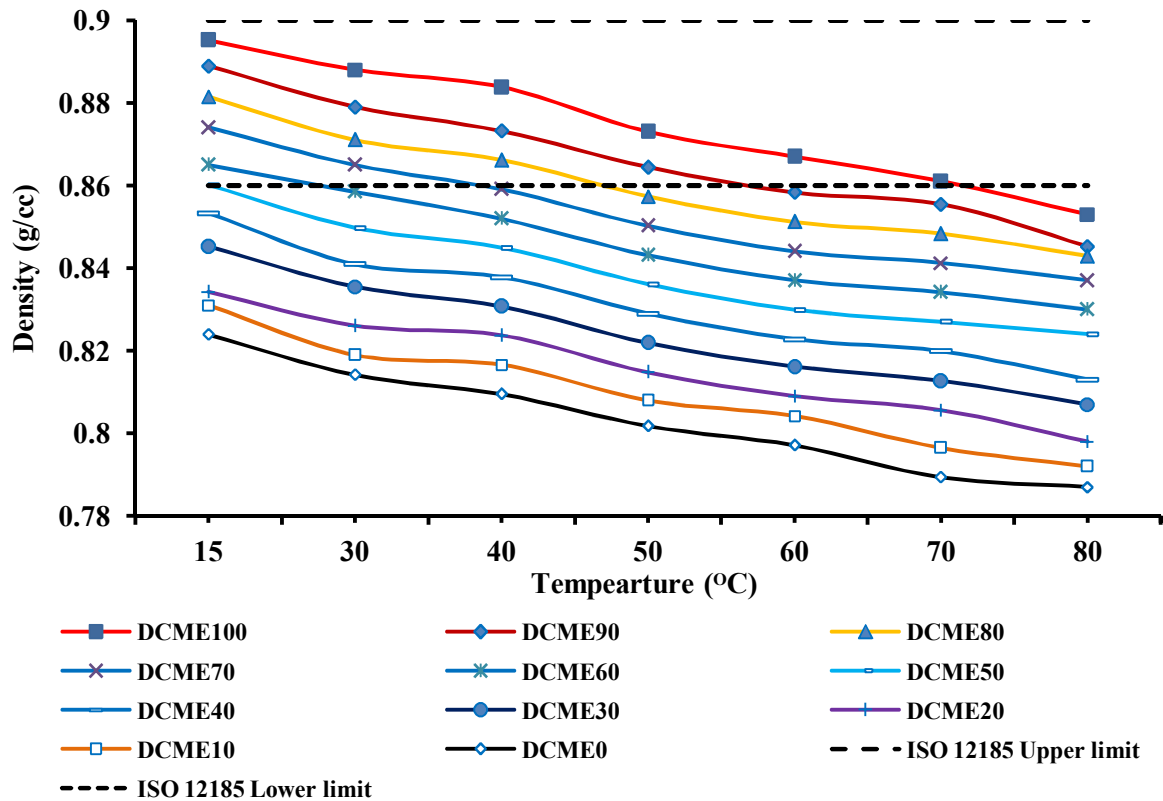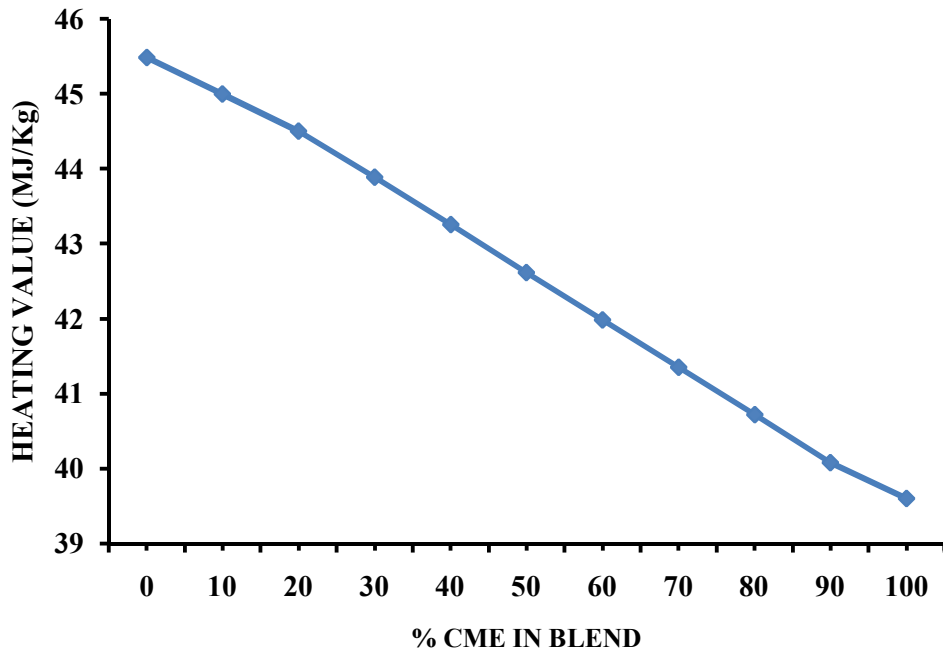*Fig. 4.7: Variation of density with temperature for various test fuels*

Density was measured using an oscillating "U" tube density meter as elaborately discussed in the earlier sections. It is also a key fuel property, with potential to directly

influence the engine performance, emission and combustion behavior. Many important characteristics, such as cetane rating and heating value, are related to the density [113]. Fuel density will influence engine output power due to a difficulty in fuel mass injection [114]. In the present investigation, the density of CME and its blends were determined at temperatures 15°C and 30-80 °C with 10°C increase in every step. At 15°C, CME100 exhibited density of 0.8952 g/cc as compared to 0.8239g/cc showed by the neat diesel. The density of CME and its blends were less sensitive to temperature than viscosity. It may be observed that within the entire range of temperature variation, the change in density of CME100 was merely 4.3%. CME100 and all its blends were well within the prescribed ISO12185 standard for density.

4.2.3 Calorific Value

Fig. 4.8: Variation of calorific value with temperature for various test fuels

A bomb calorimeter was used to determine the calorific value of the test fuels as discussed briefly in the earlier sections. Calorific value of various blends of CME and diesel is shown in Fig.4.8. It may be observed that CME100 was having a calorific value of 39.6 MJ/Kg as compared to 45.49MJ/Kg in case of mineral diesel. The variation of calorific value with volume fraction of CME in the test fuel was linear.

4.2.4 Cold flow plugging point (CFPP)
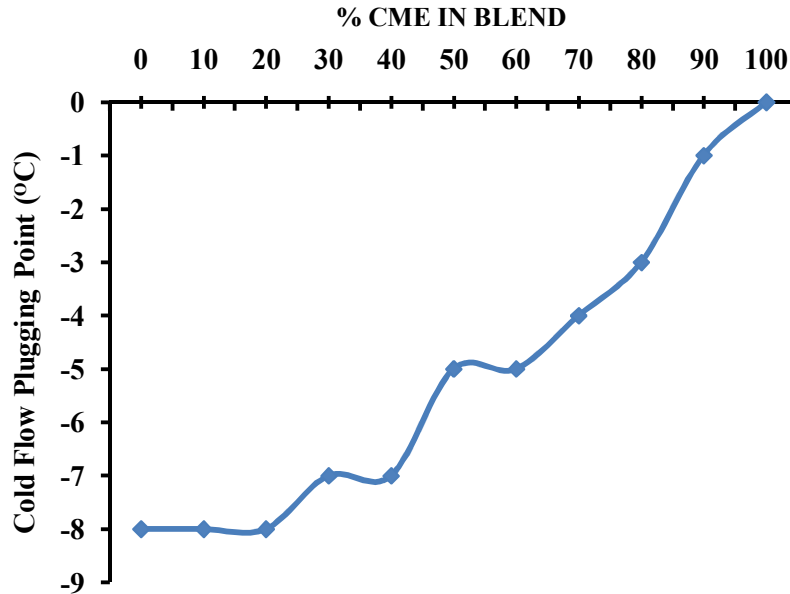
Fig. 4.9: CFPP for various test fuels

Variation in CFPP for the test fuels is shown in Fig. 4.9. It may be observed that neat diesel exhibited CFPP of -8°C where as CME100 showed CFPP of 0°C. Therefore, the flow properties of CME are inferior to diesel. As India is mostly a tropical country, 0°C CFPP may be acceptable for diesel engine application in Indian context. However, the cold flow properties of CME may be improved by some additives, however, no such studies were carried out. Moreover, the variation of CFPP with increasing volume fraction of CME in the test fuels was not linear.

4.2.4 Oxidative stability

As describe earlier, the biodiesel rancimat method was used for oxidation stability study. The EN14112 standard was followed with 10 L/h air flow and 110 °C bath temperature. The total induction time showed by the CME100 sample was 3.97 hours as against the standard of three hours. Therefore, the oxidation stability of CME100 was found to be within the limits of European biodiesel standard. However, the stability of the oil was not excellent and just marginally over the prescribed limit. Therefore, addition of oxidation stability improvers to the CME may be studied before commercial scale production or usage. Fig. 4.10 shows the conductivity and induction time curve for oxidation stability study using biodiesel rancimat.
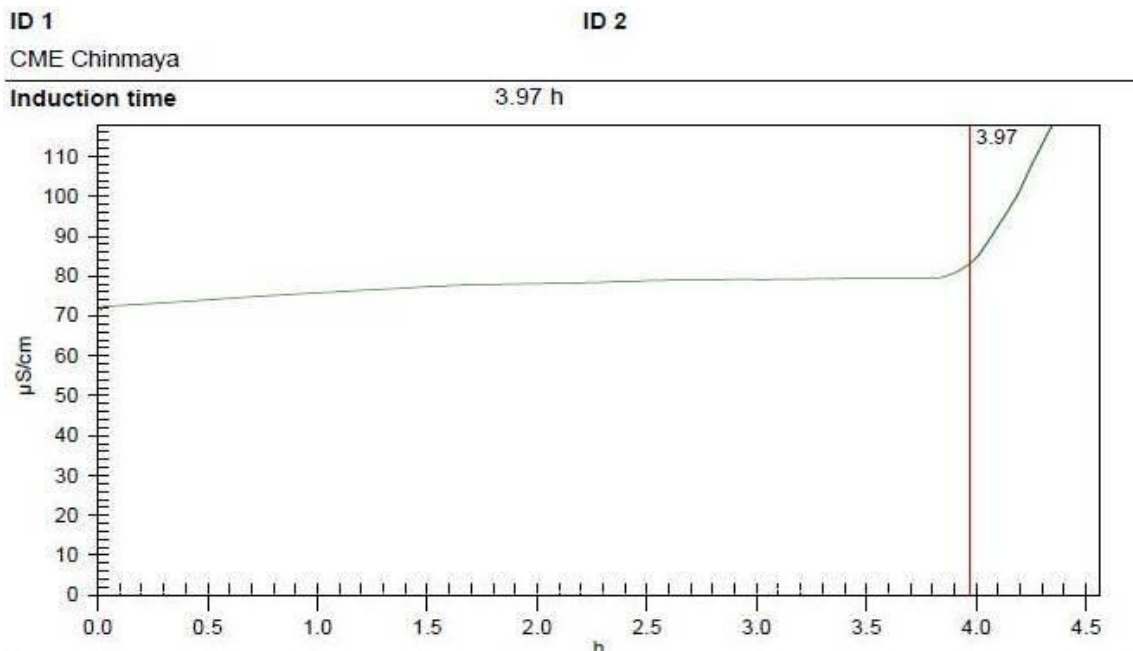
Fig. 4.10: Oxidation stability of CME100

4.2.5 Fatty Acid Profile

The fatty acids profile of the neat Calophyllum biodiesel was obtained using the gas chromatography equipment as discussed d in the earlier sections. The scanned copy of the peaks obtained during the chromatography test is shown in Fig. 4.11
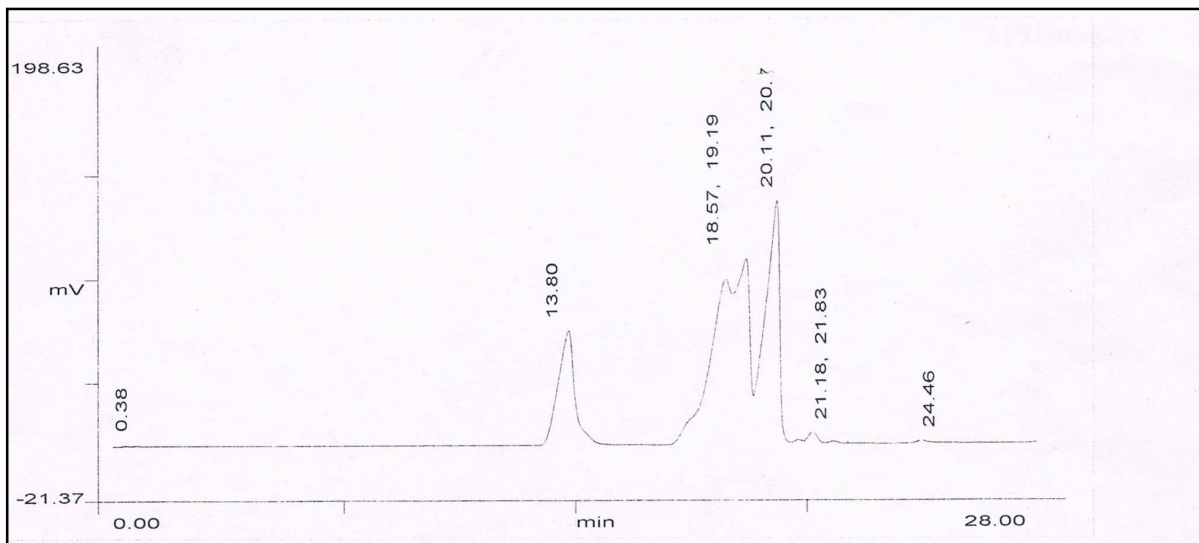
Fig. 4.11: The results of gas chromatography

Each fatty acid corresponds to one peak. The area of that peak to the summation of the area under all other peaks provided the % composition of the respective fatty acid. Table 4.5 shows the detailed fatty acid profile of Calophyllum methyl ester.

Table 4.5: Fatty acid profile for Calophyllum methyl ester

Fatty Acid	Chemical Structure	Formula	Weight (g/mol)	(% wt)
Palmitic acid	C16:0	$C_{16}H_{32}O_2$	256.42	16.18
Stearic acid	C18:0	$C_{18}H_{36}O_2$	284.48	22.01
Oleic acid	C18:1	$C_{18}H_{34}O_2$	282.47	29.46
Linoleic acid	C18:2	$C_{18}H_{32}O_2$	280.5	31.06
Linolenic acid	C18:3	$C_{18}H_{30}O_2$	278.4	00.70
Arachidic acid	C20:0	$C_{20}H_{40}O_2$	304.47	00.19
Saturated	--------	----------	---------	**38.38**
Unsaturated	--------	----------	---------	**61.22**
Total	--------	----------	---------	**99.6**

Table 4.5 suggests that CME100 was rich in Oleic and Linoleic acids. It may be observed that 61.22% composition by weight of CME contained unsaturated fatty acids and only 38.38% saturated fatty acids. Due to availability of double bonds and poly-unsaturated fatty acids, CME tends to have higher inclination to react with oxygen. This is consistent with the previous observation of comparatively inferior oxidation stability of CME. However, availability of unsaturated fatty acids also has some advantages. Due to high reaction tendency, the CME when injected in to the diesel engine suddenly broke in to lighter compounds reducing the ignition delay. The unsaturated fatty acids also have a positive say on the cetane rating of the fuel.

Various equipments used for determination of physico-chemical and fuel properties and the corresponding standards are provided in table 4.6. A comparative assessment of various physico-chemical properties of CME was carried out with Jatropha methyl ester in table 4.7

Table 4.6: List of equipments used for property measurements and the standards

Sl No	Property	Equipment	Manufacturer	ASTMD6751	ASTMD6751 LIMITS
1	Kinematic viscosity	Petrotest viscometer	Anton Parr, UK	D445	1.9-6 cSt
3	Oxidative stability	873 Rancimat	Metrohm, Switzerland	D675	3 hours
4	Density	U tube density meter	Anton Parr, UK	D1298/ISO12185	0.86-0.9g/cc
5	CFPP	Automatic NTL 450	Normalab, France	D6371	Not specified
6	Calorific value	Parr 6100 Bomb calorimeter	IKA, UK	Not specified	Not specified

Table 4.7: Comparison of physicochemical properties between the methyl esters of Calophyllum and Jatropha

| Sl No	Property	Calophyllum Methyl Ester	Jatropha Methyl Ester
1	Viscosity at 40°C	5.5 cSt	4.94 cSt
3	Viscosity at 80°C	4.1 cSt	1.85 cSt
4	Density at 40°C	0.8838 g/cc	0.8642 g/cc
5	Density at 15°C	0.8952 g/cc	0.8791 g/cc
6	CFPP	0°C	10°C
7	Calorific value	39.60 NJ/Kg	39.738 MJ/Kg

On the basis of the data provided in the table 4.6 and 4.7, it may be concluded that Calophyllum methyl ester was well within the limits of international biodiesel standards. Its various critical physico-chemical characteristics closely matched with the methyl ester of Jatropha curcas recognized by Government of India as the best oil seed for biodiesel production.

4.2 RESULTS OF ENGINE TRIALS

4.2.1 Engine Performance Results

4.2.1.1 Brake thermal efficiency (BTE)

Brake thermal efficiency is a vital engine performance parameter. It is the ratio between useful mechanical work obtained at the engine shaft and the energy of the injected fuel, the latter being the product of mass flow rate and heating value of the fuel [62]. Variation of brake thermal efficiency with brake mean effective pressure for the test fuels is shown in Fig. 4.12.
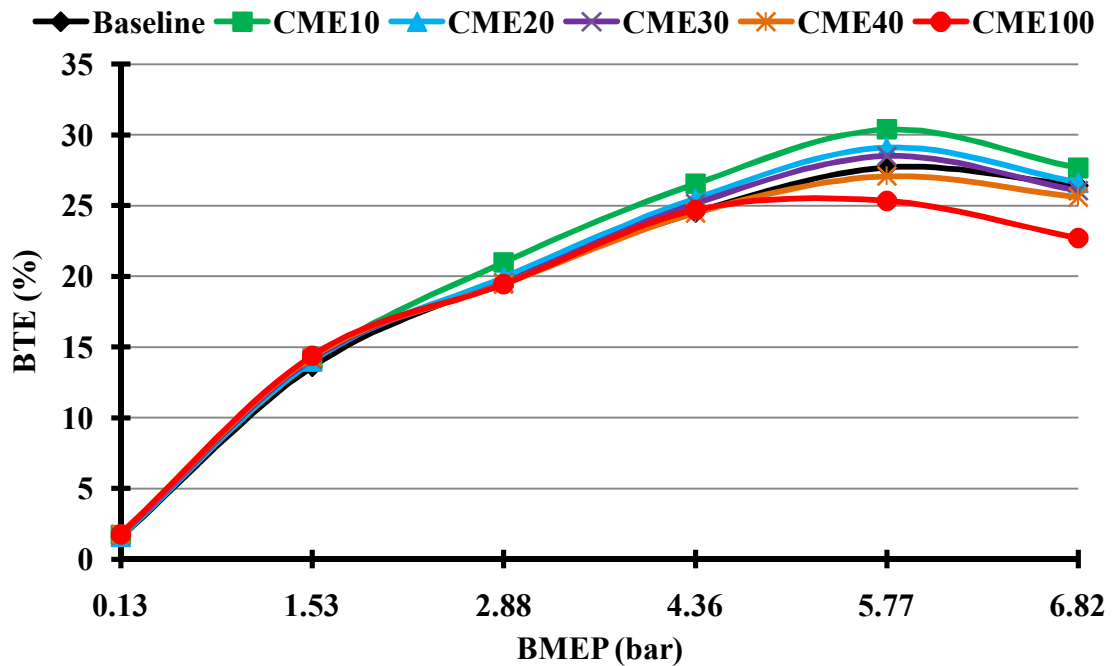
Fig. 4.12: Variation of brake thermal efficiency with brake mean effective pressure

It was observed that with increase in load, brake thermal efficiency of the engine was increased for all test fuels. This was attributed to the fact that at higher loads more power was generated and heat loss was reduced [67,38,73]. It was observed that CME10 and CME20 exhibited 27.6% and 26.6% full load BTE respectively as compared to 26.4% illustrated by diesel baseline. On the other hand, CME30 and CME40 showed 26% and 25.6% full load BTE respectively, lying close to the baseline. However, the usage of CME 100 in the engine trial demonstrated 22.7% full load brake thermal efficiency which was way lower than the baseline data. As a nutshell, it may be stated that thermal efficiency of the diesel engine was increased with increase in the volume fraction of Calophyllum Methyl Ester up to 20%. Engine operation at 30% substitution of diesel by CME was found to be the inflexion point, beyond which a reduction in thermal efficiency was observed. Neat CME operation resulted in significant reduction of higher load brake thermal efficiency as compared to mineral diesel operation. Increase in BTE up to 20% blend, inflexion at 30% and the subsequent drop in higher load BTE till neat CME operation may be attributed towards a number of factors. Firstly, biodiesel is an oxygenated fuel that leads to complete combustion even at lower equivalence ratio zones [74]. Secondly, the lower flame temperature of the blends than diesel leads towards a reduction in heat loss [117].

Thirdly, the lubricity property of CME was higher than diesel resulting in reduction in frictional power loss [77]. All these factors contribute towards improved combustion, reduced losses and higher thermal efficiency. However, beyond 20% volume fraction of CME in diesel some other characteristics of the biodiesel like lower calorific value, higher viscosity and density, poor atomization/vaporization, increase in fuel consumption etc. starts negating the gain [66,67,68]. Beyond 30% blend, the reductions in higher load thermal efficiency as compared to neat diesel operation were significant.
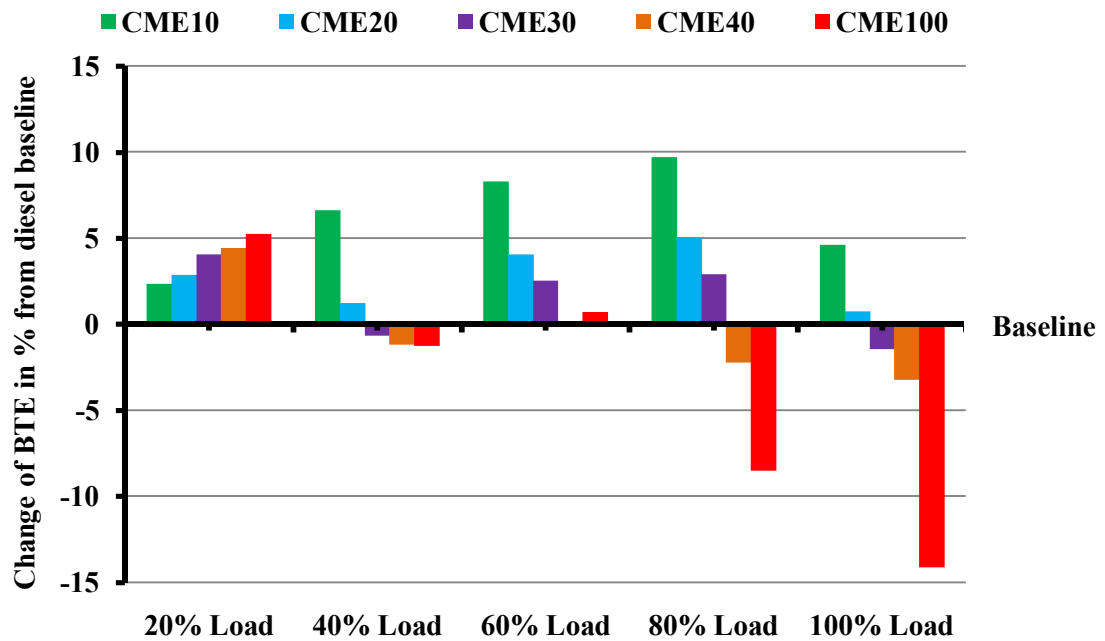

Fig. 4.13: % Variation of brake thermal efficiency from diesel baseline at various loads

Fig. 4.13 shows the % variation in brake thermal efficiency of various test fuels compared to the baseline data at all loading conditions. It is significant to note that at 20% load, the BTE exhibited by CME10, CME20, CME30, CME40 and CME100 were 2.3%, 2.8%, 4.0%, 4.45% and 5.25% respectively higher than the baseline diesel operation. This may be attributed to the fact that the higher A/F ratio at 20% load coupled with the oxygenated nature of CME led towards improved combustion even at higher volume fractions. CME10 and CME20 illustrated higher BTE at all loads compared to the baseline data.

On the other hand, CME30 truly justified the nature of inflexion by displaying a reduction of 0.66% and 1.43% in BTE at 40% and 100% loads respectively where as an increase of 2.55% and 2.91% in BTE at 60% and 80% loads respectively compared to the baseline diesel data. In the light of the above results, it may be concluded that the engine performance in terms of brake thermal efficiency was improved with biodiesel blends up to 20% substitution. Beyond 30% volume fraction of CME in the fuel, resulted in reduction of thermal efficiency as compared to the diesel baseline. Similar type of results were obtained by several researchers [73,74, 75,76,77,118,119] working on biodiesel derived from polanga, waste cooking oil, mahua oil, karanja oil, apricot oil, rape seed oil etc.
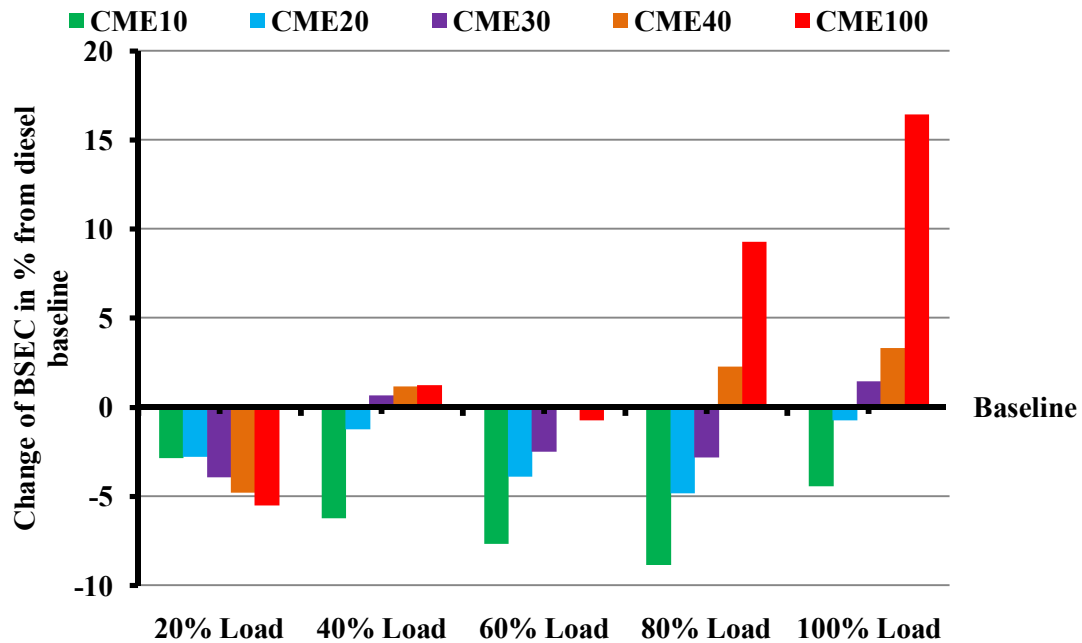
4.2.1.2 Brake specific energy consumption (BSEC)
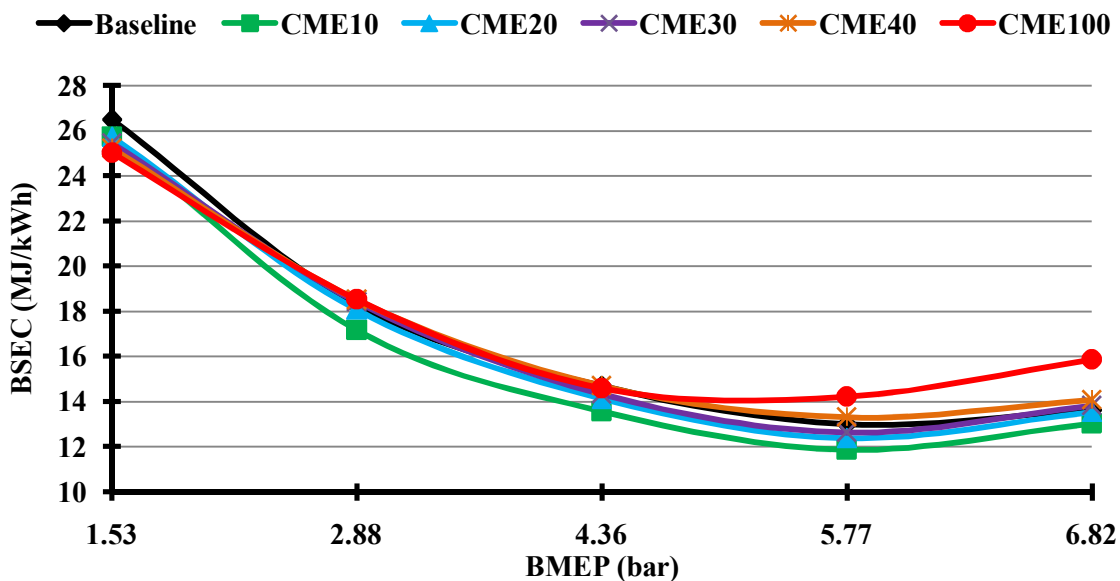
Fig. 4.14: Brake specific energy consumption VS brake mean effective pressure plot

Comparative assessment of volumetric consumption of fuel is an important parameter to explain the engine performance exhibited by various test fuels. In this context, brake specific fuel consumption which is a ratio between fuel mass flow rates to the brake power has been used as a conventional parameter. However, BSFC has not been considered as a reliable parameter when the calorific values and densities of test fuels vary considerably [73]. In the present case CME100 exhibited 8.65% higher density and 12.94% less calorific value than diesel. Therefore, brake specific energy consumption was considered as more reliable assessment method for comparison of volumetric fuel consumption in this case.

Variation of BSEC with brake mean effective pressure for the test fuels under designated conditions of load is shown in Fig.4.14. It may be observed that CME10, CME20, CME30, CME40 and CME100 brandished full load BSEC of 289.42MJ/kWh, 278.17MJ/kWh, 315.03MJ/kWh, 325.54MJ/kWh and 358.95MJ/kWh respectively as compared to 299.57MJ/kWh illustrated by the baseline diesel operation. Therefore, it may be concluded that up to 20% volume fraction of CME in the blend, full load BSEC was found to get reduced whereas, beyond 30% substitution of diesel by biodiesel led to increased full load BSEC compared to the neat diesel operation. The reduction in BSEC at lower volume fractions of CME may be attributed towards the enhanced combustion as discussed earlier. However, the increase in BSEC beyond 30% substitution of biodiesel in the fuel was mainly due to the combined effects of the relative fuel density, viscosity and heating value of the blends. The higher density of Calophyllum biodiesel has led to more discharge of fuel for the same displacement of the plunger in the fuel injection pump, thereby increasing the specific energy consumption [67].

Fig. 4.15: %Variation of brake specific energy consumption from diesel baseline at various loads

Fig. 4.15 shows the variation in BSEC from diesel baseline for various test fuels under the designated loading conditions. It was observed that BSEC was found to get reduced with increase in CME volume fraction at 20% load. Various reductions shown by the test fuels compared to the baseline data were 2.84%, 2.79%, 3.91%, 4.79% and 5.52% for

CME10, CME20, CME30, CME40 and CME100 respectively. It may be observed that CME10 and CME20 exhibited reduction in BSEC compared to the baseline data at all loading conditions. On the contrary CME40 and CME100 illustrated higher BSEC than neat diesel data after 40% load. CME30 demonstrated 0.66% and 1.45% increase at 40% and 100% loads respectively compared to the baseline data. However, at 60% and 80% loads, CME30 exhibited 2.49% and 2.82% reduction in the respective BSEC.

4.2.2 Engine Emissions Results

4.2.2.1 Carbon monoxide
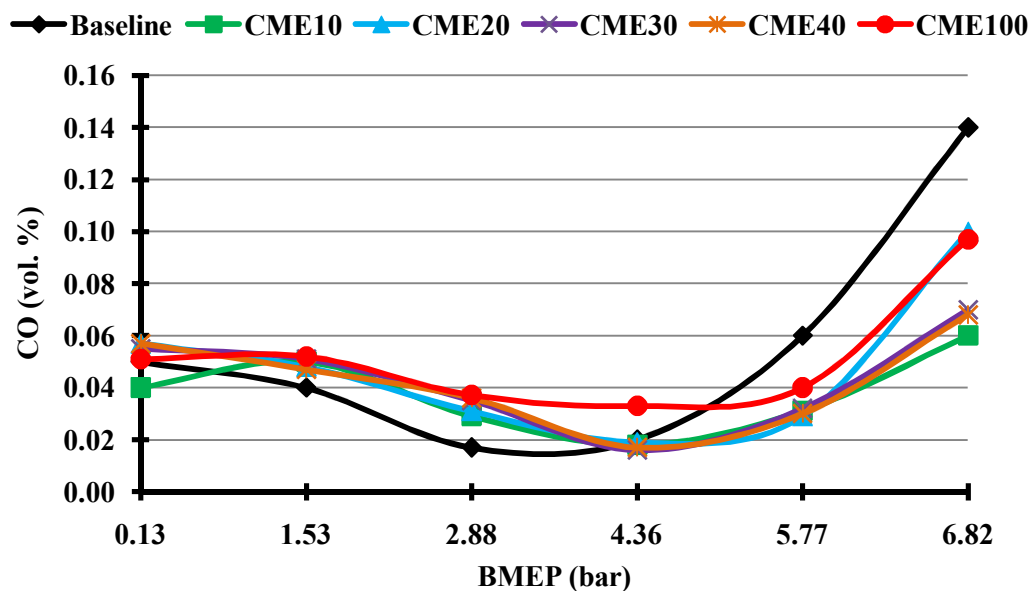
Fig. 4.16: Emission of carbon monoxide with brake mean effective pressure

Carbon monoxide is considered as a major diesel engine pollutant. The formation of CO during combustion in diesel engines is primarily attributed to lower fuel-air equivalence ratios of combustible mixtures [120]. However, factors like combustion chamber design, atomization rate, start of injection timing, fuel injection pressure, engine load, speed etc. may affect formation of CO at varied influences [121]. Volumetric emissions of CO with brake mean effective pressure for various test fuels is shown in Fig.4.16. It may be noted that initially the emissions of CO get reduced with increase in load for all test fuels. However, after 60% load a steep hike in CO emission was observed irrespective of test fuels. This may attributed to the fact that at no load condition, in-cylinder temperatures are fairly low leading towards incomplete combustion; however, with increase in load, temperature gets elevated

due to burning of more fuel injected in to the cylinder. At higher temperatures improved burning of the fuel reduces CO emissions [74,75]. Interestingly beyond 60%load, higher amount of fuel injection in to the engine leads to incomplete combustion and steep increase in CO emissions. At higher loads CME and its blends exhibited lower CO emissions as compared to the baseline data. A load specific analysis of variation of CO emissions from various blends compared to the baseline data is shown in Fig. 4.17
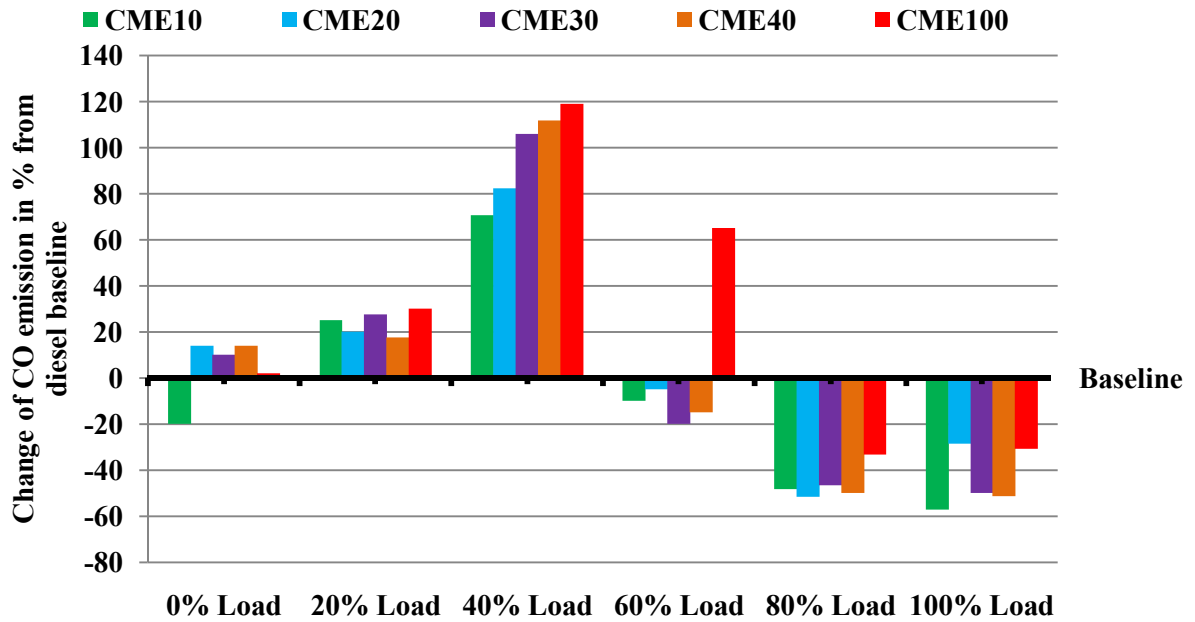

Fig. 4.17: %Variation of CO emission for various test fuels compared to the diesel baseline

It was observed in the engine trial that up to 40% engine load, CME and its blends illustrated higher CO emissions than the diesel baseline as indicated in the Fig.4.17. This may be attributed to the theory that the air–fuel mixing process is affected by the difficulty in atomization of biodiesel due to its higher viscosity resulting in locally rich mixtures of biodiesel and consequent higher CO emissions [78]. This also can be explained in terms of the premixed lean combustion in presence of excess air in these loads that makes the effect of biodiesel on CO emission reductions less tangible. However, the net volumetric CO emissions in these loads were less than 0.06% and hence insignificant. However, at 80% load CME10, CME20, CME30, CME40 and CME100 demonstrated 48.3%, 51.67%, 46.67%, 50% and 33.33% reductions respectively in emissions of carbon monoxide as compared to the diesel baseline operation at this load. Similarly at full load 57.14%, 28.57%, 50%, 51.42% and 30.71% reductions in carbon monoxide emissions were observed for CME10,

CME20, CME30, CME40 and CME100 test fuels respectively as compared to the full load neat diesel operation. The reduced emissions of CO for CME and its blends at higher loads may be attributed by the fact that biodiesel is an oxygenated fuel with lesser C/H ratio than diesel resulting in enhanced combustion [122]. One significant observation in the experiment reiterates that the reduction in CO emissions are not a function of CME volume fraction in the test fuel i.e. reductions in CO emissions are evident with increase in CME volume fractions in the test fuel, but the trend is not linear. Similar type of observations were reported by Last et.al.[123] and Lapuerta et.al.[62].

4.2.2.2 Total hydrocarbon emissions
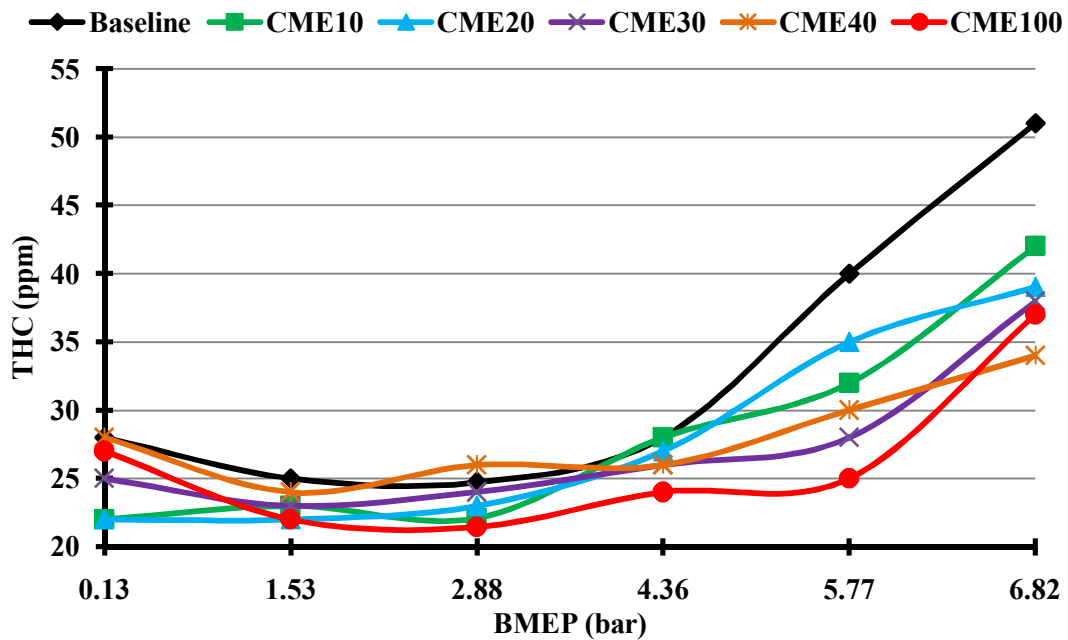
Fig. 4.18: Emission of total hydrocarbons with brake mean effective pressure

Emission of total hydrocarbons with brake mean effective pressure is shown in Fig. 4.18. The detail mechanism of formation of hydrocarbons inside engine cylinder during combustion and its theoretical study is still at infancy and elusive [126]. However, certain factors like in engine cylinder crevices, engine configuration, fuel structure, combustion temperature, oxygen availability, residence time etc. are presumed to affect the hydrocarbon emissions in compression ignition engines [124,125]. In the present study reduction in emissions of hydrocarbons was reported with increase in CME volume fractions, however, the trend was not linear. At partial loads, there was no significant variation in THC

emissions between diesel and the blends. However, at full load, CME 10, CME20, CME30, CME40 and CME100 demonstrated volumetric emissions of 42, 39, 38, 34 and 37 ppm respectively as compared to 51 ppm illustrated by the baseline data of diesel. % Variation in THC emissions exhibited by various test fuels at the designated conditions of load is shown in Fig. 4.19.
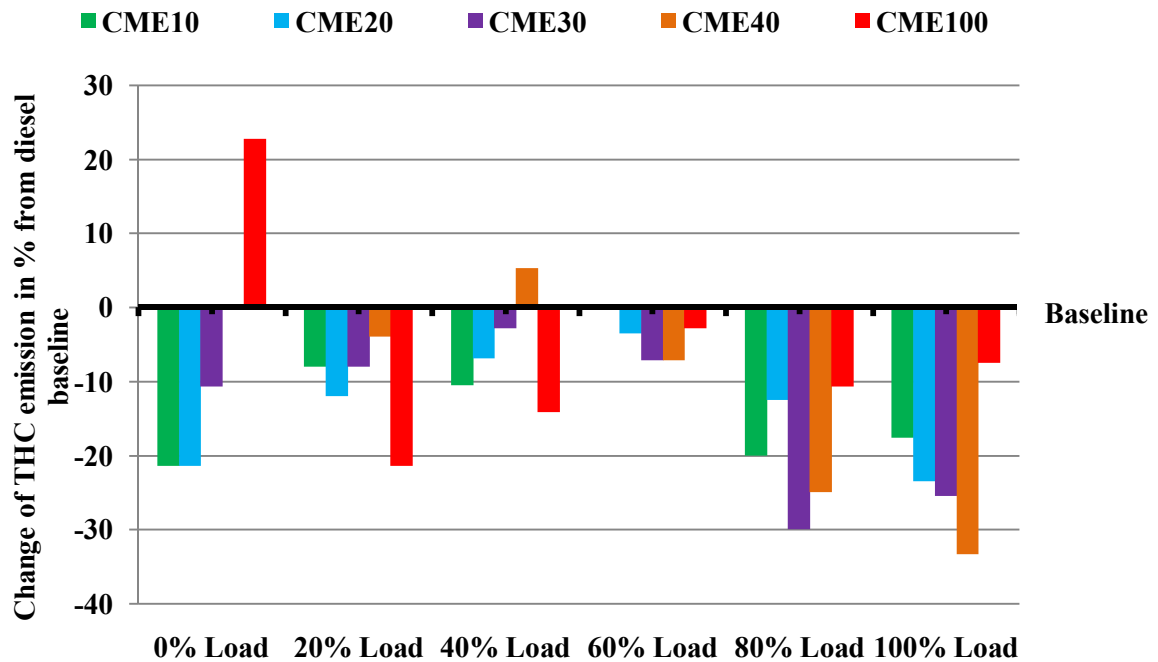
Fig. 4.19: %Variation of THC emission for various test fuels compared to the diesel baseline

It may be observed in the Fig.4.19 that all most all the test fuels under all operating conditions of loads demonstrated reductions in THC emissions as compared to the baseline data of diesel. At full load 17.64%, 23.53%, 25.49%, 33.33% and 7.5% reductions in emissions of CO was reported for CME10, CME20, CME30, CME40 and CME100 test fuels respectively. Two basic explanations may be suitable to describe the reductions in THC emissions with increased volume fractions of CME in the test fuel. Firstly, up to 30% blend of CME in diesel, higher in-cylinder pressures and bulk gas temperature was reported compared to the neat diesel operation that prevented the condensation of heaviest hydrocarbons at the sampling line (These phenomena will be explained in detail in the subsequent sections of combustion study). Secondly, CME was reported to have higher cetane rating and lower ignition delay than diesel. Therefore, a combined effect of higher in-

cylinder temperature, higher cetane rating and reduced ignition delay resulted in reduced emissions of THC by CME and its blends compared to the baseline data of diesel [77,127].
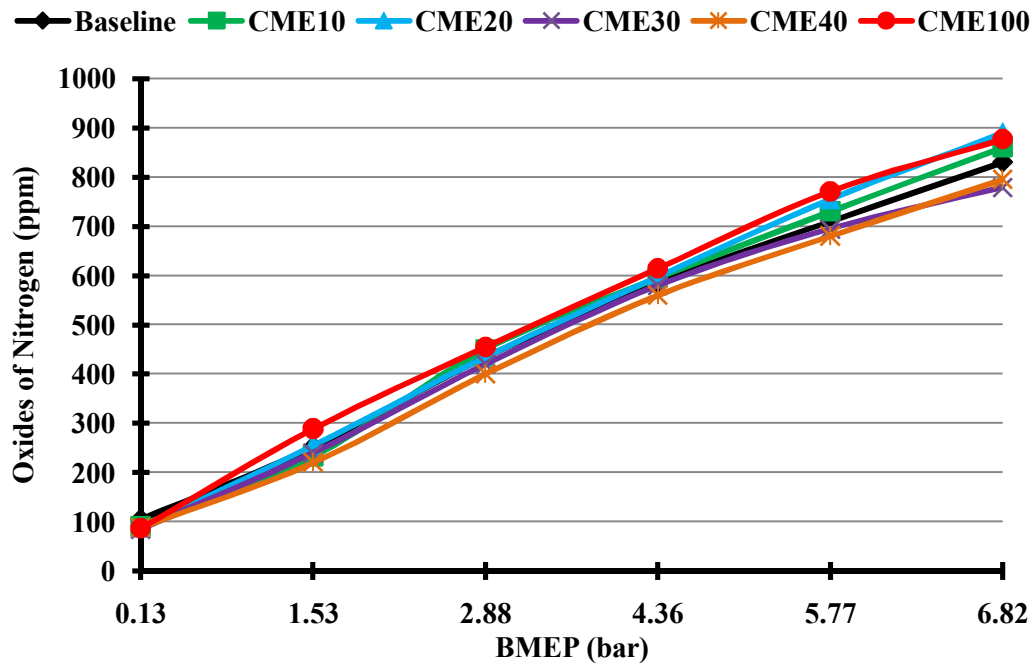
4.2.2.2 Oxides of nitrogen emissions

Fig. 4.20: Emission of oxides of nitrogen with brake mean effective pressure

Oxides of nitrogen popularly referred as NO_x are the critical diesel engine emissions of major concern. It mostly comprises of nitric oxide (NO) and nitrogen dioxide (NO_2), formed by "Zeldovich Mechanism". Combustion flame temperature, availability of oxygen and time for oxygen-nitrogen reaction are the major factors controlling NO_x formation in diesel engines [78,128,129]. Fig.4.20 shows the volumetric emissions of NO_x demonstrated by various test fuels under the designated operating loads. It may be observed that NO_x emissions increased with increase in engine load for all test fuels. This may be attributed to the fact that increase in engine loading leads to increase in in-cylinder pressure and bulk gas temperature. As NO_x formations are highly temperature dependent phenomena, hence, an almost linear increase in the formation of NO_x was observed with loading for all test fuels [73]. The results suggested that CME10, CME20 and CME100 exhibited 860, 890 and 877 ppm volumetric emissions of NO_x at full load which was higher than 830 ppm showed by the baseline data of diesel. However, the maximum difference was less than 60ppm. On the other hand CME30 and CME40 demonstrated reduction in NOx emissions at full load as compared

to the baseline data. Load specific % variations in NOx emissions for various test fuels as that of the baseline data is shown in Fig. 4.21
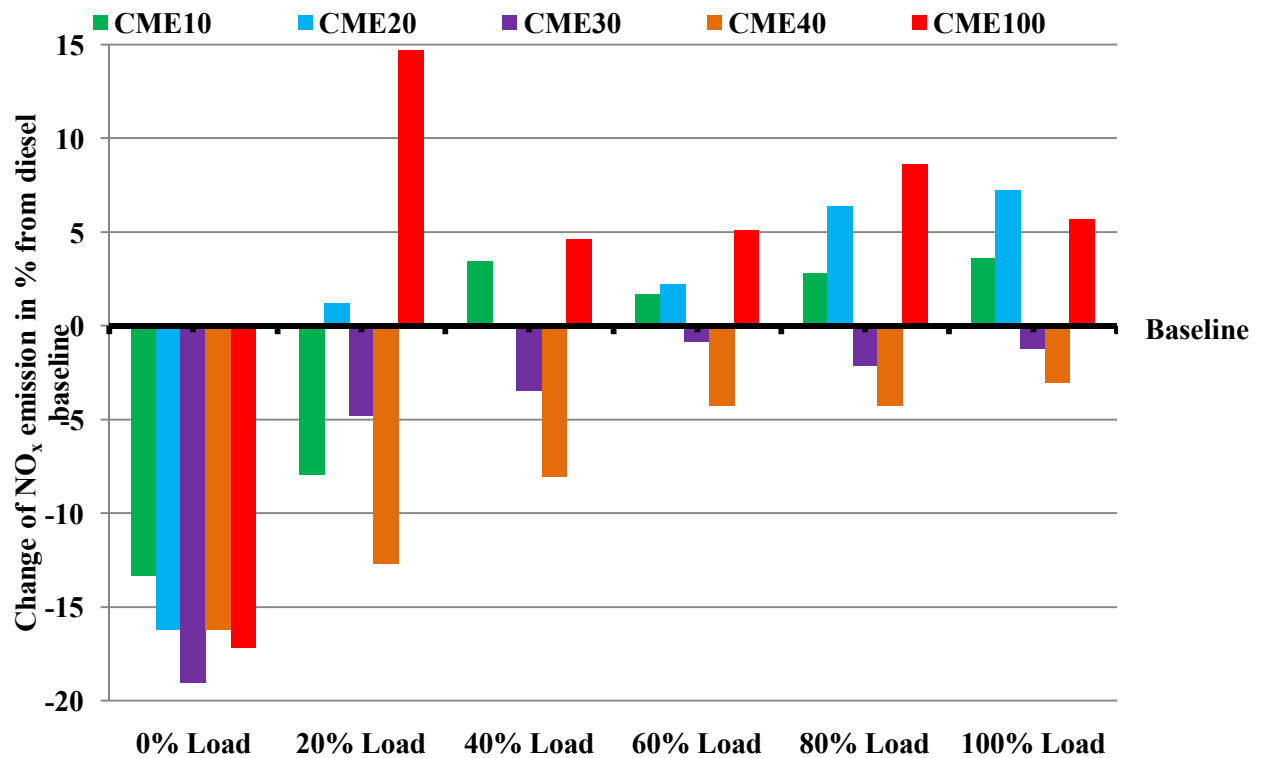
Fig. 4.21: %Variation of NO$_x$ emission for various test fuels compared to the diesel baseline

It may be observed in the Fig.4.21 that the NO$_x$ emisions at no load condition was lower for CME and its blends compared to the baseline data. However, at this load most of the emissions were less than 100 ppm and hence insignificant. Beyond 40% load, it may be observed that CME and its blends deomnstrated higher emissions of NO$_x$ compared to the baseline data (except CME30 and CME40). This may be attributed to the fact that CME is an oxygentade fuel and the adiabatic flame temperature was higher than neat diesel operation for up to 30% blend. So therefore, higher combustion temepratures was the predominant factor for increased NOx emissions for CME10 and CME20, where as excess avaialbility of oxygen was the predominat factor for increased NOx emissions for CME100. On the contrary a marginal drop in NOx emisisons for CME30 and CME40 compared to the baseline data may be due to a slight drop in in-cylinder temperature reported in the experiment (To be discussed in the subsequent sections). Similar results were reported by Nabi et.al.[130]. Another critical observation in the NOx emissions pattern suggests that the variations in NOx emissions wereless than 7% and 60 ppm comapred to the baseline data. This may be

explained with the theory suggested by Zheng et.al.[131]. which states that biodiesel with equal cetane rating with diesel produces more NOx. However, biodiesel with higher cetane rating than diesel leads to comparable NOx emissions with the baseline data as higher cetane rating causes reduced ignition delay and less exposure of the fuel at high tempearture premixed burning phase. As explaine earlier, CME has higher cetane rating than diesel hence, its NOx emissions are allmost comparable with the baseline data.
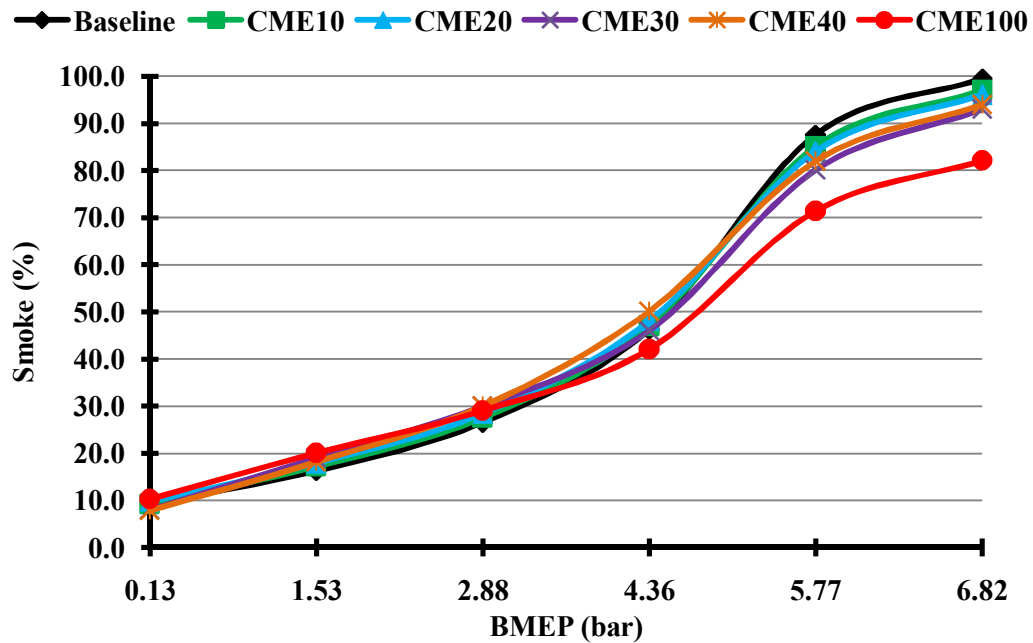
4.2.2.3 Smoke opacity

Fig. 4.22: Smoke opacity with brake mean effective pressure

Fig.4.22 shows the variation of smoke opacity with brake mean effective pressure for various test fuels. Smoke is one of the most unpleasant emissions in diesel engines. It can be seen from Fig. 4.19 that smoke level increased sharply with increase in load for all fuels tested. It was mainly due to the decreased air–fuel ratio at such higher loads when larger quantities of fuel are injected in to the combustion chamber, much of which goes unburnt into the exhaust [74,119]. It may be observed that CME and its blends demonstrated reduced emissions of smoke at higher loads. At full loadCME10, CME20, CME30, CME40 and CME100 showed smoke opacities of 97%, 96%, 93%, 93.9% and 82.1% as compared to 99.5% exhibited by baseline diesel at full load. The reduction in smoke opacity at higher loads with increase in CME volume fraction may be attributed to a number of factors such as higher oxygen content in CME that contributes towards complete fuel oxidation even at

locally rich zones [62], lower C/H ratio and absence of aromatic compounds. Higher number of carbon atoms in a fuel molecule leads towards higher smoke and soot formations where as higher number oxygen and hydrogen atoms leads to lower smoke and soot [132]. It may be observed that at part loads CME and its blends exhibited higher smoke opacities than the baseline. % Variation in smoke opacities exhibited by CME and its blends with the baseline data of diesel at various loads is shown in Fig. 4.23
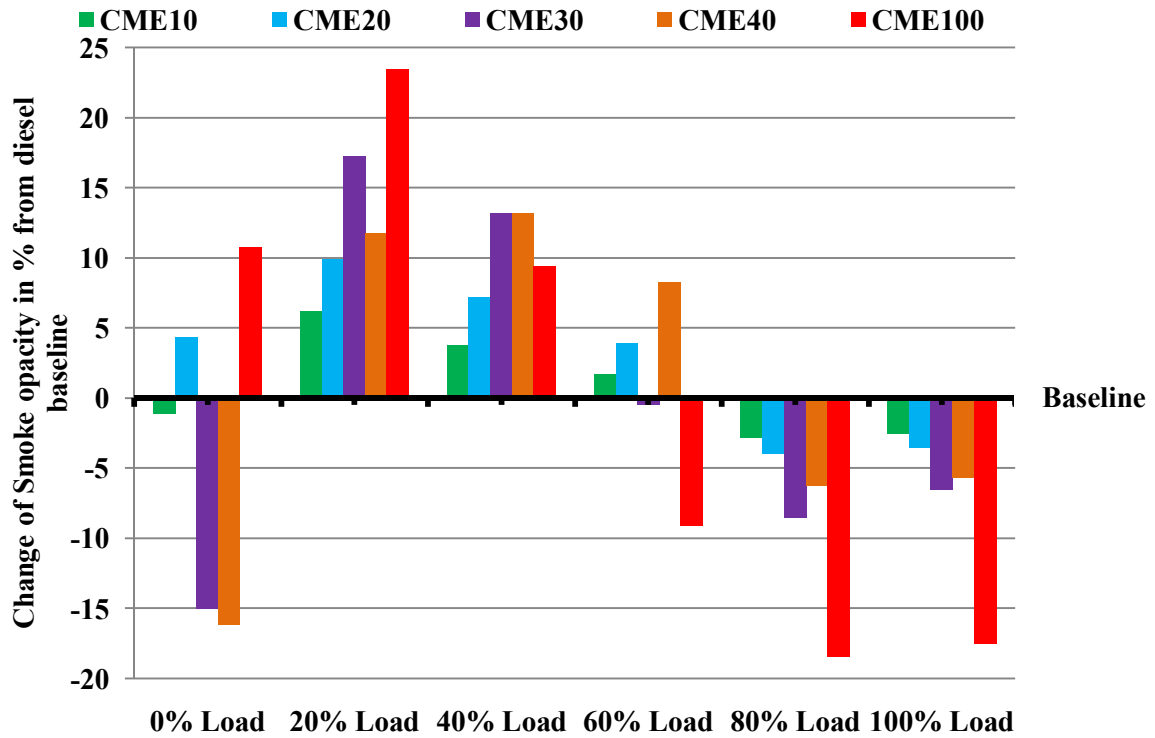
Fig. 4.23: %Variation of smoke for various test fuels compared to the diesel baseline

Fig.2.3 shows that at 20%, 40% and 60% of the engine load, CME and its blends exhibited higher smoke as compared to the baseline data of diesel. This may be attributed to the fact that higher viscosities of biodiesel and lower in-cylinder temperatures at lower and medium engine loads leads to poor atomization, locally rich mixtures and higher emissions of smoke [5,18,31]. However, just like previously reported emissions, the smoke opacities at lower and medium loads are less than 50% and hence, significantly lower than the higher load smoke of 90% and higher. Similar types of results were reported by various researchers [74,76,77,78,119] working on a variety of vegetable oils and their esters.
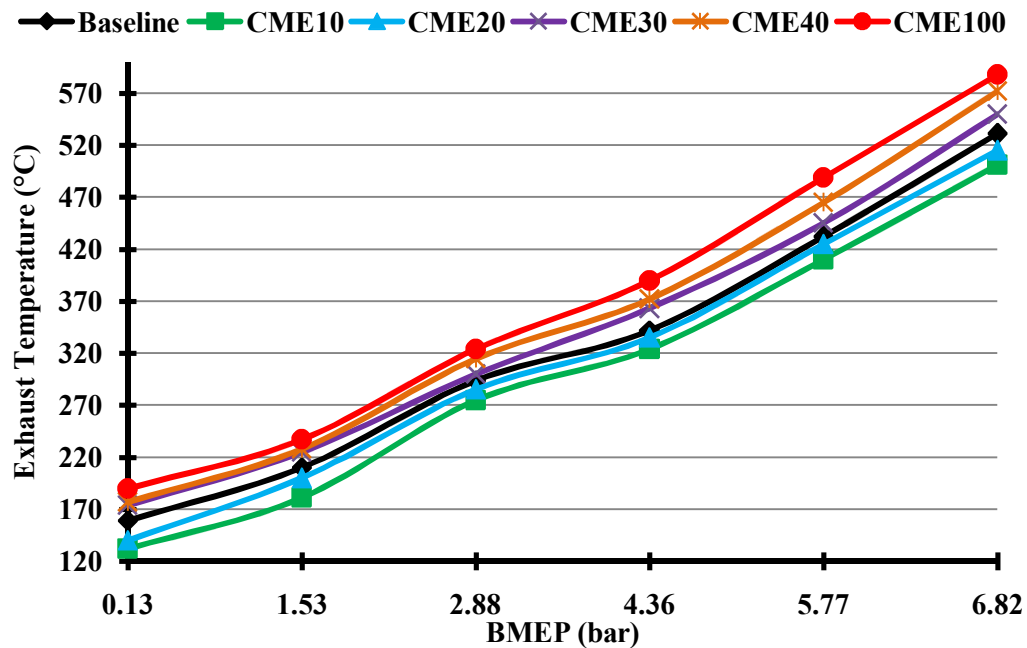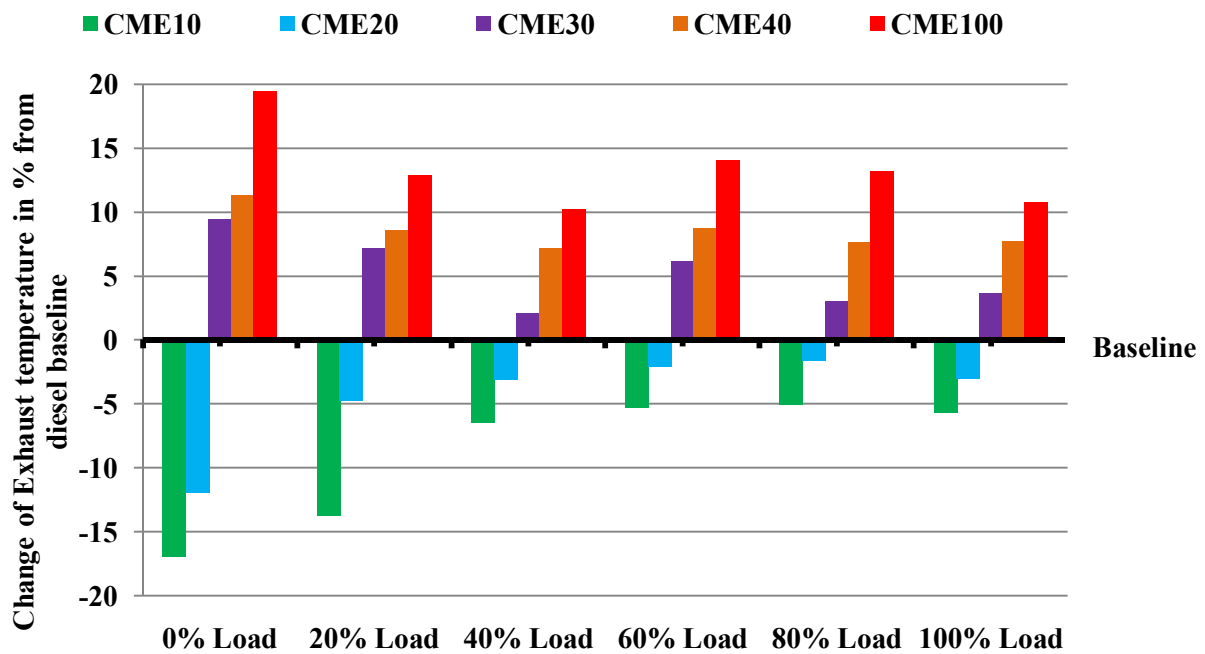
4.2.2.3 Exhaust temperature

Fig. 4.24: Engine exhaust temperature with brake mean effective pressure

The variation of exhaust gas temperature with brake mean effective pressure is shown in the Fig.4.24. It may be observed that temperature of the engine exhaust gases varies linearly with load for all test fuels. Temperature in the baseline diesel increased from 159°C at no load to 531°C at full load with an almost linear increase of 74°C at every 20% load applied on the engine shaft. The same linear pattern was observed with other test fuels with different temperature rise rate with loads. The increase in exhaust temperature with loads may be due to increased amount of fuel burnt inside the engine at higher loads to generate the requisite brake mean effective pressure [74]. An interesting exhaust gas temperature pattern was observed for CME and its blends. CME10 and CME20 exhibited lower exhaust temperatures whereas CME30 showed a marginal increase in exhaust gas temperature compared to the baseline data of diesel. On the other hand CME40 and CME100 both demonstrated higher exhaust gas temperatures compared to the neat diesel operation. % Variation of exhaust gas temperature from the baseline data of diesel at various loads is shown in Fig. 4.25

CME30, CME40 and CME100 exhibited 3.58%, 7.72% and 10.73% of higher exhaust temperature respectively compared to the baseline data at full load. On the contrary,

CME10 and CME20 showed 5.65% and 3.01% lower full load exhaust temperature as that of the baseline data of diesel. The lower exhaust temperature of CME10 and CME20 may be due to the lower combustion duration of these fuels so that most of the increased heat release was converted into useful work resulting in reduced exhaust temperature [67,68]. Lower exhaust loss may be the possible reason for higher engine performance for CME10 and CME20 as discussed earlier. However, after CME30 higher exhaust temperatures compared to the diesel baseline were observed mostly due to increased combustion duration, increased heat loss etc. which may be further evident from the reduced engine performances reported by the higher blends [74]. Results consistent with the present experiment were reported by various researchers [68,78,133,134] working on a variety of vegetable oil esters.

Fig. 4.25: %Variation of exhaust temperature for various test fuels compared to the diesel baseline

4.2.2.3 Carbon dioxide

Fig.4.26shows the variation in emission of carbon dioxide with brake mean effective pressure at various loads. Carbon dioxide in the exhaust gases is an indication of complete combustion. It may be observed that CME10 and CME20 exhibited higher CO_2 emissions as compared to the neat diesel operation at all loads. At full load CME10 and CME20 showed 7% by volume emission of CO_2 as compared to 6.8% demonstrated by the baseline data.

This indicates complete combustion and higher heat release for CME10 and CME20. The same was evident from higher BTE and lower BSEC indicated by theses test fuels in the earlier sections. However CME30 and other higher CME blends showed reduction in CO_2 emissions compared to the baseline data. %Variation in CO_2 emissions at various loads is shown in Fig. 4.27.
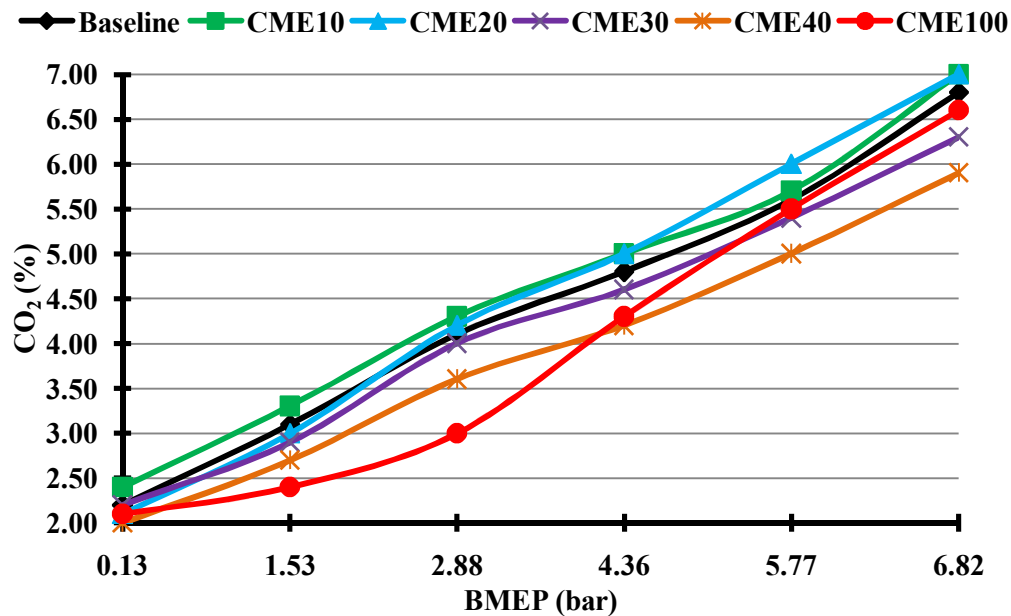
Fig. 4.26: Carbon dioxide emissions with brake mean effective pressure

As discussed above, beyond 20% blend of CME in diesel, emissions of CO_2 was reduced as compared to the baseline data with further increase in CME volume fraction in the test fuel. Higher percentage of CME blends emits lower amount of CO_2 emissions as a consequence of higher viscosity of CME. Fuel spray cone angle, in which air entrainment depends, decreases with increased fuel viscosity. Decrease in cone angle results in reduction of amount of air entrainment in the spray. Lack of enough air in the fuel spray impedes completion of combustion and decreases formation of CO_2 emissions [119].
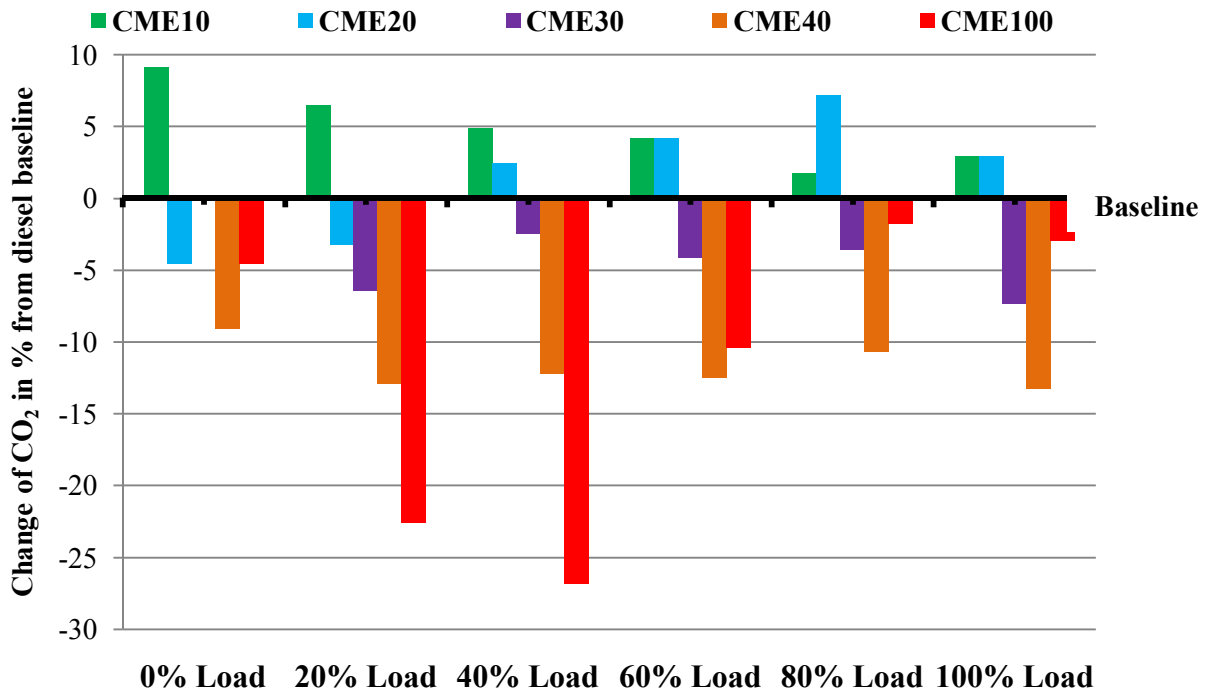
Fig. 4.27: %Variation CO_2 emission for various test fuels compared to the diesel baseline

4.2.3 Engine Combustion Results

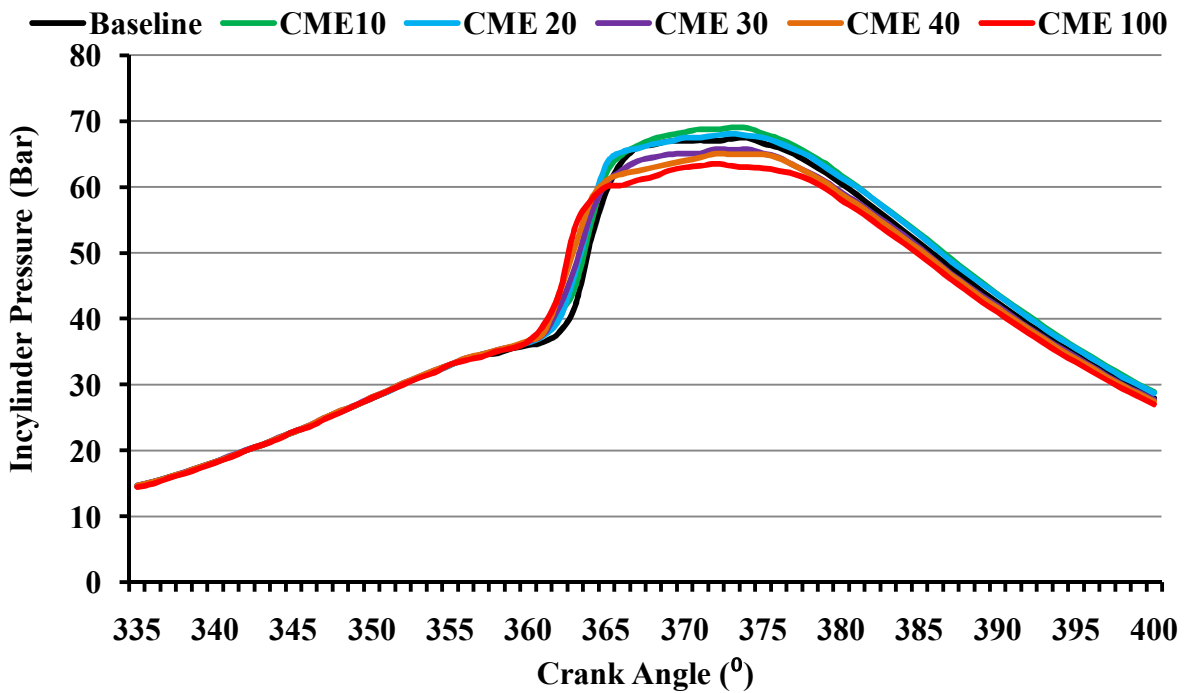### 4.2.3.1 In-cylinder pressure and pressure rise rate

Fig. 4.28: Full load pressure crank angle diagram for various test fuels
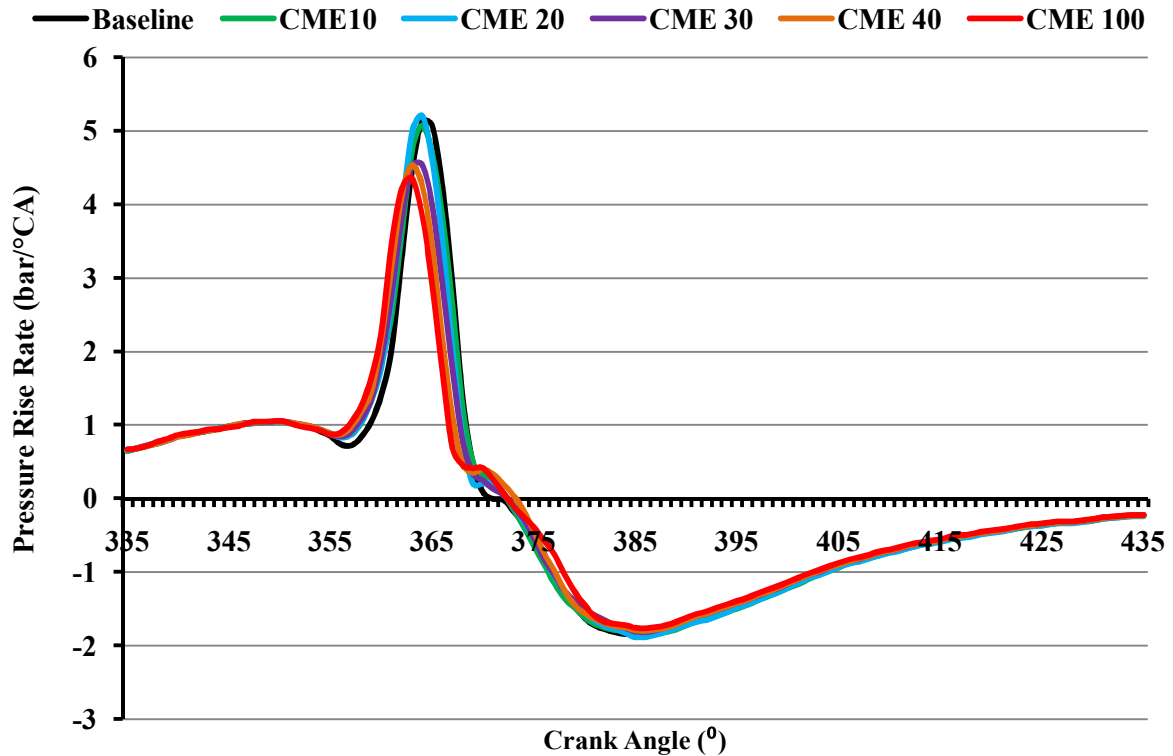
Fig. 4.29: Full load pressure crank angle diagram for various test fuels

The variation of full load in-cylinder pressure with crank angle is shown in Fig. 4.28 and the pressure rise rate is shown in Fig.4.29 for the test fuels. For the purpose of clarity, in visualisation of firing pressure for different test fuels, the pressure data between 335°CA and 400°CA was taken for in-cylinder pressure. It may be observed that at full load neat diesel exhibited 67.51 bar pressure corresponding to 374°CA. CME10 and CME20 showed full load peak pressure of 69.06 bar and 68.12 bar respectively corresponding to 373°CA same for both case. The higher and earlier peak pressure observed for CME10 and CME20 compared to the baseline data of diesel may be explained by the fact that at lower fractions of CME in the blend, the fuel became more oxygenated due to CME and the higher viscosity of CME was not felt due to lower proportions. Moreover, the higher cetane rating of CME compared to neat diesel led to improved combustion. This may be validated by the fact that that CME10 and CME20 exhibited higher full load BTE and lower exhaust temperature compared to the baseline data. However, CME30, CME40 and CME100 showed peak in-cylinder pressure of 65.81 bar, 65.1 bar and 63.53 bar corresponding to 372°CA. The lower in-cylinder pressure exhibited by the blends of CME beyond 20% substitution may be due to

the reduced heating value of the fuel and increasing difficulty in atomization and vaporisation. Despite of reduced peak pressure, neat CME and all of its blends indicated earlier peak pressure compared to the baseline confirming the higher cetane rating of the fuel. It may be observed that the rate of pressure rise was higher for CME10, CME20 and the diesel baseline compared to other blends. The higher pressure rise rate of these test fuels was evident from the noisy engine operation when running on these test fuels. Similar types of results were obtained by Sahoo et.al. [80] and Shivalakshmi et.al.[58].

4.2.3.2 Heat release rate

The rate of heat release was calculated from the pressure crank angle data using the Sorenson's heat release model elaborately discussed in the section 3.7.7. Heat release per crank angle was calculated using the equation (3.15). The heat release curve for various test fuels is shown in Fig. 4.27. It may be observed that the peak heat release rate of diesel was 73.58 J/°CA. CME10, CME20, CME30, CME40 and CME100 exhibited peak heat release rates of 69.62, 70.71, 62.82, 60.04 and 57.14 J/°CA respectively. Notably, the crank angle corresponding to the peak heat release was lower for CME and its blends. Therefore it may be stated that CME and its blends exhibited an earlier and slower rate of heat release compared to the baseline data of diesel. Fig. 4.31 shows the cumulative heat release for various test fuels. It may be observed that CME10 and CME20 exhibited higher amount of total heat release in a cycle as compared to the baseline data of diesel. However, beyond CME30, a reduction in total heat release was reported mainly on account of poor combustion and reduced heating values. It may be observed in the Fig.4.30 that the premixed and diffusion heat release phases for all the test fuels were distinctly visible. By combining the results of Fig. 4.30 and 4.31, the total cyclic heat release and phase wise heat release for various test fuels were evaluated and shown in the Fig. 4.32. Two interesting observations were drawn from the heat release pattern. Firstly, CME10 and CME20 showed marginally higher total cyclic heat lease of 1111.20 Joules/cycle and 1100.57 Joules/cycle respectively compared to 1066.04 showed by the baseline data. Other higher blends of CME indicated lower total heat release. Secondly, the percentage of heat release in the diffusion phase with the total heat release was found to increase in CME volume fraction in the test fuel. Results in the similar spirits were reported by Sahoo et.al. [80], Dhar et. al.[81] and Qi et.al. [78].
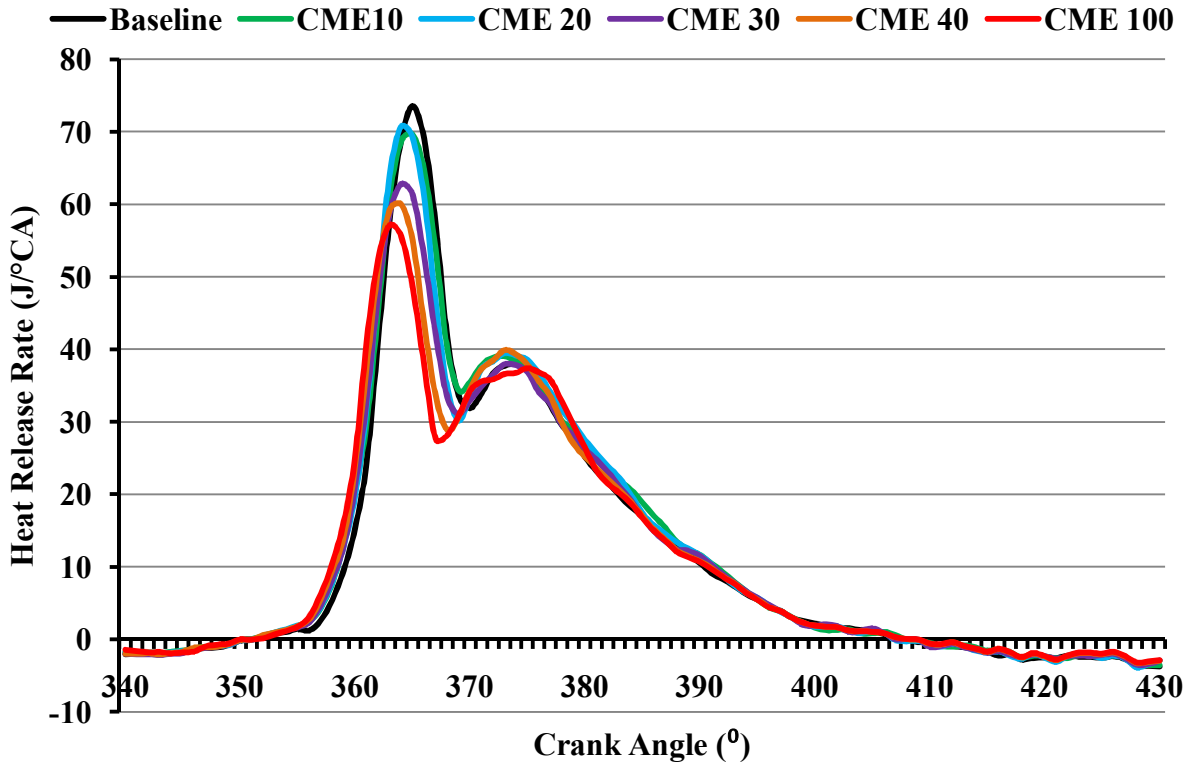
Fig. 4.30: Full load heat release rate diagram for various test fuels
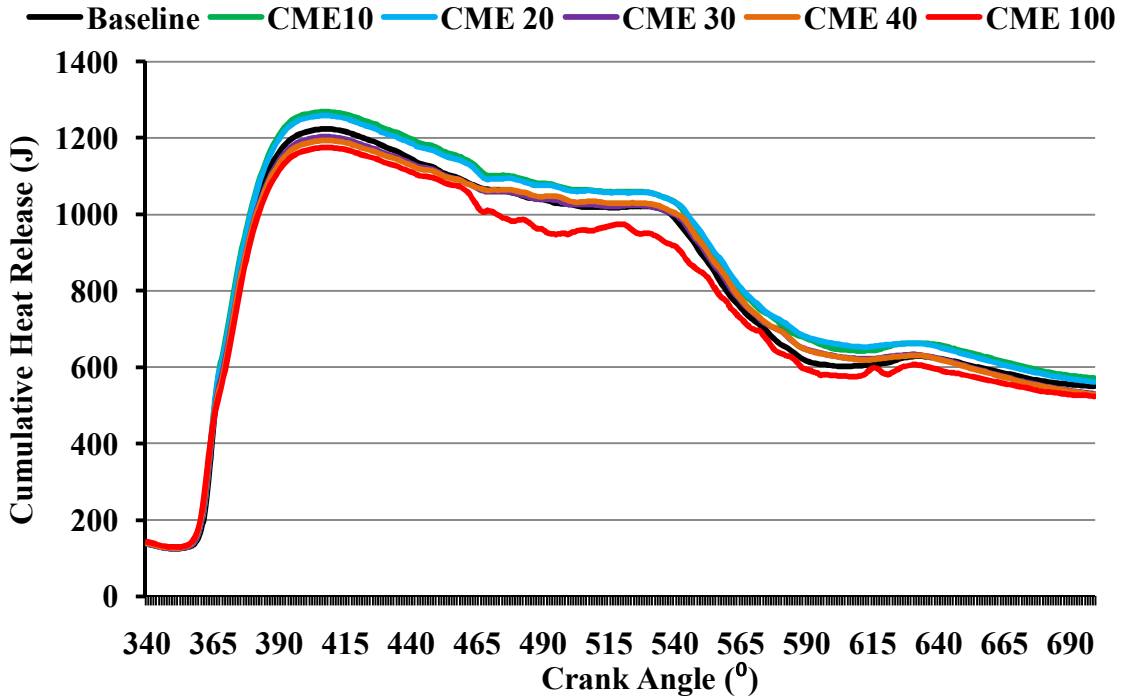
Fig. 4.31: Cumulative heat release diagram for various test fuels
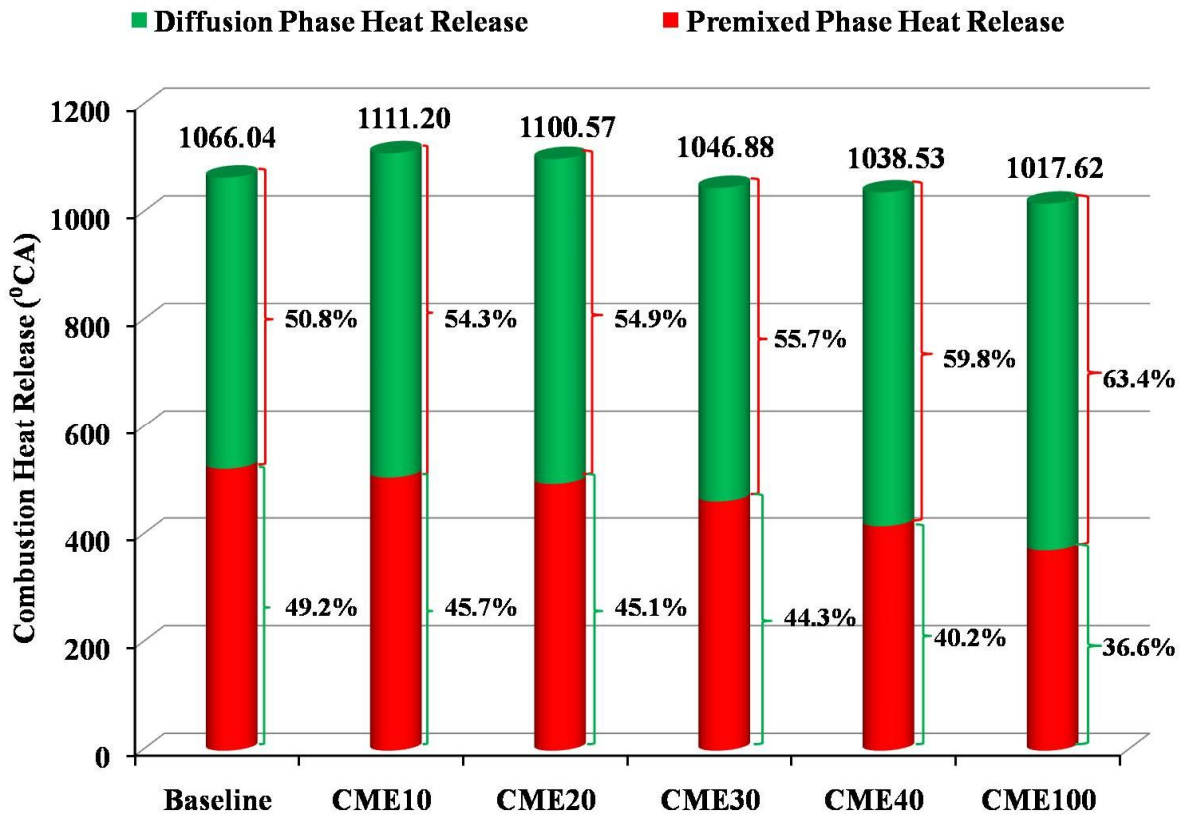
Fig. 4.32: Total cyclic heat release and phase wise heat release for various test fuels at full load

4.2.3.3 Mass fraction burnt

Mass fraction burnt was calculated as per the equation (3.29), discussed in the previous sections. The ignition delay of individual test fuels and total combustion duration was calculated from the mass fraction burnt. Ignition delay was calculated as the difference between the crank angle corresponding to the beginning of fuel injection and the crank angle for MFB=0.05. Similarly the total combustion duration was calculated as the crank angle corresponding to MFB of 0.05 to 0.95.Fig.4.33 and Fig.4.34 shows that total combustion duration was reduced for CME10 and CME20 to 19° and 20° of crank rotation respectively as compared to the 21° crank rotation for the baseline data. However, CME30 and other higher blends exhibited higher total combustion durations. Notably, diffusion phase combustion duration was found to increase with increase in CME volume fraction in the test fuels suggesting smoother engine operation. Fig.4.35 suggests an almost linear reduction in ignition delay with increase in CME volume fraction in the test fuel.
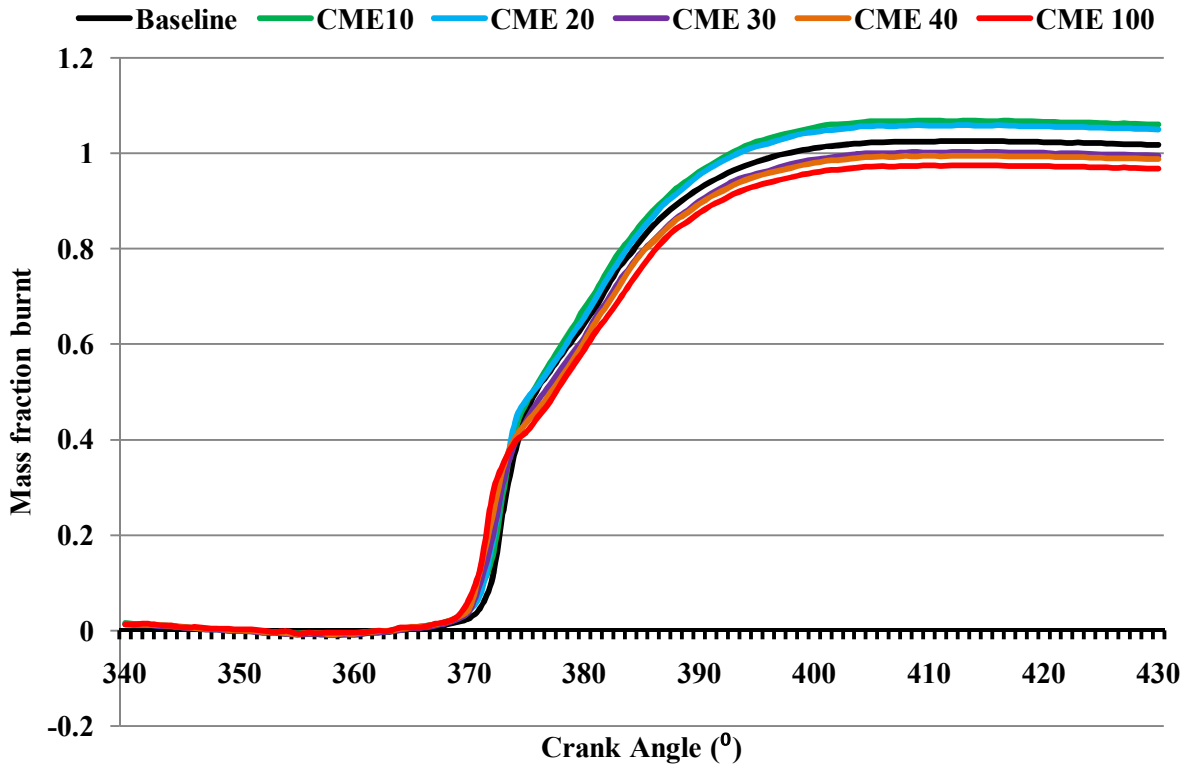
Fig. 4.33: Mass fraction burnt for various test fuels
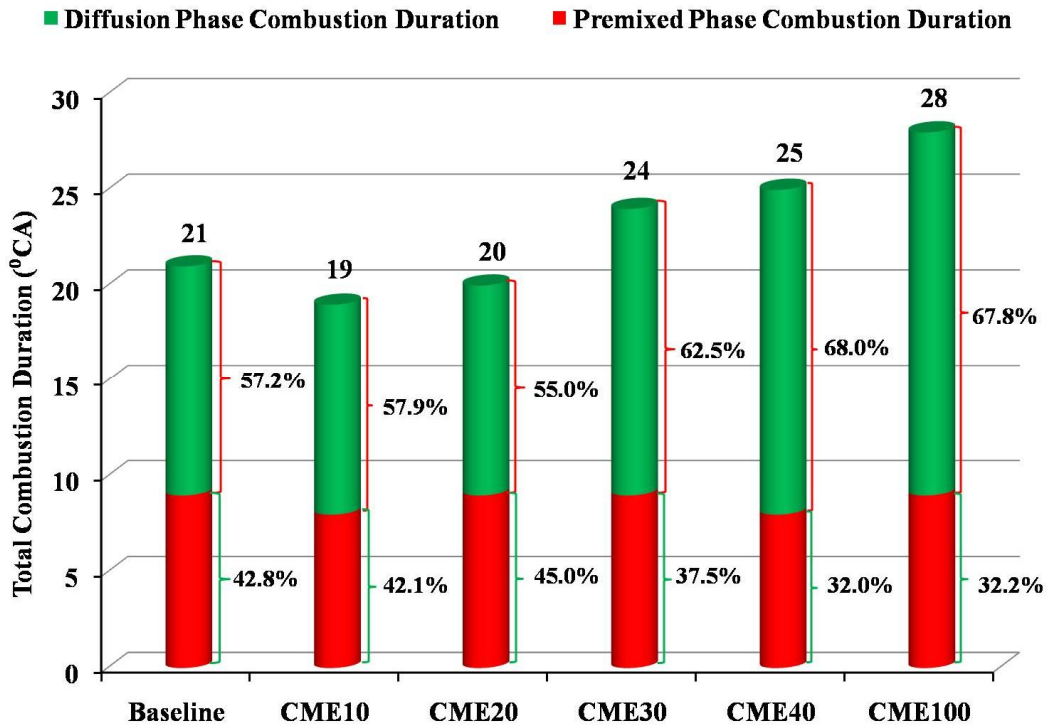
Fig. 4.34: Total and phase wise combustion duration for various test fuels
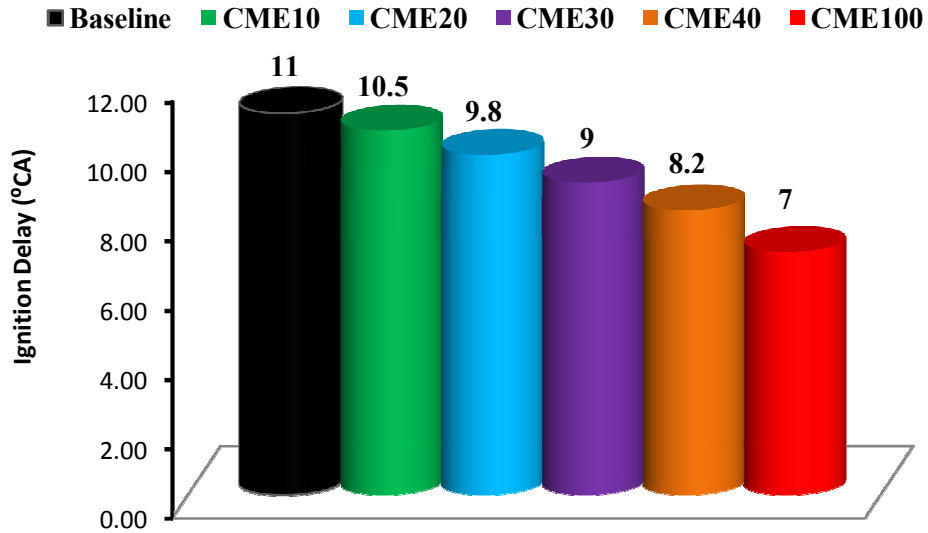
Fig. 4.35: Ignition delay for various test fuels

4.2.3.4 In-cylinder thermodynamics.

In-cylinder bulk gas temperature and the wall heat transfer rate were calculated as per equation (3.23) and (3.26) respectively as described in the section 3.7.7. Fig.4.36 shows the variation in in-cylinder bulk gas temperature for various test fuels. CME10 and CME20 showed higher bulk gas temperature than the diesel baseline. Despite the fact, the exhaust temperature of CME10 and CME20 was lower than the baseline data of diesel. It may be explained by the fact that the pressure rise rate was high and the combustion duration of both these fuels were low resulting in higher conversion of heat energy into mechanical thrust leading to lower exhaust temperatures. However, the emission of NOx was higher for these test fuels as discussed in the emission section. Fig.4.37 shows the rate of wall heat transfer for various test fuels. It may be observed that the loss of heat to the cylinder walls was found to get reduced with increase in the volume fraction of CME in the test fuels. However, the magnitude of wall heat transfer is very low and barely affects the net heat release rate. The pattern was studied only to indicate the suitability of CME in diesel engines.

Fig. 4.36 In-cylinder bulk gas temperature for various test fuels
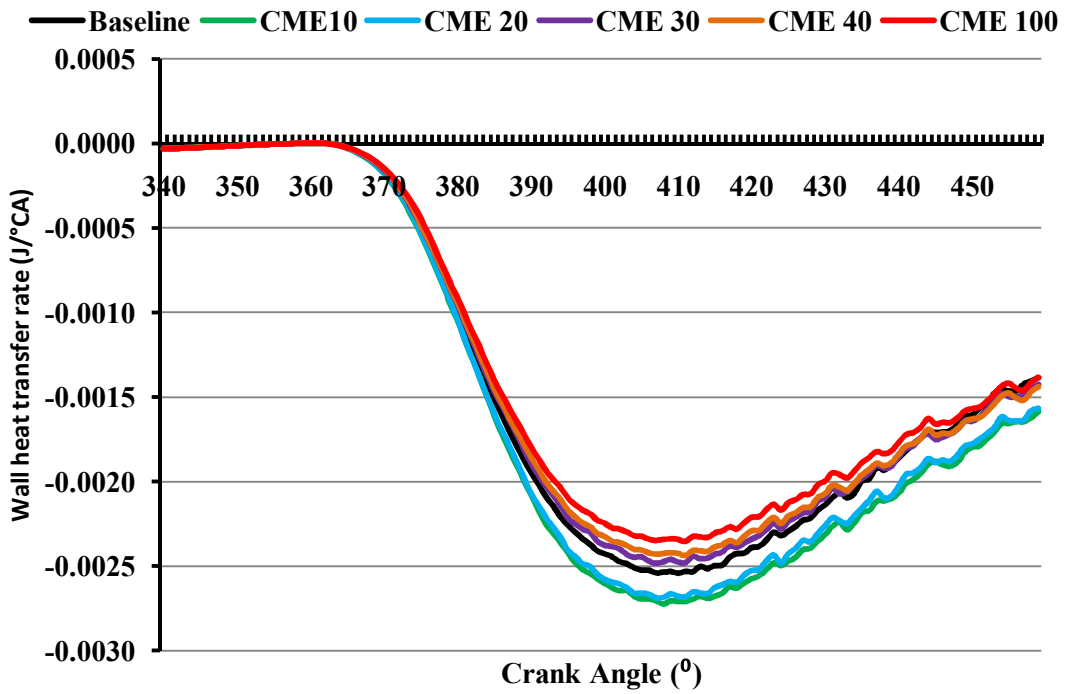
Fig. 4.37 Wall heat transfer for various test fuels

Table 4.8 shows various in-cylinder and combustion characteristics of the test fuels.

Table 4.8 Various in-cylinder and combustion characteristics of the test fuels

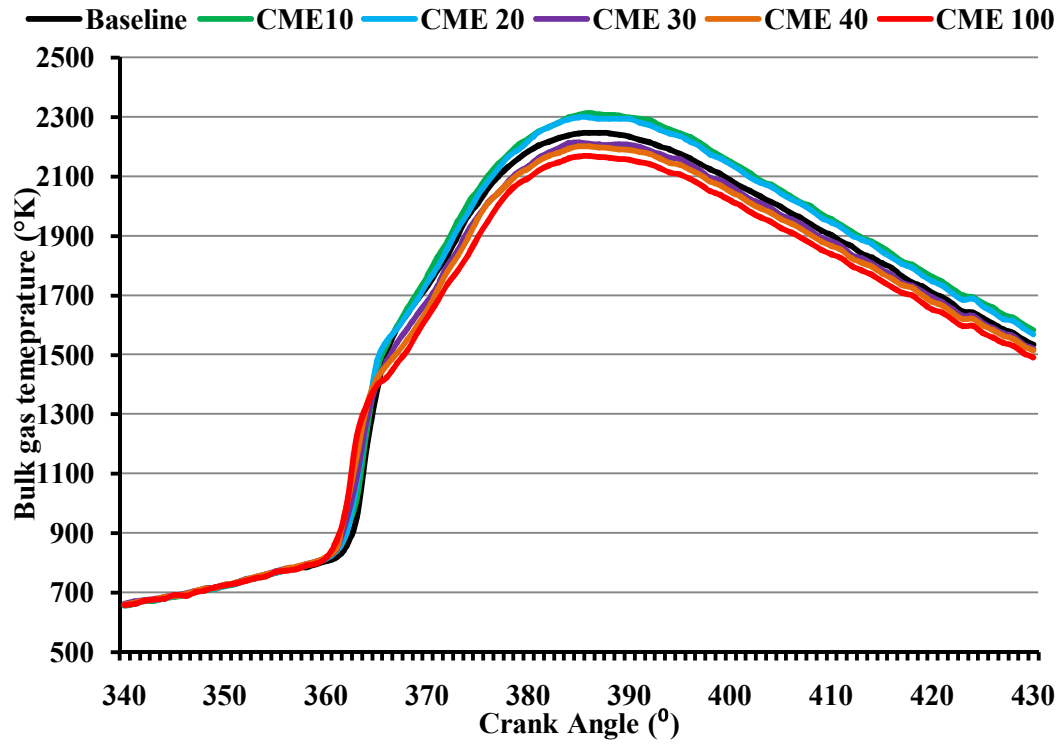| Sl No	Test Fuel	Peak Pressure (bar)	Peak HRR (J/°CA)	CHR (J)	TCD (°CA)	Ignition delay (°CA)
1	Diesel	67.51	73.58	1066.04	21	11
2	CME10	69.06	69.62	1111.2	19	10.5
3	CME20	68.12	70.71	1100.57	20	9.8
4	CME30	65.81	62.82	1046.88	24	9
5	CME40	65.1	60.04	1038.53	25	8.2
6	CME100	63.53	57.14	1017.62	28	7

As an outcome of an exhaustive engine trial and the subsequent analysis, it may be satisfactorily stated that Calophyllum methyl ester is an excellent diesel engine fuel. Up to 30% blend of CME in diesel may be applied in any unmodified diesel engine with improved performance, emission (except NO_x) and combustion characteristics. CME derived from Calophyllum vegetable oil employing a two stage acid and base catalyzed transesterification is an excellent alternative renewable fuel for diesel engine applications.

4.3 MODEL VALIDATIONS AND RESULTS OF NUMERICAL SIMULATION

4.3.1 Model Validation

For the validation of the numerical model, the ignition delay period, peak in-cylinder pressure and the shapes of experimental and simulation pressure profiles. The matching of simulated and experimental pressure traces are shown in Fig. 4.38. Although the general shape of the simulated in-cylinder pressure profiles matched the experimental measurements, there is noticeable discrepancy beyond 400°CA point due to the possible effects of blow-by. The experimental cases also have marginally 'slimmer' peaks as compared to the simulated cases due to the sharper predicted pressure spike. This sharper spike could be attributed to the relatively small size of the surrogate fuel molecules which are relatively more combustible as compared to the actual larger size fuel molecules. In general, the accuracy of the models is deemed good and these models are utilized for all the subsequent simulations.
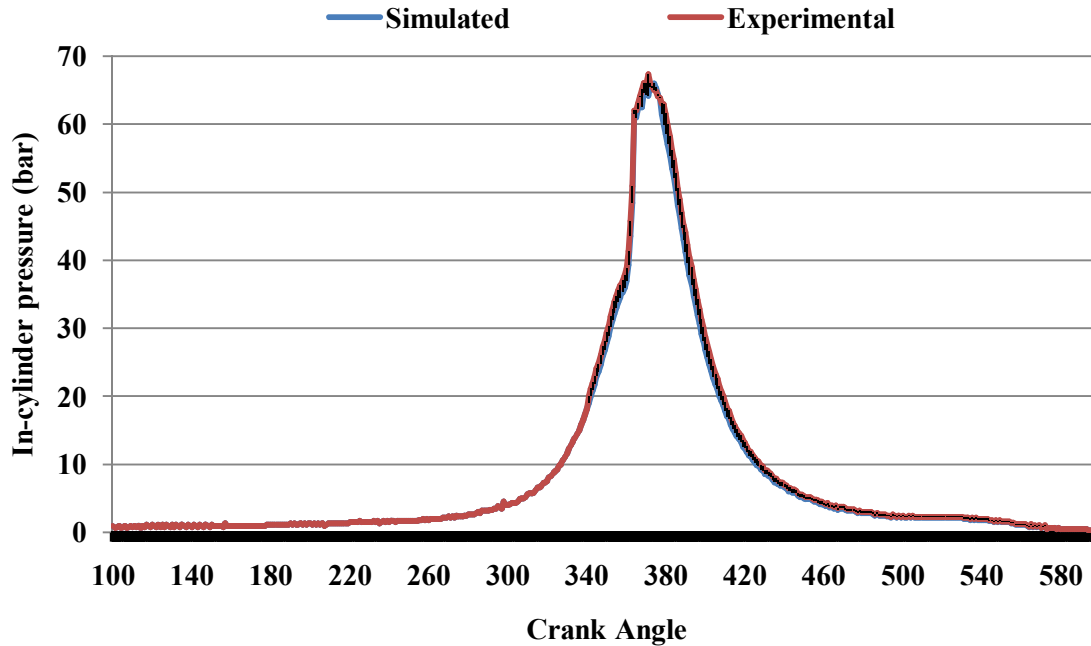
Fig. 4.38 Simulated and experimental pressure traces

4.3.2 Results

Fig. 4.39 depicts the spatial plots of mole fraction of NO when fuelled with CME at 370°CA and 390°CA.Th. The regions where NO are formed at high concentration match those where temperatures are high, at above the 2000 K range. CME has concentrated regions of high gas temperature. As such, the local in-cylinder peak gas temperature achieved for CME was lower than that of mineral diesel. On the other hand, the extremely high local in-cylinder gas temperature regions for the biodiesel cases were mainly concentrated in the bowl. This indicated that local regions away from the bowl which were cooler were not able to form thermal NO. However, the overall formation of NO was high. It can be seen that as time advanced from 370°CA, the high gas temperature regions moved away from the injection point. At +390°CA, gas temperature remained relatively high throughout the bowl, squish and near to the injector regions. Hence, the high gas temperature regions which were sustained late into the expansion stroke for the CME case also extended the NO formation window. Thus, the engine-out NO concentration was considerably higher for CME which was consistent with the experimental data.

MOLE FRACTION OF NO$_x$
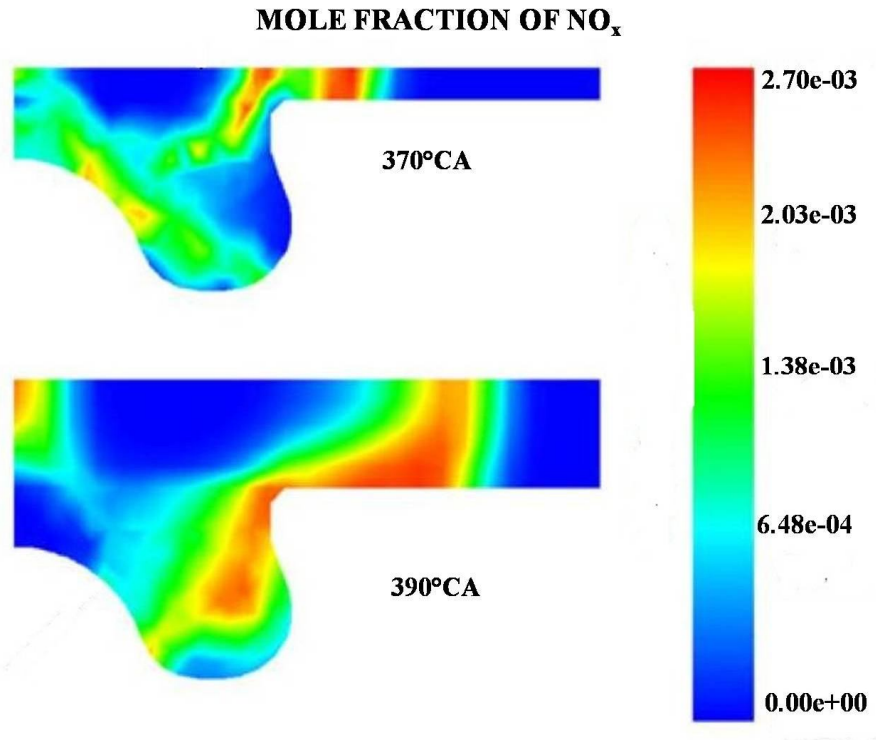
Fig. 4.39 Mole fraction of NOx using CME100 at 370°CA and 390°CA

CONCLUSION AND FUTURE WORKS

5.1 CONCLUSION

In the present work, four basic aspects of alternative fuel application in diesel engine were investigated. They include the optimization of process parameters for the production of biodiesel from Calophyllum vegetable oil, physico-chemical and fuel characterization of Calophyllum biodiesel, exhaustive diesel engine trials using biodiesel to determine various performance, emission and combustion characteristics and setting up a numerical model and its validation. The results for the present investigation are discussed below.

5.1.1 Biodiesel production optimization using response surface methodology

1. The statistically significant model for the esterification stage was a quadratic model.
2. The optimal point conditions predicted in the esterification stage was 4.74% FFA, 1.5% catalysts (PTSA) concentration and reaction temperature of 65°C for a reaction time of 60 munities.
3. The statistically significant model for the transesterification stage was a cubic model.
4. For the transesterification of the oil to biodiesel, the optimal yield was predicted as 96.48% under the reaction conditions of 0.88% catalyst (KOH) concentration, reaction temperature of 62.75^{o}C for the reaction time of 90 minutes.
5. The methanol to oil molar ratio of 1:6 and agitation speed of 400 rpm was same in both the stages.

5.1.2 Physico-chemical and fuel characterisation.

1. The fatty acid profile of the Calophyllum biodiesel indicated 16.18% palmitic acid, 22.01% stearic acid, 29.46% oleic acid, 31.06% linoleic acid and others in traces.

2. The density of CME100 was 0.89 g/cc at 15°C, viscosity was 5.55cSt at 40°C, oxidative stability was 3.97 hours and CFPP of 0°C. All the physico-chemical parameters were found to be within the limits of corresponding ASTM standards.

5.1.3 Results for engine trial

1. CME10 and CME20 exhibited 27.6% and 26.6% full load brake thermal efficiency respectively as compared to 26.4% illustrated by the diesel baseline. CME30, CME40 and CME100 showed lower full load BTE than neat diesel operation.

2. Similarly CME10, CME20, CME30, CME40 and CME100 brandished full load brake specific energy consumption (BSEC) of 289.42MJ/kWh, 278.17MJ/kWh, 315.03MJ/kWh, 325.54MJ/kWh and 358.95MJ/kWh respectively as compared to 299.57MJ/kWh illustrated by the baseline diesel operation.

3. The full load carbon monoxide, smoke and total hydrocarbon emissions of CME and its blends were lower than the diesel baseline by a margin of 20% to 50%. CME10 and CME20 exhibited lower exhaust temperature and carbon dioxide (CO_2) emission at all loads compared to the neat diesel operation.

4. However, other higher blends of CME showed comparatively higher exhaust gas temperature. CME and its blends showed higher oxides of nitrogen emissions than mineral diesel operation at almost all the loads.

5. The total combustion duration (TCD) of CME10 and CME20 were 19 and 20 crank angle degrees (°CA) as compared to 20, 24, 25 and 28 °CA exhibited by neat diesel, CME30, CME40 and CME100 respectively.

6. With increase in volume fraction of CME in the blend ignition delay was reduced from 11°CA for neat diesel to 7°CA for neat CME.

7. The combustion heat release (CHR) for CME10 and CME20 were1111.20 Joules and 1100.57 Joules respectively as compared to 1066.04 Joules for the baseline neat diesel data.

8. Other higher blends of CME exhibited lower heat release than the baseline diesel data. Another notable observation in combustion study was the trend of increased % heat release in the diffusion phase with increase in CME volume fraction that leads to smoother engine operation.

5.1.4 Numerical simulation

1. The model was highly congruent with the actual engine set up with profile matching and peak pressure difference of 1.5%.
2. The NO emissions of the model were found to be consistent with the experimental data.

6.2 FUTURE WORKS

The knowledge so gained during the present research work may be extended in the following directions for further research.

1. Molar ratio and agitator rpm may be considered as factors for biodiesel production optimization.
2. Effect of cold flow property and oxidation stability improvers may be studied.
3. Quasi-dimensional heat release model may be developed for more accurate heat release characterization.
4. Comprehensive combustion simulation may be carried out to evaluate the performance, emission and combustion behavior of the model using various permutation and combination of CME and diesel.

[1]   A text book on "Science Concepts" by Alvin Silverstein, Virginia Silverstein and Laura Silverstein Nunn. Second Edition, ISBN 978-0-8225-8655-5. Publisher-Twenty First century books. pp: 5-7.

[2]   http://physics.about.com/od/glossary/g/energy.htm. Data taken on 22.06.2013

[3]   A text book on "Energy its use and Environment" by Hinrichs and Kleinbach. Fifth edition, ISBN-13: 978-1-111-99083-1. Publisher – Cengage Learning Co. pp: 1-3.

[4]   BPSR-2011.

[5]   http://maninair.in/gdp-growth-rate-india. Data taken on 22.06.2013.

[6]   Chauhan B.S, Kumar N, Jun Y.D, Lee K.B. Performance and emission study of preheated Jatropha oil on medium capacity diesel engine. Energy 35 (2010), pp: 2484-2492.

[7]   http://data.worldbank.org. Data taken on 27.06.2013.

[8]   International energy agency annual survey conducted in the financial year 2009-2010..http://www.iea.org/stats/pdf_graphs/INTPESPI.pdf

[9]   Basic Statistics on Indian Petroleum & Natural Gas, 2009-10. Ministry of Petroleum & Natural Gas, Government of India, New Delhi, Economic Division.

[10]   Basic Statistics on Indian Petroleum & Natural Gas, 2010-11. Ministry of Petroleum & Natural Gas, Government of India, New Delhi, Economic Division.

[11]   Gill S.S, Tsolakis A, Dearn K.D, Fernandez R.J. Combustion characteristics and emissions of Fischer Tropsch diesel fuels in IC engines. Progress in Energy and Combustion Science 37 (2011), pp: 503-523.

[12]   OECD Key environmental indicators 2008. OECD Environmental Directorate, Paris, France.

[13]   Wang L, Yu H. Biodiesel from Siberian apricot (Prunussibirica L.) seed kernel oil. Bioresource Technology 112 (2012) 355–358.

[14]   Agarwal A.K. Bio-fuels (alcohols and biodiesel) applications as fuels for internal combustion engines. Prog Energ Combust 2007;33:233-71.

[15]   Chauhan B.S, Kumar N, Cho H.M. Performance and emission studies on an agriculture engine on neat Jatropha oil. Journal of Mechanical Science and Technology 24 (2) (2010), pp: 529-535.

[16] Chauhan B.S, Kumar N, Pal S.S, Jun Y.D. Experimental studies on fumigation of ethanol in a small capacity diesel engine. Energy 2011; 36:1030-8.

[17] Mishra R.D, Murthy M.S. Straight vegetable oils usage in a compression ignition engine—A review. Renewable and Sustainable Energy Reviews 14 (2010) 3005–3013.

[18] Achten W.M.J, Verchot L, Franken Y.J, Mathijs E, Singh V.P, Aerts R. Jatropha bio-diesel production and use. Biomass Bioenergy (2008). 32 1063–84

[19] Lin L, Ying D, Chaitep S, Vittayapadung S. Biodiesel production from crude rice bran oil and properties as fuel. Applied Energy 86 (2009) 681–688.

[20] Barnwal B. K, Sharma M. P. Prospects of biodiesel production from vegetable oils in India; Renewable and Sustainable Energy Reviews (2005), Vol.9, pp.363–378.

[21] http://planningcommission.nic.in/plans/planrel/fiveyr/welcome.html. Data taken on 27.06.2013.

[22] http://mofpi.nic.in/ContentPage.aspx?CategoryId=687. Data taken on 27.06.2013.

[23] http://www.bioenergyconsult.com/tag/national-biodiesel-mission/. Data taken on 27.06.2013.

[24] http://www.jatrophabiodiesel.org/indianPrograms.php. Data taken on 27.06.2013.

[25] http://mnre.gov.in/file-manager/UserFiles/biofuel_policy.pdf. Data taken on 27.06.2013.

[26] Friday J.B, Okano, D. Agro species profiles for Pacific Island -forestry.2006, ver. 2.1.

[27] Azam M.M, WarisA, Nahar N.M. Prospects and potential of fatty acid methyl esters of some non-traditional seed oils for use as biodiesel in India. Biomass and Bio-energy (2005);29(4):293–302.

[28] Pinzi S, Garcia I.L, Gimenez F.J.L, Castro M.D.L, Dorado G, Dorado M.P. The ideal vegetable oil-based biodiesel composition: a review of social, economic and technical implications. Energy & Fuels (2009); 23:2325–41.

[29] Kumar A, Sharma S. Potential non-edible oil resources as biodiesel feed-stock: an Indian perspective. Renewable and Sustainable Energy Reviews (2011); 15(4):1791–800.

[30] Venkanna B.K, Venkataramana R.C. Biodiesel production and optimization from Calophyllum Inophyllum Linn oil (hone oil) — a three stage method. Bio-resource Technology (2009) ;100(21):5122–5.

[31] No S.Y. Inedible vegetable oils and their derivatives for alternative diesel fuels in CI engines: a review. Renewable and Sustainable Energy Reviews (2011) ;15(1):131–49.

[32]   Atabani A.E, Silitonga A.S, Ong H.C, Mahlia T.M.I, Masjuki H.H, Badruddin I.A, Fayaz H. Non-edible vegetable oils: A critical evaluation of oil extraction, fattyacid compositions, biodiesel production, characteristics, engine performance and emissions production". Renewable and Sustainable Energy Reviews18(2013)211–245.

[33]   Atadashi I.M, Aroua M.K, Abdul Aziz A.R, Sulaiman N.M.N. Production of biodiesel using high free fatty acid feedstocks. Renewable and Sustainable Energy Reviews 16 (2012) 3275– 3285.

[34]   Chen Y.H, Chen J.H, Chang C.Y, Chang C.C. Biodiesel production from tung (Vernicia montana) oil and its blending properties in different fatty acid compositions. Bioresource Technology 101 (2010) 9521–9526.

[35]   Usta N, Aydoğˇan B, Çon A.H, Ugˇuzdogˇan E, Özkal S.G. Properties and quality verification of biodiesel produced from tobacco seed oil. Energy Conversion and Management 52 (2011) 2031–2039.

[36]   Teixeira da Silva de La Salles K, Meneghetti S.M.P, Ferreira de La Salles W, Meneghetti M.R, Dos Santos I.C.F, da Silva J.P.V, de Carvalho S.H.V, Soletti J.I. Characterization of Syagrus coronata (Mart.) Becc. oil and properties of methyl esters for use as biodiesel. Industrial Crops and Products 32 (2010) 518–521.

[37]   Silitonga A.S, Ong H.C, Mahlia T.M.I, Masjuki H.H, Chong W.T. Characterization and production of Ceiba pentandra biodiesel and its blends. Fuel 108 (2013) 855–858.

[38]   Lin L, Ying D, Chaitep S, Vittayapadung S. Biodiesel production from crude rice bran oil and properties as fuel. Applied Energy 86 (2009) 681–688.

[39]   Wang L, Yu H. Biodiesel from Siberian apricot (Prunus sibirica L.) seed kernel oil. Bioresource Technology 112 (2012) 355–358.

[40]   Wang R, Zhou W, Hanna M.A, Zhang Y.P, Bhadury P.S, Wang Y, Song B, Yang S. Biodiesel preparation, optimization, and fuel properties from non-edible feedstock, Datura stramonium. Fuel 91 (2012) 182–186.

[41]   Benjumea P, Agudelo J, Agudelo A. Basic properties of palm oil biodiesel–diesel blends. Fuel 87 (2008) 2069–2075.

[42]   Berman P, Nizri S, Wiesman Z. Castor oil biodiesel and its blends as alternative fuel. Biomass and bioenergy 35(2011)2861-2866.

[43]   Bucy H.B, Baumgardner M.e, Marchese A.J. Chemical and physical-properties of algal methyl ester biodiesel containing varying levels of methyl eicosapentaenoate and methyl docosahexaenoate. Algal Research 1 (2012) 57–69.

[44]   Chakraborty M, Baruah D.C, Konwer D. Investigation of terminalia (Terminalia belerica Robx.) seed oil as prospective biodiesel source for North-East India. Fuel Processing Technology 90 (2009) 1435–1441.

[45]   Chammoun N, Geller D.P, Das K.C. Fuel properties, performance testing and economic feasibility of Raphanus sativus(oilseed radish) biodiesel. Industrial Crops and Products 45 (2013) 155– 159.

[46]   Chu J, Xu X, Zhang Y. Production and properties of biodiesel produced from Amygdalus pedunculata Pall. Bioresource Technology 134 (2013) 374–376.

[47]   Kaya C, Hamamci C, Baysal A, Akba O, Erdogan S, Saydut A. Methyl ester of peanut (Arachis hypogea L.) seed oil as a potential feedstock for biodiesel production. Renewable Energy 34 (2009) 1257–1260.

[48]   Atapour M, Kariminia H.R, Moslehabadi P.M. Optimization of biodiesel production by alkali-catalysed transesterification of used frying oil. Process Safety and Environmental Protection x x x (2 0 1 3) xxx–xxx. PSEP-338.

[49]   Ilham Z, Saka S. Optimization of supercritical dimethyl carbonates method for biodiesel production. Fuel 97 (2012) 670–677.

[50]   Kafuku G, Mbarawa M. Biodiesel production from Croton megalocarpus oil and its process optimization. Fuel 89 (2010) 2556–2560.

[51]   Kılıç M, Uzun B.B, Pütün E,Pütün A.E. Optimization of biodiesel production from castor oil using factorial design. Fuel Processing Technology 111 (2013) 105–110.

[52]   Lee H.V, Yunus R, Juan J.C, Taufiq-Yap Y.H. Process optimization design for jatropha-based biodiesel production using response surface methodology. Fuel Processing Technology 92 (2011) 2420–2428.

[53]   Omar W.N.N.W, Amin N.A.S. Optimization of heterogeneous biodiesel production from waste cooking palm oil via response surface methodology. Biomass and bio-energy 35(2011)1329-1338.

[54]   Wu X, Leung D.Y.C. Optimization of biodiesel production from camelina oil using orthogonal experiment. Applied Energy 88 (2011) 3615–3624.

[55] Yücel Y. Optimization of biocatalytic biodiesel production from pomace oil using response surface methodology. Fuel Processing Technology 99 (2012) 97–102.

[56] Yun H, Wang M, Feng W, Tan T. Process simulation and energy optimization of the enzyme-catalysed biodiesel production. Energy 54 (2013) 84-96.

[57] Uzun B.B, Kılıç M, Özbay N, Pütün A.E, Pütün E. Biodiesel production from waste frying oils: Optimization of reaction parameters and determination of fuel properties. Energy 44 (2012) 347-351.

[58] Sivalakshmi S, Balusamy T. Effect of biodiesel and its blends with diethyl ether on the combustion, performance and emissions from a diesel engine. Fuel 106 (2013) 106–110.

[59] Shehata M.S. Emissions, performance and cylinder pressure of diesel engine fuelled by biodiesel fuel. Fuel xxx(2013)xxx–xxx.

[60] Nabi M.N, Hoque S.M.N, Akhter M.S. Karanja (Pongamia Pinnata) biodiesel production in Bangladesh, characterization of karanja biodiesel and its effect on diesel emissions. Fuel Processing Technology 90 (2009) 1080–1086.

[61] Ganapathy T, Gakkhar R.P, Murugesan K. Influence of injection timing on performance, combustion and emission characteristics of Jatropha biodiesel engine. Applied Energy 88 (2011) 4376–4386.

[62] Lapuerta M, Jose O.A, Ferna´ndez R. Effect of biodiesel fuels on diesel engine emissions. Progress in Energy and Combustion Science 34 (2008) 198–223.

[63] Muralidharan K, Vasudevan D, Sheeba K.N. Performance, emission and combustion characteristics of biodiesel fuelled variable compression ratio engine. Energy 36 (2011) 5385-5393.

[64] Mofijur M, Masjuki H.H, Kalam M.A, Atabani A.E. Evaluation of biodiesel blending, engine performance and emissions characteristics of Jatropha curcas methyl ester: Malaysian perspective. Energy 55 (2013) 879-887.

[65] Chen L.Y, Chen Y.H, Hung Y.S, Chiang T.H, Tsai C.H. Fuel properties and combustion characteristics of jatropha oil biodiesel–diesel blends. Journal of the Taiwan Institute of Chemical Engineers 44 (2013) 214–220.

[66] Canakci M, Ozsezen A.N. Arcaklioglu E. Erdil A. Prediction of performance and exhaust emissions of a diesel engine fuelled with biodiesel produced from waste frying palm oil. Expert Systems with Applications 36 (2009) 9268–9280.

[67]   Chauhan B.S, Kumar N, Cho H.M. A study on the performance and emission of a diesel engine fuelled with Jatropha biodiesel oil and its blends. Energy 37 (2012) 616-622.

[68]   Chauhan B.S, Kumar N, Cho H.M, Lim H.C. A study on the performance and emission of a diesel engine fuelled with Karanja biodiesel and its blends. Energy 56 (2013) 1-7.

[69]   Dhar A, Kevin R, Agarwal A.K. Production of biodiesel from high-FFA neem oil and its performance, emission and combustion characterization in a single cylinder DICI engine. Fuel Processing Technology 97 (2012) 118–129.

[70]   Liaquat A.M, Masjuki H.H, Kalam M.A, Fattah I.A.R, Hazrat M.A, Varman M, Mofijur M, Shahabuddin M. Effect of coconut biodiesel blended fuels on engine performance and emission characteristics. 5th BSME International Conference on Thermal Engineering. Procedia Engineering 56 (2013) 583 – 590.

[71]   Özener O, Yüksek L, Ergenç A.T, Özkan M. Effects of soybean biodiesel on a DI diesel engine performance, emission and combustion characteristics. Fuel xxx (2012) xxx–xxx.

[72]   Selvam D.J.P, Vadivel K. Performance and emission analysis of DI diesel engine fuelled with methyl esters of beef tallow and diesel blends. International Conference on Modelling Optimization and Computing-(ICMOC-2012). Procedia Engineering 38; (2012); 342 – 358.

[73]   Sahoo P.K, Das L.M, Babu M.K.G, Naik S.N. Biodiesel development from high acid value polanga seed oil and performance evaluation in a CI engine. Fuel 86 (2007) 448–454.

[74]   Raheman H, Ghadge S.V. Performance of compression ignition engine with mahua (Madhuca indica) biodiesel. Fuel 86 (2007) 2568–2573.

[75]   Godiganur S, Murthy C.H.S, Reddy R.P. 6BTA 5.9 G2-1 Cummins engine performance and emission tests using methyl ester mahua (Madhuca indica) oil/diesel blends. Renewable Energy 34 (2009) 2172–2177.

[76]   Rehman H, Phadatare A.G. Diesel engine emissions and performance from blends of karanja methyl ester and diesel. Biomass and Bio-energy 27 (2004) 393 – 397.

[77]   Buyukkaya E. Effects of biodiesel on a DI diesel engine performance, emission and combustion characteristics. Fuel 89 (2010) 3099–3105.

[78] Qi D.H. Chen H, Geng L.M. Bian Y.Z. Experimental studies on the combustion characteristics and performance of a direct injection engine fuelled with biodiesel/diesel blends. Energy Conversion and Management 51 (2010) 2985–2992.

[79] Qi D.H. Chen H, Geng L.M. Bian Y.Z, Liu J, Ren X.C.H. Combustion and performance evaluation of a diesel engine fuelled with biodiesel produced from soybean crude oil. Renewable Energy 34 (2009) 2706–2713.

[80] Sahoo P.K, Das L.M. Combustion analysis of Jatropha, Karanja and Polanga based biodiesel as fuel in a diesel engine. Fuel 88 (2009) 994–999.

[81] Bari S, Idris S. CFD modelling of the effect of guide vane swirl and tumble device to generate better in-cylinder air flow in a CI engine fuelled by biodiesel. Computers and fluids. DOI: http://dx.doi.org/10.1016/j.compfluid.2013.06.011. Accepted, yet to publish.

[82] Battistoni M, Grimaldi C.N. Numerical analysis of injector flow and spray characteristics from diesel injectors using fossil and biodiesel fuels. Applied Energy 97 (2012) 656–666.

[83] Bunce M, Snyder D, Adi G, Hall C, Koehler J, Davila B, Kumar S, Garimella P, Stanton D.S, Chaver G. Optimization of soy-biodiesel combustion in a modern diesel engine. Fuel 90 (2011) 2560–2570.

[84] Luo Z, Plomer M, Lu T, Som S, Longman D.E, Sarathy S.M, Pitz W.J. A reduced mechanism for biodiesel surrogates for compression ignition engine applications. Fuel 99 (2012) 143–153.

[85] Ismail H.M, Ng H.K, Gan S, Lucchini T. Computational study of biodiesel–diesel fuel blends on emission characteristics for a light-duty diesel engine using OpenFOAM. Applied Energy 111 (2013) 827–841.

[86] Ismail H.M, Ng H.K, Gan S, Lucchini T, Onorati A. Development of a reduced biodiesel combustion kinetics mechanism for CFD modelling of a light-duty diesel engine. Fuel 106 (2013) 388–400.

[87] Ng H.K, Gan S, Ng J.H, Pang K.M. Simulation of biodiesel combustion in a light-duty diesel engine using integrated compact biodiesel–diesel reaction mechanism. Applied Energy 102 (2013) 1275–1287.

[88] Ng H.K, Gan S, Ng J.H, Pang K.M. Development and validation of a reduced combined biodiesel–diesel reaction mechanism. Fuel 104 (2013) 620–634.

[89] Pang K.M, Ng H.K, Gan S. Development of an integrated reduced fuel oxidation and soot precursor formation mechanism for CFD simulations of diesel combustion. Fuel 90 (2011) 2902–2914.

[90] Som S, Longman D.E, Ramírez A.I, Aggarwal S.K. A comparison of injector flow and spray characteristics of biodiesel with petrodiesel. Fuel 89 (2010) 4014–4024.

[91] Chopade G, Kulkarni K.S, Kulkarni A.D, Topare S. Solid heterogeneous catalysts for production of biodiesel from trans-esterification of triglycerides with methanol : a review. Acta Chimica & Pharmaceutica Indica (2012) ; 2(1):8–14.

[92] Strayer R.C, Blake J.A, Craig W.K. Canola and higher ucicrape seed oil as substitutes for diesel fuel: preliminary tests. Journal of the American Oil Chemists' Society (1983);60:1587–92.

[93] Yusuf N.N.A.N, Kamarudin S.K, Yaakub Z. Overview on the current trends in biodiesel production. Energy Conversion and Management (2011); 52(7):2741–51.

[94] Parawira W. Biodiesel production from Jatropha curcas: a review. Scientific Research and Essays (2010) ;5(14):1796–808.

[95] Leung D.Y.C, Wu X, Leung M.K.H. A review on biodiesel production using catalysed transesterification. Applied Energy (2010) ;87:1083–95.

[96] Park Y.M, Lee J.Y, Chung S.H, Park I.S, Lee S.Y, Kim D.K. Esterification of used vegetable oils using the heterogeneous WO3/ZrO2 catalyst for production of biodiesel. Bioresource Technology (2010); 101(1):S59–61.

[97] Leung D.Y.C, Wu X, Leung M.K.H. A review on biodiesel production using catalysed transesterification. Applied Energy 87 (2010) 1083–1095.

[98] Brandy N. The Response Surface Methodology, Master of Science in Applied Mathematics & Computer Science, Thesis Submitted to the Faculty of the Indiana University South Bend, unpublished article. (2007) ; pp 54-70.

[99] Faletti, J. J., S. C. Sorenson, and C. E. Goering. 1984. Energy release rates from hybrid fuels. Transactions of the ASAE 27(2): 322-325.

[100] Hanson, A. C. 1989. A diagnostic quasi-dimensional model of heat transfer and combustion in compression-ignition engines. Unpublished. Ph.D. thesis. Pietermaritzburg, South Africa: Dept. of Agricultural Engineering, University of Natal.

[101] Huang Z.H, Jiang D.M, Zeng K, Liu B, Yang Z.L. "Combustion characteristics and heat release analysis of a DI compression ignition engine fuelled with diesel-dimethyl carbonate blends". Proc Inst Mech Eng, Part D, J Automobile Eng (2003); 217(D7):595–606.

[102] Crowell, T. J.. Evaluation of enhanced ethanol with fumigation as a diesel fuel replacement. Unpublished. M.S. thesis (1989). Urbana, Ill.: University of Illinois.

[103] Eichelberg, G. Some new investigations on old combustion engine problems. Engineering (1939) ; 148: 463-464, 547-560.

[104] Heywood J.B. Internal Combustion Engine Fundamentals. McGraw-Hill. 1988, ISBN 0-07-100499-8.

[105] Kobayashi T, Tsubokura M. CFD applications in automotive industry. Notes Numer Fluid Mech Multidiscip Des (2009) ;100:285–95.

[106] Reitz R.D, Rutland C.J. Development and testing of diesel engine CFD models. Prog Energy Combust Sci (1995) ;21:173‑96.

[107] Morgan R, Wray J, Kennaird D.A, Heikal M.R. The influence of injector parameters on the formation and break-up of a diesel spray. SAE Paper; (2001) [2001-01-0529].

[108] Golovitchev V.I. Towards universal EDC-based combustion model for compression ignited engine simulations. SAE Paper; (2003) [2003-01-1849].

[109] Ng J-H. Experimental and computational studies of combustion and emission characteristics of biodiesel fuels in a light-duty diesel engine. PhD thesis, University of Nottingham Malaysia Campus; (2011).

[110] Noordin M. Y., Venkatesh V.C, Elting S, Abdullah A. Application of response surface methodology in describing the performance of coated carbide tools when turning AISI 1045 steel, Journal of Materials Processing Technology, **145,** 2004; pp 46-58.

[111] Razali N, Mootabadi B, Salamatinia B, Lee K.T and Abdullah A.Z. Optimization of Process Parameters for Alkali-Catalysed Transesterification of Palm Oil Using Response Surface Methodology, Sains Malaysiana **39**, (2010) ; pp 805-809.

[112] Brandy N. The Response Surface Methodology, Master of Science in Applied Mathematics & Computer Science, Thesis Submitted to the Faculty of the Indiana University South Bend, unpublished article. (2007); pp: 54-70

[113] Tat M.E, Gerpen J.V. The specific gravity of biodiesel and its blends with diesel fuels. JAOCS (2000) ;77:115‑9.

[114] Bahadur N.P, Boocock D.G.B, Konar S.K. Liquid hydrocarbons from catalytic pyrolysis of sewage sludge lipid and canola oil: evaluation of fuel properties. Energy Fuels (1995); 9:248‑56.

[115] EN 14112, Determination of Oxidation Stability (Accelerated Oxidation Test), European Standard, (2003).

[116] ASTM D7170, Standard Test Method for Determination of Derived Cetane Number (DCN) of Diesel Fuel Oils — Fixed Range Injection Period, Constant Volume Combustion Chamber Method, ASTM International, 2009.

[117] Singh Pranil J, KhurmaJagjit, Singh Anirudh. Preparation, characterization, engine performance and emission characteristics of coconut oil based hybrid fuels. Renewable Energy, (2010);35:2065-70

[118] Muralidharan K, Vasudevan D, SheebaK.N. Performance, emission and combustion characteristics of biodiesel fuelled variable compression ratio engine. Energy 36 (2011) 5385-5393.

[119] Gumus M, Kasifoglu S. Performance and emission evaluation of a compression ignition engine using a biodiesel (apricot seed kernel oil methyl ester) and its blends with diesel fuel. Biomass and bio-energy 34(2010)134–139.

[120] Cheng C.H, Cheung C.S, Chan T.L, Lee S.C, Yao C.D. "Experimental investigation on the performance, gaseous and particulate emissions of a methanol fumigated diesel engine". The Science of the Total Environment (2008); 389: 115–124.

[121] Sayin C, Ozsezen A.N, Canakci M. The influence of operating parameters on the performance and emissions of a DI diesel engine using methanol-blended-diesel fuel. Fuel (2010); 89:1407–1414.

[122] Nabi N, Akhter S, Shahadat M.Z. Improvement of engine emissions with Transport Construction Foundation from Ministry of Transport of conventional diesel fuel and diesel–biodiesel blends.   Bioresour Technol People's Republic of China No. 200631826253. (2006); 97:372–8.

[123] Last R.J, Kruger M, Durnholz M. Emissions and performance characteristics of a 4-stroke, direct injected diesel engine fuelled with blends of biodiesel and low sulphur diesel fuel. SAE paper, no. 950054; (1995).

[124] Sayin C. Engine performance and exhaust gas emissions of methanol and ethanol–diesel blends. Fuel (2010); 89:3410–3415.

[125] Challen B, Baranescu R. Diesel engine reference book. 2nd edition. Woburn, MA: SAE and Butterworth Heinemann; (1999).

[126] Rakopoulos C.D, Rakopoulos D.C, Hountalas D.T, Giakoumis E.G, Andritsakis E.C. Performance and emissions of bus engine using blends of diesel fuel with bio-diesel of sunflower or cottonseed oils derived from Greek feedstock. Fuel (2008) ; 87:147–57.

[127] Monyem A, Van Gerpen J.H, Canakci M. The effect of timing and oxidation on emissions from biodiesel-fueled engines. ASAE (2001) ;44:35–42.

[128] Chao M.R, Lin T.C, Chao H.W, Chang F.S, Chen C.B. Effects of methanol-containing additive on emission characteristics from a heavy-duty diesel engine". Sci Total Environ (2001); 279:167–79.

[129] Stone R. Introduction to internal combustion engines. 3rd edition. Warrendale: SAE Inc.; (1999).

[130] Nabi N, Rahman M, Akhter S. Biodiesel from cotton seed oil and its effect on engine performance and exhaust emissions. ApplThermEng (2009);29:2265–70.

[131] Zheng M, Mulenga M.C, Reader G.T, Wang M, Ting D.S.K, Tjong J. Biodiesel engine performance and emissions in low temperature combustion. Fuel (2008) ;87(6):714–22.

[132] Tree D.R, Svensson K.I. Soot processes in compression ignition engines. Prog Energy Combust Sci (2007); 33:272–309.

[133] Senthil K.M, Ramesh A, Nagalingam B. An experimental comparison of methods to use methanol and jatropha oil in a compression ignition engine. J Biomass Bioenerg (2003);25:309–18.

[134] Ramadhas AS, Muraleedharan C, Jayaraj S. Performance and emission evaluation of a diesel engine fueled with methyl esters of rubber seed oil. J Renew Energ (2005);30:1700–89.

APPENDIX-I

Technical Specifications of AVL Di-Gas Analyser

Measurement principle	CO, HC, CO_2	Infrared measurement
	O_2	Electrochemical measurement
	NO (option)	Electrochemical measurement
Operating temperature	+5 to +45ºC	Keeping measurement accuracy
	+1 to +50ºC	Ready for measurement
	+5 to +35ºC	with integral NO sensor (Peaks of : +40ºC)
Storage temperature	-20 to +60ºC	
	-20 to +50ºC	With integrated O_2 sensor
	-10 to. +45ºC	With integrated NO sensor
	0 to +50ºC	With water in filter and / or pump
Air humidity	90% max.,	non-condensing
Power drawn	150 VA	
Dimensions	432 x 230 x 470 mm	(w x h x l)
Weight	16 Kg	

Measurement Ranges of AVL Di-Gas Analyser

Parameter	Measurement Range	Resolution
CO	0-10% vol	0.01% vol
CO_2	0-20% vol	0.1% vol
HC	0-20000 ppm vol	1 ppm
NO_X	0-5000 ppm vol	1 ppm
O_2	0-25% vol	0.01% vol

APPENDIX-II

Technical Specifications of AVL 437 Smoke Meter

Accuracy and Reproducibility   ± 1% full scale reading

Heating Time   Approx. 20 min

Light source   Halogen bulb 12 V / 5W

Colour temperature   3000 K ± 150 K

Detector   Selenium photocell dia. 45 mm ,

Max. Sensitivity in light   In Frequency range: 550 to 570 nm. Below 430 nm and above 680 nm sensitivity is less   than 4% related to the maximum sensitivity

Maximum Smoke   250ºC Temperature at entrance